

2-D RENDERING AND ANALYSIS OF A
HORIZONTAL ZINC SELENIDE
AEROSOL REACTOR VIA
COMPUTATIONAL FLUID
DYNAMICS

By

BRENT LEWIS FOSTER

Bachelor of Science

Oklahoma State University


Stillwater, Oklahoma

1997

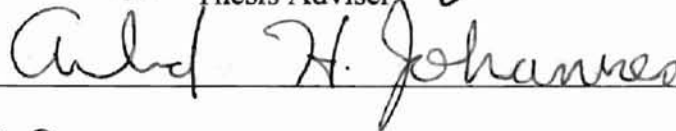
Submitted to the Faculty of the Graduate College of the
Oklahoma State University in partial fulfillment
of the requirements for the Degree of
MASTER OF SCIENCE
July, 1999

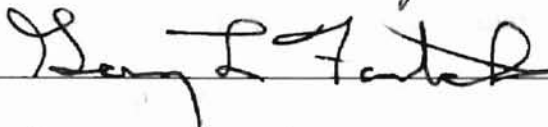
2-D RENDERING AND ANALYSIS OF A
HORIZONTAL ZINC SELENIDE
AEROSOL REACTOR VIA
COMPUTATIONAL FLUID
DYNAMICS

Thesis Approved:



Thesis Adviser







Dean of the Graduate College

ACKNOWLEDGEMENTS

I would like to express my heartfelt appreciation to my graduate advisor, Dr. Afshin Ghajar, for his endless patience and dedication for seeing me through to completion of this thesis. Without his active participation, the time spent as a graduate student would have been more formidable. This appreciation is extended to the other professors associated with this research, Drs. A. J. Johannes and Gary Foutch, for their input and guidance. Dr. D. G. Lilley also deserves thanks for his kind support and suggestions.

Gratitude must also be expressed towards my fellow research associates and friends. I would like to thank Trey Morrison and Chris Shay for helping me understand many chemistry related concepts which presented me with some difficulty and for helping me to realize I still have much to learn about chemistry. Jake Nikolic is due special recognition for being a friend and colleague throughout my undergraduate years and continuing with me on into graduate studies. Bret Collier and Ryan Cambern deserve thanks for providing occasional distractions and reminding me there is life outside of scholastic studies.

Many others have contributed to the success of this thesis and are due mention. Appreciation is given to Dr. Bruce Gerhold for providing needed insight and a different enlightening perspective. Additionally, I would like to thank Tom Potts and others at Eagle-Picher Inc. for providing the opportunities for this research. The School of

Mechanical and Aerospace Engineering and Eagle-Picher are jointly due thanks for providing OCAST support throughout my time as a graduate student at Oklahoma State University.

I am forever grateful to my family. Undying appreciation is expressed to my parents, Patsy and Curley Foster. They were always there for me providing emotional and financial support. My brother, Captain Brian Foster, USAF, also deserves recognition for perpetually providing words of encouragement.

TABLE OF CONTENTS

Chapter	Page
I. INTRODUCTION.....	1
1.1 Background.....	1
1.2 Semiconductors.....	2
1.3 Eagle-Picher Process.....	5
1.4 Objectives.....	7
II. LITERATURE REVIEW.....	9
2.1 Introduction.....	9
2.2 II-VI Production Methods.....	10
2.3 Aerosol Reactors and Processes.....	15
2.4 Numerical and CFD Modeling.....	21
2.5 Heat and Mass Transfer.....	29
III. DESCRIPTION OF CURRENT II-VI SYNTHESIS PROCESS.....	34
3.1 Introduction.....	34
3.2 Physical Description of Reactor Components.....	34
3.3 Reactor Operation Procedures.....	38
3.4 Initial Assessment of Process Operation.....	41
IV. FLUENT CFD SUITE.....	43
4.1 Background.....	43
4.2 Suite Overview.....	44
4.3 GeoMesh.....	49
4.3.1 DDN.....	51
4.3.2 P-Cube.....	51
4.3.3 Leo.....	52
4.4 FLUENT/UNS.....	53
4.4.1 Governing Equations.....	53
4.4.2 FLUENT/UNS Numerical Scheme.....	60

Chapter	Page
V. FLUENT/UNS 2-D MODEL DEVELOPMENT.....	69
5.1 Introduction.....	69
5.2 Pre-CFD Process Assessment.....	70
5.3 FLUENT/UNS 2-D CFD Model Development.....	73
5.4 Correlation of Computational Model.....	78
5.5 Model Simplifications and Assumptions.....	81
5.6 Convergence and Model Feasibility Considerations.....	82
5.7 Presentation and Evaluation of Results.....	87
VI. PROCESS PARAMETER VARIATIONAL INVESTIGATION.....	95
6.1 Introduction.....	95
6.2 Reactor Temperature Zones.....	97
6.3 Reactant Stream Argon Flow Rates.....	100
6.4 Reactant Flow Rates.....	102
6.5 Comparison of Results.....	105
6.6 Optimized Model.....	106
VII. SUMMARY, CONCLUSIONS, AND RECOMMENDATIONS.....	111
7.1 Scope and Purpose Summary.....	111
7.2 Conclusions.....	112
7.3 Recommendations.....	113
REFERENCES.....	115
APPENDIX A - REACTOR AND BOILER DIMENSIONS.....	122
APPENDIX B - ZINC AND SELENIUM VAPOR PRESSURE DATA.....	128
APPENDIX C - HSC CHEMISTRY DATA.....	131
APPENDIX D - CASE PROCESS CHARACTERISTICS.....	135
APPENDIX E - FLUENT/UNS CFD MODEL DOCUMENTATION.....	141
E.1 DDN.....	141
E.2 P-Cube.....	144
E.3 Leo.....	149
E.4 FLUENT/UNS.....	149
E.5 Thermophysical Properties.....	163
APPENDIX F - COMPUTATIONAL STUDY DATA.....	181

LIST OF TABLES

Table		Page
1-1	Typical Energy Gap of Some II-VI Compounds.....	4
2-1	Common Models for Simulating Multiphase Flow.....	24
2-2	Typical Ranges of Arrhenius Parameters.....	26
5-1	Summary of Representative Parameters.....	72
5-2	Activation Energies Estimated by Various Methods.....	78
5-3	Reactant Loadings and Yields.....	80
5-4	Pre-exponential Factor Iteration for Case BA97202.....	80
5-5	Pre-exponential Factor Iteration for Case BA97195.....	81
5-6	Determination of Final Pre-exponential Factor.....	81
5-7	Typical Residual Termination Criteria.....	83
5-8	Typical Residual Values for Baseline Model.....	86
5-9	Evaluation of Variability of Process Solution for Case Corr1-1.....	86
6-1	Front Zone Temperature Variation Effects on Yield.....	98
6-2	Middle Zone Temperature Variation Effects on Yield.....	99
6-3	Rear Zone Temperature Variation Effects on Yield.....	99
6-4	Zinc Inlet Argon Flow Rate Effects on Yield.....	101
6-5	Selenium Inlet Argon Flow Rate Effects on Yield.....	102
6-6	Zinc Reactant Flow Rate Effects on Yield.....	104

Table	Page
6-7 Stoichiometric Reactant Flow Rate Effects on Yield.....	104
6-8 Characteristic Values for Optimal Case Opt1.....	107
B-1 Coefficients and Temperature Ranges for Vapor Pressure Functions.....	129
B-2 Vapor Pressure of Zinc at Various Temperatures.....	129
B-3 Vapor Pressure of Selenium at Various Temperatures.....	130
C-1 Thermochemical Data for Reaction $\text{Se}_2(\text{g}) + 2\text{Zn}(\text{g}) = 2\text{ZnSe}(\text{g})$	132
C-2 Thermochemical Data for Reaction $\text{ZnSe}(\text{g}) = \text{ZnSe}(\text{s})$	133
C-3 Thermochemical Data for Reaction $\text{Zn}(\text{s}) + \text{Se}(\text{s}) = \text{ZnSe}(\text{s})$	134
D-1 Case BA97202 Process Characteristics.....	137
D-2 Case BA97195 Process Characteristics.....	139
E-1 DDN Geometry Coordinates.....	142
E-2 Various Species Properties.....	165
E-3 Lennard-Jones Parameters for Species.....	167
E-4 Thermophysical Properties for Quartz.....	169
E-5 Zn(g) Species Ideal Gas Density.....	169
E-6 Zn(g) Species Dynamic Viscosity Based on Chapman-Enskog Theory.....	170
E-7 Zn(g) Species Thermal Conductivity Based on Monatomic Theory.....	170
E-8 Final Polynomial Coefficients and Constant Values for Zn(g) Species.....	171
E-9 $\text{Se}_2(\text{g})$ Species Specific Heat.....	171
E-10 $\text{Se}_2(\text{g})$ Species Ideal Gas Density.....	172
E-11 $\text{Se}_2(\text{g})$ Species Dynamic Viscosity Based on Chapman-Enskog Theory.....	172
E-12 $\text{Se}_2(\text{g})$ Species Thermal Conductivity Based on the Eucken Method.....	173

Table	Page
E-13 Final Polynomial Coefficients and Constant Values for $\text{Se}_2(\text{g})$ Species.....	173
E-14 $\text{ZnSe}(\text{g})$ Species Specific Heat.....	173
E-15 $\text{ZnSe}(\text{g})$ Species Ideal Gas Density.....	174
E-16 Final Polynomial Coefficients and Constant Values for $\text{ZnSe}(\text{g})$ Species....	174
E-17 $\text{Ar}(\text{g})$ Species Ideal Gas Density.....	175
E-18 $\text{Ar}(\text{g})$ Species Dynamic Viscosity.....	176
E-19 $\text{Ar}(\text{g})$ Species Thermal Conductivity.....	177
E-20 Final Polynomial Coefficients and Constant Values for $\text{Ar}(\text{g})$ Species.....	178
E-21 Binary Diffusion Coefficients for $\text{Ar}(\text{g})$ - $\text{Se}_2(\text{g})$ Combination.....	178
E-22 Binary Diffusion Coefficients for $\text{Ar}(\text{g})$ - $\text{Zn}(\text{g})$ Combination.....	179
E-23 Binary Diffusion Coefficients for $\text{ZnSe}(\text{g})$ - $\text{Se}_2(\text{g})$ Combination.....	179
E-24 Binary Diffusion Coefficients for $\text{Zn}(\text{g})$ - $\text{Se}_2(\text{g})$ Combination.....	180
E-25 Final Polynomial Coefficients for Binary Diffusivity Combinations.....	180
F-1 Computational Study Data.....	182

LIST OF FIGURES

Figure		Page
1-1	Relative Comparisons of Energy Gap.....	3
2-1	Early Example of Vapor Growth Technique.....	13
2-2	Gas Phase Processes Contributing to Particle Formation.....	18
2-3	Commercial Scale Aerosol Process.....	20
2-4	Design Procedure for Jet Type Aerosol Reactor.....	21
2-5	Secondary Flow Vector Plot.....	31
3-1	Current Eagle-Picher Reactor.....	35
4-1	Program Interactions for FLUENT Software Package.....	45
4-2	Program Interactions for FLUENT/UNS and RAMPANT Software Packages.....	46
4-3	Program Interactions for the NEKTON Software Package.....	47
4-4	GeoMesh Session Manager Window.....	49
4-5	Overview of FLUENT/UNS Numerical Scheme.....	61
4-6	One-Dimensional Representation of Control Volume.....	63
5-1	Energy Changes Occurring in a Hypothetical Reaction.....	77
5-2	Typical Residual Behavior for Solution Considering Gravity.....	85
5-3	Velocity Vectors at Front of Chemical Reactor.....	88
5-4	Contours of Velocity Magnitude.....	90

Figure	Page
5-5	Contours of Static Temperature..... 91
5-6	Contours of Zn Concentration..... 92
5-7	Contours of Se ₂ Concentration..... 93
5-8	Contours of ZnSe Concentration..... 94
6-1	Contours of ZnSe Concentration for Optimum Case..... 110
A-1	Reactor Tube Dimensions..... 123
A-2	Zinc Transfer Arm Dimensions..... 124
A-3	Selenium Transfer Arm Dimensions..... 125
A-4	Zinc Boiler Dimensions..... 126
A-5	Selenium Boiler Dimensions..... 127
E-1	DDN Model Representation..... 142
E-2	DDN Geometry - Front of Reactor..... 143
E-3	DDN Geometry - Rear of Reactor..... 143
E-4	P-Cube Model Representation..... 144
E-5	Boundary Condition Specification Panel..... 145
E-6	P-Cube Boundary Condition Designations - Front of Reactor..... 146
E-7	P-Cube Boundary Condition Designations - Rear of Reactor..... 146
E-8	Rendering of Boundary Conditions in P-Cube..... 147
E-9	Bunch Node Distribution Panel..... 147
E-10	P-Cube Node Distribution - Front of Reactor..... 148
E-11	P-Cube Generated Mesh for Front of Reactor..... 148
E-12	Final Domain Rendering as Indicated by FLUENT/UNS..... 149

NOMENCLATURE

English Letters

A	Pre-exponential factor, $\text{m}^3/\text{kmol}\cdot\text{s}$
c_p	Specific heat at constant pressure, $\text{J}/\text{kg}\cdot\text{K}$
D	Diameter, m
D_{AB}	Diffusivity of component A in component B, m^2/s
E_a	Activation energy, J/kmol
eV	Electron-volt
ΔH	Change in enthalpy, kcal, J
ΔH_{react}	Heat of reaction, J/kmol
g	Acceleration due to gravity, $9.81 \text{ m}/\text{s}^2$
ΔG	Change in Gibbs free energy, kcal
Gr	Grashof number, dimensionless
k	Rate constant, $\text{m}^3/\text{kmol}\cdot\text{s}$
k	Thermal conductivity, $\text{W}/\text{m}\cdot\text{K}$
k	Turbulent kinetic energy, m^2/s^2
K	Equilibrium constant, dimensionless
k_0	Pre-exponential factor, $\text{m}^3/\text{kmol}\cdot\text{s}$
\dot{m}	Mass flow rate, kg/s

M	Molecular Weight, kg/kmol
N	Avogadro's number, 6.023×10^{23} molecules/mol
P	Pressure, mmHg, Pa
Pe	Peclet number, dimensionless
Pr	Prandtl number, dimensionless
r	Reaction rate, kmol/m ³ -s
R	Ideal gas constant, 8314 J/kmol-K
R ²	Regression coefficient, dimensionless
Re	Reynolds number, dimensionless
ΔS	Change in entropy, cal
Sc	Schmidt number, dimensionless
T	Temperature, K
T _b	Bulk temperature, K
T _m	Temperature at the melting point, K
T _{min}	Minimum temperature, K
T _{max}	Maximum temperature, K
T _w	Wall temperature, K
V	Velocity, m/s
\tilde{V}_m	Molar volume at the melting point, cm ³ /mol
Y	Yield, %

Greek Letters

α	Thermal diffusivity, m^2/s
β	Coefficient of thermal expansion, $1/\text{K}$
Δ	Change in
ε	Maximum energy of attraction between two molecules, erg
ε	Turbulence dissipation rate, m^2/s^3
ν	Kinematic viscosity, m^2/s
κ	Boltzmann constant, 1.30×10^{-16} erg/K
μ	Dynamic viscosity, Pa-s
ρ	Density, kg/m^3
σ	Molecule collision diameter, m
σ	Characteristic diameter, Å
Ω_D	Diffusion collision integral parameter, dimensionless
Ω_k	Collision integral parameter, dimensionless
Ω_μ	Collision integral parameter, dimensionless

Subscripts and Superscripts

A	Component A
B	Component B
e	Location of face shared between cells P and E
E	Center of cell E, to the right (or east) of cell P

o	Out (at the exit)
P	Center of cell P
w	Location of face shared between cells P and W
W	Center of cell W, to the left (or west) of cell P

Abbreviations

2-D	Two-Dimensional
3-D	Three-Dimensional
ACT	Assumed Combined Temperature
C	Centigrade
CFD	Computational Fluid Dynamics
CVT	Chemical Vapor Transport
EP	Eagle-Picher Inc.
g	Gas phase
K	Kelvin
LED	Light Emitting Diode
MOCVD	Metalorganic Chemical Vapor Deposition
MOVPE	Metalorganic Vapor Phase Epitaxy
PDF	Probability Density Function
PVT	Physical Vapor Transport
RNG	Renormalization Group
SIMPLE	Semi-Implicit Method for Pressure-Linked Equations

CHAPTER I

INTRODUCTION

1.1 Background

Group II-VI semiconducting compounds are so named based on the location of their constituent elements in the periodic table. The Group II elements include zinc (Zn), cadmium (Cd), and mercury (Hg). These are found in Group 2B and are all metals, hence they are excellent conductors of heat and electricity. The elements comprising Group VI typically associated only with semiconductor material processes include sulfur (S), selenium (Se), and tellurium (Te). These are found in Group 6A and all Group 6A elements are commonly referred to as chalcogens, or “chalk formers” (Brown et al., 1994). Sulfur and selenium are considered nonmetals while tellurium is considered a metalloid. Nonmetals, as can probably be deduced, are poor conductors of heat and electricity. Metalloids contain some properties of both metals and nonmetals.

Another term often used to characterize metalloid elements and compounds is semiconductors. Eagle-Picher Inc. (EP) is a successful company with many proprietary processes focusing on semiconducting materials production. An alliance was formed between Eagle-Picher and Oklahoma State University for the design and optimization of a chemical reactor for the production of II-VI semiconducting compounds, specifically

zinc and cadmium selenides and sulfides. The goals also included improving the efficiency of the process currently in operation. The research focus within this thesis concentrates on the understanding and improvement of the current process with the realization that what is learned could be applied to a new system. To aid in the understanding of the importance of this research, a brief introduction to semiconductor behavior has been included. Following the semiconductor introduction will be a summary of the Eagle-Picher process of interest and the objectives of the research.

1.2 Semiconductors

The benefits of semiconductors can be seen everywhere in our daily lives. They are in everything from televisions and watches to cellular phones and computers. Semiconductors have increasingly allowed companies to design smaller and more sophisticated devices and opened new doors to other applications. For example, the computer industry has seen a dramatic increase in speed and operation efficiency over the years while continually decreasing product space requirements. To gain a better understanding for the purpose of research activities discussed within this thesis, a discussion of semiconductors is presented.

Beiser (1986) provides a sufficient overview of band theory as related to semiconductors. The use of energy bands is a method to characterize the sharply defined energy levels in a crystal structure of component atoms. When atoms are brought close together, such as that in a crystal structure, their electron shells interact to form a collective system of electrons. Resulting from changes occurring in the crystal structure

such as shifting of atom energy levels, the energy bands materialize. These bands are typically composed of many energy levels, however, they are so near one another the boundaries are almost indistinguishable. Chang (1991) explains closely spaced energy levels which are filled by orbitals are called the “valence bands” while closely spaced empty outer levels which overlap are called “conduction bands.” Beiser (1986) continues further by indicating electrons can only have energy values that fall within an energy band. These energy bands may or may not overlap. If they do not overlap then the material is noted to have a forbidden (or energy) gap, or a group of electron energy values the crystal may not possess. A representation of common energy gap behavior for various substances is shown in Figure 1-1. As shown by the figure, there is usually an

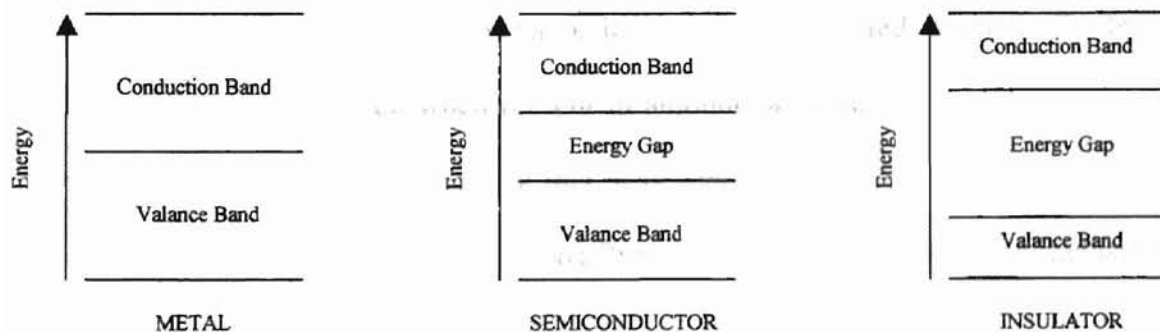


Figure 1-1. Relative Comparisons of Energy Gap (Chang, 1991)

imperceptible or non-existent gap for metals. This means delocalized electrons are easily able to move throughout the material and therefore conduct electricity or heat. For semiconductors, there is only a small gap, therefore needing a fixed small amount of energy before they begin to conduct electricity or heat. Insulators have a seemingly large gap and it is very difficult for electrons to make the jump across the gap. Characteristic values for energy gaps of compounds of interest to this research at room temperature are

shown in Table 1-1. Physicists commonly consider an energy gap of about 4 eV as a way of distinguishing semiconductors from insulators (Van Vlack, 1989).

Table 1-1. Typical Energy Gap of Some II-VI Compounds (Kaldis, 1982)

Compound	Energy Gap (eV)
ZnS	3.66
ZnSe	2.67
CdS	2.42
CdSe	1.73

Very pure semiconductors whose behavior is not dictated by the amount of impurities are known as pure (or intrinsic) semiconductors (Jones and Childers, 1990). It is known that the properties of semiconductors can be altered dramatically by the inclusion of impurities, even when present in amounts as small as one part per million (Jones and Childers, 1990). Knowing this, it is apparent why manufacturers constantly strive to produce a product as pure as possible or to stringently control the inclusion of impurities.

Industry also has needs for impure (or extrinsic) semiconductors as well (Jones and Childers, 1990). These are normally characterized as being either n-type or p-type semiconductors. Semiconductors where an impurity has increased the number of negative charge carriers are known as n-type, while semiconductors containing more positive carriers are known as p-type (Jones and Childers, 1990). Both n-type and p-type semiconductors have the energy gap significantly reduced as a result of impurity

inclusions and conductivity may be increased by as much as a factor of 100,000 (Chang, 1991).

Jones and Childers (1990) also discuss a few specific examples of the applications of semiconductors, one of these being light emitting diodes (LEDs). LEDs emit radiation in the form of light due to the return of an electron from the conduction band to the valence band. Most LEDs, depending on the compounds they are created from, can be found in red, green, and yellow. This appears to be an area of intense investigation based on a review of the available literature. Authors such as Aoki et al. (1996), and Bottcher and Hartmann (1995) investigated various aspects of ZnSe compounds and indicated their potential for blue LEDs and laser applications. These works and many others are reviewed in Chapter II.

1.3 Eagle-Picher Process

The system of research interest can be described as an aerosol batch reactor where vapor phase species come together and interact forming a condensable product. The species begin as solid elemental source materials (usually zinc and selenium) and are heated to boiling in semi-isolated areas to form the vapor phase species. They are then introduced to the reaction zone at very low flow rates (less than 1×10^{-4} kg/s) with the aid of the non-reactive carrier gas argon. The overall process is carried out at high temperatures (in excess of 1000 K) and is also quite exothermic. The product powder deposits itself primarily on the bottom of the reaction tube with smaller amounts coating

the walls of the remaining reaction area. After the batch process has run to completion, the desired product is collected from inside the tube.

The product is generally of high purity (as much as six nines, or 99.9999%) and is used in-house as well as supplied to other companies for use in creating semiconductor materials. The need for high purity in these materials has been emphasized in the previous section. Common high purity compound production by Eagle-Picher can be attributed predominantly to the vapor phase reaction methods employed. Other methods utilized in the industry for the production of the desired product powders tend to employ wet-chemical methods. When these types of processes are used, further purification steps are often required to obtain the high purity product.

The current process setup employed by Eagle-Picher has many shortcomings they wish to improve. In the beginning stages, sweeping improvements to the process were going to be accomplished by the design, construction, and operation of a new large-scale reactor. In fact, one of the major obstacles was reactor scale-up. Initially, Eagle-Picher estimated production would have to be increased by as much as a factor of 100 to be in a position to meet future market demands for these materials. Due to changing market conditions, however, the production target was scaled back to two orders of magnitude. Therefore, focus turned towards the design of a new reactor based on the lower estimated production demands as well as optimization of the current process. Many of the shortcomings with the process control, process run time, and other reactor operation characteristics as related to the development of a new reactor design have been addressed by Morrison (1998) and Shay (1998). The research discussed within this thesis is principally concerned with providing Eagle-Picher with additional means of increasing

production by optimization of the current process. This was carried out by applying the computational fluid dynamics (CFD) code FLUENT/UNS to one of the II-VI compound production processes. Zinc selenide was chosen as the primary compound for investigation based chiefly on safety and environmental concerns. It was concluded the results of the final analysis of the system could also be used to further optimize the other II-VI processes. The commercial FLUENT/UNS code allows analyses of complex geometries and heat transfer effects in flowing and reacting systems. It was chosen based on availability and potential for application towards the research process. More complete coverage is given to initial evaluation of the current reactor system in Chapter III.

1.4 Objectives

Eagle-Picher has consistently remained a driving force for the advancement of semiconductor materials. To remain at the forefront of this technology, new process developments and enhancements need to be discovered and applied on a continuing basis. The objectives outlined below summarize the contributions this thesis strives to accomplish for the understanding and advancement of the II-VI processes investigated. The objectives are as follows:

1. Evaluate the operation of the current system by analysis of historical and experimental data and information.
2. Characterize and document process parameters and phenomena previously unknown or not readily determined from the literature.

3. Develop and provide confidence in a two-dimensional (2-D) CFD model of the present system to aid in evaluation processes.
4. Optimize the current chemically reacting system with the use of systematic parameter variation within the 2-D CFD model.
5. Document procedures utilized in applying the FLUENT/UNS CFD code in evaluation of the chemically reacting system, therefore providing a source of information to be used by others in analysis of similar systems.

Completion of the objectives was accomplished by the use of traditional engineering methods coupled with current technological applications, i.e. the Fluent CFD Suite.

The following Chapter (Chapter II) provides a comprehensive literature review of the material related to the current research. Chapter III gives a description of the investigated process. The Fluent CFD Suite is then discussed in Chapter IV. Chapter V presents the computational model development while Chapter VI discusses model parameter variations. Finally, in Chapter VII, conclusions and recommendations are summarized.

CHAPTER II

LITERATURE REVIEW

2.1 Introduction

The processes utilized by Eagle-Picher discussed in Chapter I are quite unique. This technology has evolved over the last fifty years and has been maintained as an in-house trade secret. Therefore, due to the scarcity of material related directly to the scope of study in this thesis, relevant information has been assembled from a diverse collection of sources. The objective of this literature review is to expose the reader to many aspects of II-VI materials production. The goal of the second section of this chapter is to discuss the available literature directly related to II-VI compounds and some of their applications. The third section covers characteristics and performance of aerosol reactors. General CFD resources are examined and specific applications are discussed in the fourth section. In the fifth and final section, heat and mass transfer resources deemed relevant to the present study are considered.

2.2 II-VI Production Methods

Production methods found in the literature mostly centered around the growth of high-purity crystals. While the final goals of these procedures are different when compared to the focus of this research, portions of the information presented and many of the techniques discussed are certainly applicable to the current process. Moreover, the product created from the process discussed in this research is later used in some of the additional procedures described in this section.

Aven and Prener (1967) provide a good source of initial explanation on many interesting aspects of the II-VI compounds. Most of the topics covered are related to crystal growth by various methods and semiconductor attributes such as band structure, crystallography, and energy transfer processes. Related topics of interest include thermodynamic considerations and general growth techniques for crystals with processes that parallel the current research. Some discussion is oriented toward the basic properties of the source elements involved and phase equilibria information (or the lack thereof). Mention is also given to the limitations of the crystal preparation due to the phase equilibria. Some of the limitations can be attributed to the combination of high temperatures, costs for contaminant free stable containers (quartz is a common material for these processes), and non-negligible dissociation pressures. The authors also indicate there are two basic methods by which crystals are generally produced: liquid phase and vapor phase. Many examples of these two general classifications have been found in the literature and are discussed further. Characteristics of the vapor phase methods in common with the current research will also be communicated.

Single crystals with significant volume can be created utilizing melt growth techniques (Aven and Prener, 1967). Crystal growth by one method generally involves the sealing of a preformed compound (such as that created by the current process of interest) in a quartz tube. Due to transport limitations, a three-zone heating arrangement is commonly used. The compound is melted within the assembly and the entire tube moves at a constant fixed rate from a higher temperature to a lower temperature until the desired final position has been reached. To suppress vapor phase mass transport, an overpressure from one of the components is usually applied by maintaining a reservoir at a constant temperature in some other area of the assembly. An additional method involves placing stoichiometric proportions of the elements in a quartz ampoule. This ampoule is then heated in a furnace and passed through a sharp temperature gradient inducing the crystal growth.

Triboulet (1975) examined some of the difficulties with the melt growth methods of the II-VI compounds and also provided some comparisons of the properties between the II-VI and III-V compounds. He points out the importance of observing the shape of the liquidus curve near the congruent melting point and indicates for II-VI compounds, it is imperative to have precise control over the thermal conditions. A small temperature variation could drastically change the phase equilibria. He goes further into phase transitions in the solid state and discusses contamination in the melt growth procedures.

Nonstoichiometry effects on ZnSe and CdSe due to varying pressures from Cd, Zn, and Se were investigated by Rau (1978). His work was carried out using melt growth techniques in evacuated silica ampoules. The results of each component pressure in contact with ZnSe and CdSe were recorded and plotted. He also notes selenium appears

to be strongly absorbed by CdSe and ZnSe, while Zn and Cd are not. Additional study on stoichiometric effects can be found in the work of Kulakov and Fadeev (1981). Their work involved investigation of pulling rates, pressures, and composition to aid in arriving at optimal growth conditions.

An excellent review of available literature on crystal growth from the melt can be found in the work of Rudolph et al. (1995). They discuss in detail the problems associated with the melt growth techniques and shed some light on the difficulties encountered with heat and mass transfer analyses on these processes. In fact, according to their work, some analyses can only be made based on extrapolation of room temperature data or by considering the behaviors of other II-VI compounds.

ZnSe crystals were grown under seeded melt growth conditions with Zn partial pressure in the work of Kikuma and Shiohara (1996). They used heavily twinned crystals to seed the process and explore crystal orientation control. Twin free single crystals are the desired end product; however, this work deliberately analyzes some of the aspects of twinning behavior. Fukuda et al. (1996) report work carried out on reducing or eliminating twinning behavior in ZnSe crystals by the vertical Bridgman method. This work also explores crystal orientation and the use of seed crystals.

The vapor phase methods have the simple requirement of a continuous supply of group II and group VI elements in vapor form (Aven and Prener, 1967). Figure 2-1 shows an early example of a vapor phase method where M and N represent the metal and chalcogen, respectively. The elemental components can be created from the dissociated preformed compound or can stem from the elements themselves (Aven and Prener, 1967). In addition, the flow of the elements to the reaction (and/or deposition) zone can

occur with or without the aid of a carrier gas. Within the literature, processes utilizing a carrier gas appear to be known as chemical vapor transport (CVT) techniques while processes without a carrier gas are known as physical vapor transport (PVT) techniques. The CVT processes to be discussed tend to have the most in common with the central focus of this research.

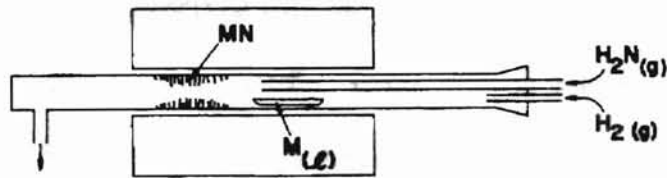


Figure 2-1. Early Example of Vapor Growth Technique (Aven and Prener, 1967)

Su (1987) gives insight into the growth rate of CdS with and without the presence of Ar gas. Convective effects on the growth rate in vertical and horizontal systems were also studied and discussed. A one-dimensional theoretical model was developed based on the work of previous authors to predict the growth rate and is compared to experimental data.

PVT mass fluxes of ZnSe were examined by Sha et al. (1995) using an in-situ dynamic technique in temperatures ranging from 1050 to 1160 °C. Paralleling the current research, the dominant vapor species were found to be Zn and Se_2 around this temperature range. A one-dimensional diffusion limited model was developed and found to agree with experimental results satisfactorily. The effects due to residual gases were also determined and the amount and composition of the gases were evaluated as well by optical absorption techniques.

The effects of argon, hydrogen, and helium on the transport rates of ZnSe by CVT were considered by Muranoi et al. (1995). Their study provided valuable information on the transport rates as they relate to pressures exerted by each of the gases. The primary purpose of this research was to find a gas that would allow the transport rate to increase so the growth temperature could be lowered and electronically active impurities could be reduced. All three gases considered produced similar high transport rates, however, higher quality crystals were observed with the use of argon.

Many other authors have contributed information related to crystal growth by PVT and CVT and can easily be found in the literature. CVT of ZnSe by iodine transport has been studied extensively by teams of researchers such as Bottcher and Hartmann (1995) and Bottcher et al. (1996). In the first work, more insight is provided on heat and mass transfer mechanisms related to the processes. In the second, convective effects are discussed. Korostelin et al. (1996a and 1996b) tend to center their work around obtaining homogeneous single crystals of II-VI compounds by both CVT and PVT processes.

Thin films are another area of research involving the II-VI compounds. Elemental gases are typically brought together at high temperatures and allowed to react with one another on a prepared interface. In contrast to single crystal growth, where the growth is desired to occur from a single seed, simultaneous nucleation is desired to achieve microcrystalline films (Aven and Prener, 1967). Certain optical qualities can only be studied through the use of these thin films. Since the processes related to thin films have a limited connection with the research contained in this thesis, mention will be given to only a few of these sources.

Metalorganic chemical vapor deposition (MOCVD) is a typical process used for creation of thin films employing the basic mechanisms mentioned earlier. Jensen (1989) has compiled a review of many issues related to MOCVD. Some of the topics of discussion range from transport phenomena to the underlying reactions. Other works such as those by Aoki et al. (1996) and Hatanakata et al. (1996) present information concerned with radical assisted growth of ZnSe films by MOCVD.

There are other techniques discussed in the literature for the deposition of thin films. Some of the other well-known processes are hot wall beam epitaxy and atomic layer epitaxy and are discussed by authors such as Sitter (1995). Additional sources applying numerical techniques related to some of these processes will be considered in the section on numerical and CFD applications.

2.3 Aerosol Reactors and Processes

Aerosol reactor technology is generally applied in manufacturing of fine particles for the ceramics and pigments industries. The usual avenue for aerosol creation is chemical reaction of two monomers in the gas phase to form a solid particle. Literature pertaining to these processes provides much insight into some of the physical and chemical attributes of the current scope of study. Within the works presented in this section, information is reviewed which aids in evaluation of process parameters and particle characteristics. These sources also attempt to analyze particle behavior within chemical reactors and by so doing, promote further understanding of process characteristics and behaviors. Many of the authors, within their works, concede that

research of effects some processes and process parameters have on the outcome of the final product is somewhat lacking and needs further investigation and evaluation. There is a substantial amount of literature available on this topic and a generous review is given in this section. In addition, current research activities are mentioned as related topics are discussed.

Many of the fundamentals of aerosol behavior are considered in detail by Friedlander (1977). While the major motivation behind the creation of this effort appears to be environmental in nature, this work is widely recognized and referred to in other sources related to commercial aerosol reactors. Much of the terminology commonly used in the aerosol industry (among others) is explained. Topics related to convective and inertial deposition, collision and coagulation, and gas-to-particle conversion are discussed as well.

Wu et al. (1986) consider the synthesis of silicon particles by a pyrolysis process on silane gas. In analysis of chemical reacting media such as the focus of this research, it is imperative to develop the reaction mechanism or at least a good representation. For the silane pyrolysis, the determined rate limiting step was postulated to be:



The activation energy for the given process was also determined to be 60 kcal/mole. Taking note of the activation energy, it was apparent the process could be manipulated by controlling the temperature. In this particular work, the reaction mechanisms were only a small part of the overall study on silane particle size distributions. However, it was noted that determination of the important factors such as these strongly parallel obstacles encountered in this research.

Reactor geometry effects on powder production and vapor deposition are considered by Pratsinis et al. (1986a). Types of configurations considered are tubular, annular, and parallel plates as applied to the production of NH_4Cl aerosol by gas phase reaction. It was concluded that annular and parallel plate reactors could create more monodisperse (all roughly the same size) particles while sacrificing lower yields when compared to tubular reactors. An extension of this work can be found in Pratsinis et al. (1986b). Reactor residence time distribution effects on NH_4Cl were also investigated by Pratsinis et al. (1986c) on continuous stirred tank reactors and tubular flow aerosol reactors.

Kodas and Friedlander (1988) address procedures for designing tubular flow reactors for the production of monodisperse particles. Their research efforts led them to conclude that nearly monodisperse aerosols could be generated by separation of particle formation and growth processes, maintaining a narrow residence time distribution, and minimizing monomer concentration gradients. Additional topics for discussion included convection effects and radial diffusing of the condensing species.

Particle control and evaluation in aerosol reactors were the topics touched on by Wu et al. (1988). In it, they allude to the fact that reaction rate, commonly dependent on temperature, controls the particle growth and evolution. To characterize aerosol systems, they derived simplified reaction and coagulation equations. Using the models, effects of reaction rate, residence time, and additional parameters were evaluated. A graphical overview of gas-phase particle formation processes is given in Figure 2-2.

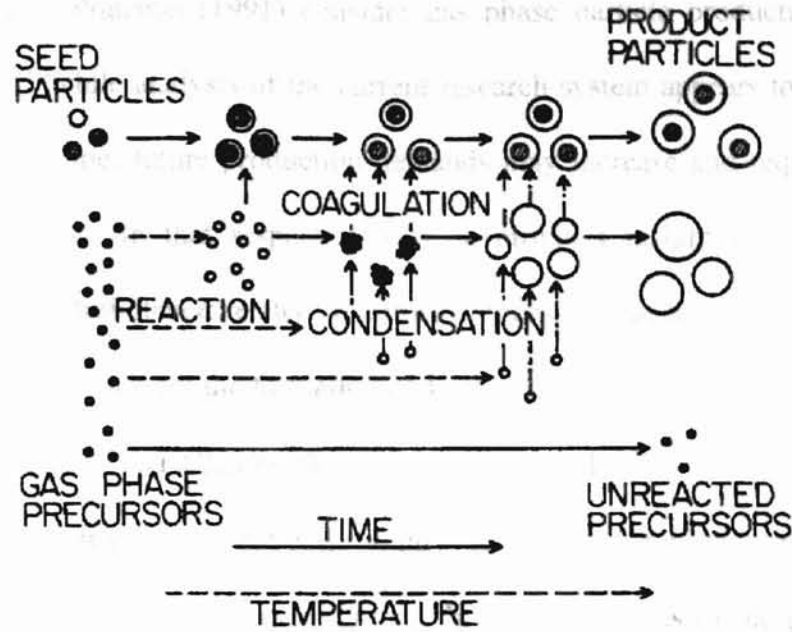
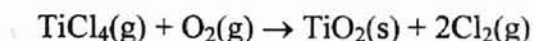


Figure 2-2. Gas Phase Processes Contributing to Particle Formation (Wu et al., 1988)

Every so often, throughout the literature, some authors combine the advances to date of certain research activities. Pratsinis (1988) compiled an exemplary work detailing aerosol activities and the considerable problems encountered. The advantages of aerosol processes over wet chemistry methods are given along with characterizations of processes and problems as they apply to individual industries in the production of carbon blacks, ceramic powders, optical fibers, and thin films for the microelectronics industry. As other literature has done in the past, the point is made that the lack of reliable correlations from system to system has created tremendous difficulties for development, design, and scale-up of industrial aerosol operations. A final conclusion, which appears to prevail in the current research, is that there is still a great deal to be learned about these processes, and therefore there is still a major dependence on basic engineering principles.

Xiong and Pratsinis (1991) consider gas phase particle production in reacting turbulent flows. While analysis of the current research system appears to operate in the highly laminar regime, future production demands may increase and require the use of higher speed flows. In that respect, this work provides insight into processes and characterization of turbulence related to aerosol processes that may be helpful. Xiong and Pratsinis (1991) consider the formation of TiO_2 by the following mechanism:



For this reaction, it was found that controlling mechanisms for particle growth included chemical reaction and Brownian coagulation. In the later stages of the process, it was found that shear-induced coagulation becomes predominant.

Specific areas where more research is needed are recognized by Stamatakis et al. (1991) with emphasis on titanium dioxide. Again, some of these parallel the needs related to the current focus of this research. They give an overview of a commercial scale aerosol process and provide the representation shown in Figure 2-3. The figure shows the general process setup, including the choice of whether to introduce the reacting species as gas phase or by liquid volatilization. In addition, particle collection is emphasized along with unused product recovery, if possible. Industrial research areas of need as indicated by their work are: nucleation processes, coagulation electrostatics, coalescence kinetics and formation of multi-component particles, in-situ processing of aerosol particles, aerosol reactor design, ultrafine particle production, and process control.

As mentioned earlier, there are currently many difficulties preventing industrial scale-up of laboratory processes. Sadakata et al. (1996) attempt to address some of these

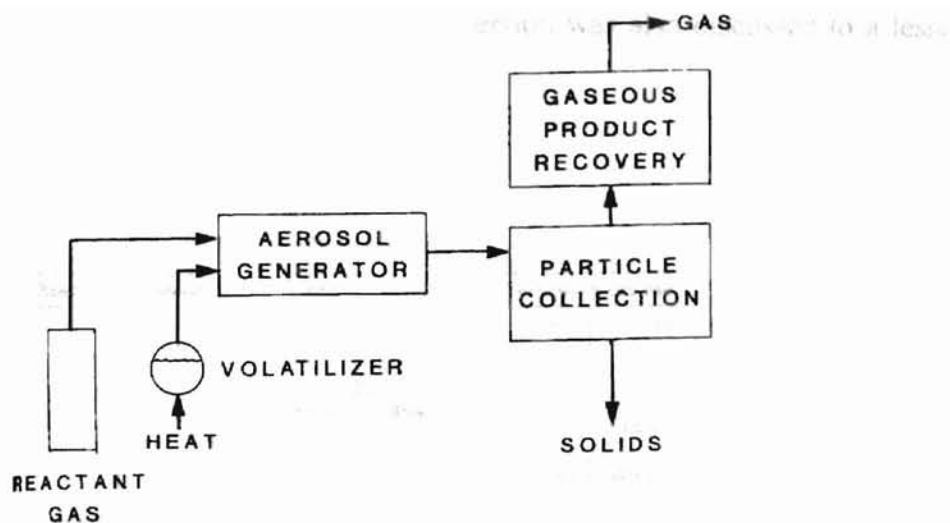


Figure 2-3. Commercial Scale Aerosol Process (Stamatakis et al., 1991)

problems by devising a systematic approach to aerosol reactor design. Their research centers around turbulent processes for the derivation of a simple scaling law which they confess the applicability to industrial processes must still be confirmed. They also discuss the general procedure for the design of an industrial scale jet type aerosol reactor and present the steps in a graphical manner as shown in Figure 2-4. This diagram has been included to indicate the complexity involved for any reactor analysis and development. In addition, it would appear this process development procedure could be adapted for application to the design of laminar flow aerosol reactors.

A number of topics associated with particle formation were addressed at the First International Forum on Particle Technology and are presented by Pratsinis and Vemury (1996). This source focused primarily on particle formation in turbulent flows. It again points to the fact that for economical mass production of particles by gas-to-particle conversion, high speed turbulent flows would be required. Other avenues were pursued as well, including structure of agglomerate powders, reactor design, and evaporation-

condensation phenomena. Particle-to-particle conversion was also discussed to a lesser extent.

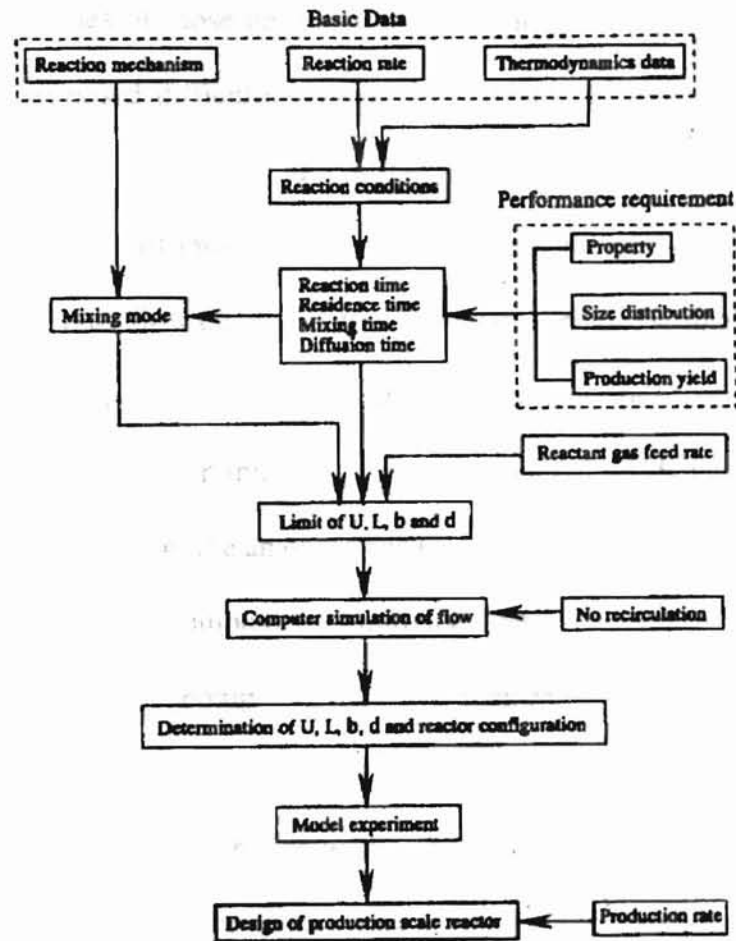


Figure 2-4. Design Procedure for Jet Type Aerosol Reactor (Sadakata et al., 1996)

2.4 Numerical and CFD Modeling

A necessity of the highly competitive business world, especially in materials production, is the optimization of processes. Due to the abundance of different material processes, the constant development of new technology, and lack of adequate scale-up

correlations as presented in the last section, engineers and scientists are faced with constant challenges. In the past, some optimization of fluid systems could only be carried out by traditional tracer studies, often on small scale models using materials with non-representative properties of those encountered in the actual process. High temperature processes have also posed difficulties, particularly related to accurate measurement of process parameters critical to execution. Further, accurate measurement of some process data requires the insertion of intrusive devices and with some of today's highly sensitive processes, this could alter flow characteristics or the outcome of the final product.

Approximately over the last two decades, a new field of engineering has developed to aid in process optimization, computational fluid dynamics (CFD). The primary goal of CFD is to provide an economically feasible means for improving flowing systems by modeling on computers. Initially, these programs were difficult to understand, very expensive computationally, and extremely limited in applicability. Progress within the last ten years has made the programs easier to understand and apply while making them more affordable as well. The information presented in this section discusses some of the potential problem areas, advances, and possible pitfalls with CFD in addition to the presentation of a few applications. Sources which tend to discuss primarily CFD background will be presented first, followed by applications to industry processes.

Advances in CFD and potential future applications are discussed by Shanley (1996). The author points out that CFD programs are becoming easier to utilize; however, users should not be lulled into a false sense of security. Input data applied to the computer models must be rigorously examined and the results validated. Some of the

advances discussed furthering the advent of CFD include parallel processing for large computer runs and automated mesh generation. Some industry applications are briefly considered emphasizing the difficulties realized with two-phase flowing systems.

Hamill (1996) gives a brief background on how CFD works, explaining that a CFD code partitions a flow area into a number of cells or control volumes, called the "grid" or "mesh." Within the confines of each cell or control volume, the Navier-Stokes equations (and others) are applied in an algebraic form and relate to neighboring cells or control volumes. Two additional points the author emphasizes are CFD provides only approximate solutions to highly complex phenomena and vendor support is extremely critical for users to become comfortable using the programs correctly and efficiently in a reasonable amount of time. The author also touches on model simplifications in addition to difficulties presented with the prediction of turbulent flow and multiphase flow. A listing of the common models applied to multiphase flows can be found in Table 2-1. The author further provides a short discussion of case studies pertaining to gas cyclone models and reformer design.

Ranade (1997) provides an overview of the thought processes, planning, and use of CFD programs as applied to chemical reactors. Typical choices allow anything from an order-of magnitude analysis to complete numerical simulation of an entire process. However, one drawback of using these tools is the methods sometimes conceal local turbulence and mixing phenomena which could have substantial impact on reactor performance. The author gives a list of tasks or activities, presented on the next page,

Table 2-1. Common Models for Simulating Multiphase Flow (Hamill, 1996)

Models	Description	Applicability
Eulerian Multifluid	Treats all phases as interpenetrating continua, with additional momentum and continuity equations needed for each phase. Phases interact via interphase transfer of transported quantities such as momentum (i.e., drag), heat, and mass	Can handle any number of separate phases: liquids, solids, gases, or chemical species, and thus can be used to model flows in which several types (or sizes) of particles or bubbles may be present. In addition, each phase may consist of distinct components, e.g., water vapor in air, or tracer dye in water
Eulerian Homogeneous	Like the Eulerian multi-fluid model, except that the different phases share the same solution field for one or more variables (e.g., momentum, temperature) while having distinct volume fraction fields	Simulates mixtures where phase properties equilibrate over distances smaller than the mesh resolution (e.g., because of high drag on small particles). Also used for free surface flows (e.g., sloshing tanks, filling processes) where the model is equivalent to the volume-of-fluid (VOF) algorithm. Some codes include surface-tension forces for free-surface flows, which may be important at small length scales
Lagrangian Particle Tracking	Tracks representative particles through the solution domain. The model can take account of momentum, heat and mass transfer between particles and the continuous phase. Stochastic models can include turbulent particle-dispersion effects	Dispersed flow, where interest is focused on the particle or droplet histories. Some CFD codes offer specific models for spray dryers and oil droplet and coal particle combustion, including devolatilization, char oxidation, and coupling to gas-phase reactions

which are commonly used to carry out an analysis of a chemical reactor using CFD. The author illustrates the procedures by application to a particular reactor. The steps are:

- Formulating the relevant transport equations
- Establishing the necessary constitutive and closure equations (the former relate fluid stresses with velocity gradients; the latter relate unknown Navier-Stokes equation correlations with known quantities)
- Formulating appropriate boundary conditions
- Selecting the most suitable numerical techniques to solve the equations

- Choosing – or developing – a suitable computer program (also referred to as a code) to implement the numerical techniques
- Validating these techniques and programs
- Developing effective flow simulation strategies for the equipment

Complex attributes of rigorous, high-temperature reactions are examined by Chen (1996). Kinetic models are commonly complex by nature and in first-level models, the chemical reactions are usually reduced to a single overall stoichiometry with similar simplifications made to the rate equations. Rigorous kinetic modeling, on the other hand, attempts to take into account all elementary mechanistic reaction steps, including free radical formation. Use of empiricism in kinetic modeling is elaborated on as well. One three-parameter expression widely used is the Arrhenius equation shown below.

$$k = A \exp\left(-\frac{E_a}{RT}\right) \quad (2-1)$$

In the expression, k stands for concentration, A for frequency factor, E_a for activation energy, R for the universal gas constant, and T for absolute temperature. Calculation of the unknown Arrhenius parameters is not an easy process and usually requires the use of thermochemical kinetic methods to estimate these values. Representative values for the Arrhenius parameters, along with example reaction mechanisms, are displayed in Table 2-2. Applications of the principles discussed are exhibited by the author in the modeling of a steam cracker and a thermal DeNO_x process.

Table 2-2. Typical Ranges of Arrhenius Parameters (Chen, 1996)

Reaction	E, kJ/mol	A, 1/s or m ³ /mol-s
<i>Initiation</i>		
Unimolecular	280–450	10 ^{16±1}
$C_2H_6 \rightarrow CH_3\cdot + CH_3\cdot$	372	9.7 × 10 ¹⁶
Bimolecular	80–280	10 ^{8±1}
$C_2H_4 + C_3H_8 \rightarrow C_2H_5\cdot + C_3H_7\cdot$	209	10 ⁷
<i>Propagation</i>		
Unimolecular		
Decomposition	100–250	10 ^{13±1}
$C_2H_5\cdot \rightarrow C_2H_4 + H\cdot$	172	9.7 × 10 ¹³
Isomerization	45–110	10 ^{9±1}
1-hexyl → 2-hexyl	11	3 × 10 ¹⁰
Bimolecular		
Hydrogen abstraction	0–130	10 ^{6±1}
$C_2H_6 + H\cdot \rightarrow C_2H_5\cdot + H_2$	38	1.1 × 10 ⁷
Radical addition	0–84	10 ^{6±1}
$CH_3\cdot + C_2H_4 \rightarrow C_3H_7$	32	3.5 × 10 ⁵
<i>Termination</i>		
Recombination	0	10 ^{6±1}
$CH_3 + CH_3 \rightarrow C_2H_6$	0	2.2 × 10 ⁷

Giridharan et al. (1995) present a method for coupling a gray radiation model with a commercial CFD code. The model was coupled to a general purpose CFD code, CFD-ACE, through radiation source terms in the energy equation. This work alludes to the difficulties encountered with the application of radiation models in heat and flow analysis. They validate their model by applying it to a number of known simple cases by another author. Application is then extended to models for a rectangular reactor for silicon deposition, a 3-D Jipelec CVD reactor, and a 3-D bell jar CVD reactor.

Harris et al. (1996) survey future trends and current and potential problems with CFD. Current problems are visualized by the use of case studies involving a stirred tank reactor and a commercial scale extruder. In relation to the stirred tank reactor, the flow

domain was the primary consideration since its shape changes with time. They also emphasize the lack of satisfactory simulation prediction for mean velocities and turbulence quantities. Turning attention to the extruder, viscosity complications of a polymer intertwined with a complex geometry representation are investigated. The authors stress that limits of computing power can be easily exceeded with complex models such as these. They further explain that when simplified models can be applied, experimental validation of these processes are frequently difficult to execute. The authors also consider turbulence and chemistry interactions in a gas phase system. In closing, the work contemplates the future trends of CFD for chemical reactor applications.

Fotiadis et al. (1990a) assess the effects of various operating conditions, reactor geometry, and heat transfer on the operation of vertical axisymmetric reactors for metal organic vapor phase epitaxy (MOVPE). This method belongs to the same family of processes as MOCVD discussed in the second section. It was previously determined that the transport processes were considerably affected by the buoyancy driven flows due to the presence of a temperature gradient. Traditional analyses related to the mentioned phenomena fail to accurately predict the induced behaviors. The authors found another effective evaluation tool to optimize the overall process, the CFD model. Models were created incorporating conduction, convection, radiation, and mass transfer. A finite element method was also utilized based on the Galerkin method. Instead of using general rectangular techniques for mesh generation, a different approach was used to accommodate arbitrarily shaped walls. A non-axisymmetric model was also examined and compared to the axisymmetric model where significant differences in the flow

patterns were discovered. In addition to the effects on a CVD reactor discussed previously, Fotiadis et al. (1990b) also consider susceptor tilt angle and reactor orientation relative to the direction of gravity. The geometries mentioned appear to be separate from the first work discussed.

Other authors have analyzed CVD process related models using commonly used commercial codes, such as FLUENT and FIDAP. In Collins et al. (1994), a CVD process for the deposition of silicon nitride is considered using FLUENT. Methodology used to develop the model is presented in a logical fashion. This work also emphasizes the empirical nature of these models and showcases the simplification of the reaction mechanism for computational purposes. Satisfactory agreement was found between the computational model and the experimental model. Other CVD works related to CFD include the epitaxial growth of silicon by Angermeier et al. (1997) and silicon dioxide deposition by Gobbert et al. (1997).

In the work by Wilck and Stratmann (1997), a multicomponent model for particle composition evaluation is developed for 2-D and 3-D applications. The developed Fortran program is named MADMAcS 1 (Multicomponent Aerosol Dynamics Modeling – Modal Approach System) and is used in conjunction with a 2-D solver for numerical flow and heat transfer. It is applied to a laminar flow aerosol reactor which has been extensively examined experimentally. Additional models found in the literature have also been compared to the developed model and the experimental data.

Kruis and Falk (1996) investigated the simulation of chemical reactions in the turbulent regime for industrial applications by the prescribed probability density function (PDF) concept. Their work weighs topics on computational time coupled with reactor

inhomogeneity and selectivity between fast reactions. It is noted that the objective of their work was not to fit the experimental results of a currently operating system, but to create a model without “reactor-dependent parameters.” These developments could then be used for design and evaluation of new reactors. The commercial CFD package PHOENICS was applied to solve the turbulent flow field using the standard k- ϵ model. Results were validated by the comparison to experimental data and adequate agreement was found.

2.5 Heat and Mass Transfer

The Eagle-Picher reactor operates at high temperatures under laminar flow (or low Reynolds number) conditions. In flow with these described characteristics, mixed convection (along with radiative heat transfer) frequently becomes a concern. Mixed convection is described as a combination of forced and free convection. Forced convection is usually flow induced by mechanical means while free convection encompasses phenomena such as buoyancy effects due to temperature gradients. This section of the literature review is provided as an overview to some of the heat and mass transfer characteristics encountered in the current research. The focus of discussion is primarily oriented towards mixed convection since there is an abundant supply of available literature on the topic and it appears to require considerable analysis in related literature concerning CVD processes.

Fotiadis et al. (1990a) describe how their CFD model of a CVD reactor adequately reproduced complex flow structures brought on by mixed convective effects,

including “recirculation cells.” Transverse temperature gradients were noted to produce the three-dimensional rolling flows. They also infer the rolling flow behavior could have been avoided if the side walls of their experimental setup had been insulated. This would have effectively decreased the temperature gradient and, in turn, would have suppressed development of the rolling flows. They further discuss how buoyancy effects in systems of higher pressure are decreased as the system pressure is decreased. Additional observations and discussions of rolling behavior encountered in CVD and MOVPE processes have also been included in works by Angermeier et al. (1997) and Fotiadis et al. (1990b).

Searches were executed to find sources directly related to materials of interest to no avail. However, the search uncovered many sources pertaining to the flow of water and air. In fact, the majority of the sources found used water as the working fluid. Mention was made by some of the authors toward the applicability of their results to similar systems such as those utilizing air. Behaviors encountered in studies of these common fluids can be compared to those of the current research. A few of these resources are discussed below to emphasize the similarities.

Of particular interest to the present research is the behavior of the flowing streams as they come together in the reaction area and travel down the reaction tube. Abou-Elail and Morcos (1983) numerically investigated the effects of buoyancy on the entrance region of horizontal rectangular channels with water as the flowing fluid. They considered aspect ratios of one and four on flows with fully developed velocity and temperature profiles with constant heat flux boundary conditions for a variety of Prandtl numbers. They contemplate how the buoyancy effects are negligible within certain axial

distances from the entrance depending on the magnitude of the Rayleigh number. Secondary flow motions usually developed due to the buoyancy effects encountered. In addition, it was presented that by increasing the Rayleigh number, the Nusselt number was also increased. The authors further present a comparison of secondary flow behavior at a particular location and aspect ratio within the entrance region. Since these characteristics are more than likely encountered in the Eagle-Picher reactor and contribute to the complexity of the analysis, a graphical representation of the physical phenomena provided by the authors is shown below in Figure 2-5.

Convection instabilities are generally described as “convective rolls” by Narusawa (1995). He numerically examines the development of these convective rolls

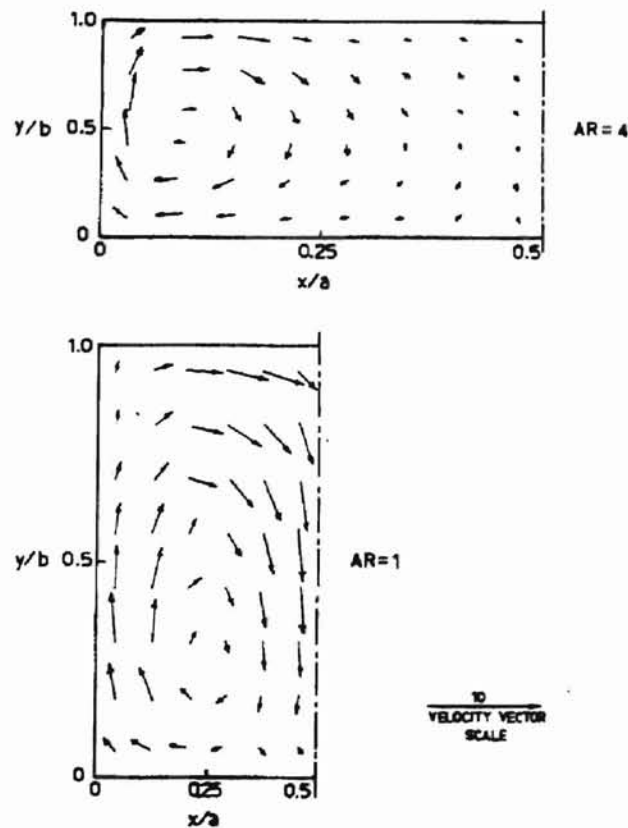


Figure 2-5. Secondary Flow Vector Plot (Abou-Ellail and Morcos, 1983)

under supercritical conditions using a finite amplitude analysis. Geometry aspect ratios were varied and free and fixed boundary conditions were applied on all four walls. The author concedes that laboratory processes involving free boundary conditions may not be readily realized, but they do however provide insight into interesting behaviors. The results are presented associating the number of convective rolls developed to the aspect ratio of the duct and natural or mixed convective conditions. In comparing the cases of free and fixed boundary conditions, it was discovered odd numbers of convective cells will not form in mixed convection due to the nonslip condition at the walls. The author further elaborates on the flowfield dependence on the aspect ratio.

In the future, possible vertical configurations may be considered for the chemical reactor described in this thesis. Related analyses of vertical pipe orientations are readily found in the literature. For example, Scheele and Hanratty (1963) consider the heat transfer characteristics for water in a vertical pipe. Their analyses focused on constant heat flux boundary conditions and constant temperature boundary conditions. Of major concern in the study was the direction of flow within the tube, upward or downward. Findings revealed, under similar circumstances, noticeable differences occur in the flowfields depending on direction of the flow. For the downward laminar flows, the transition to disturbed flow had a greater impact on the heat transfer coefficient than that for the upward flow. This conclusion appears to be readily achieved considering that the downflow laminar heat transfer coefficients tend to be smaller than their upflow counterparts under similar conditions.

As stated earlier, there is a great supply of information related to free and forced convective flows. The information utilized from these sources has been used to gain

understanding and characterize behaviors considered in the present research. Additional information can be obtained from authors such as Kyomen et al. (1996), Abid and Papini (1997), and Ishigaki (1997).

Other heat and mass transfer considerations are in need of better resolution to assess their impact on process operations. Analysis of these processes within this thesis, including mass flow, relies strongly on basic engineering mechanics and will therefore be considered within the main body of the thesis. Due to the inherent complexity of the calculations and the difficulty of locating information related to the radiative heat transfer characteristics of the current process, radiative heat transfer research is deferred to suggested advanced investigative efforts.

1/21/2013
with a great

need to determine the CFD model to be discussed later
and that is provided in Appendix A

CHAPTER III

DESCRIPTION OF CURRENT II-VI SYNTHESIS PROCESS

3.1 Introduction

As previously mentioned, Eagle-Picher has been using the current synthesis process for approximately the last fifty years to manufacture research quantities of the high purity compounds. Some of the difficulties encountered with the operation of the process have also been briefly discussed, however, before the detailed development of the CFD model can be presented and adequately understood, information regarding the physical attributes of the system must be provided. This chapter presents a discussion of the reactor system currently in use along with some possible insight as to why certain characteristics were chosen and implemented. An overview of the process operation and an initial process assessment have also been provided.

3.2 Physical Description of Reactor Components

The reactor configuration is typically composed of the reactor tube, zinc and selenium boilers, and the condenser system. A simplified depiction is presented in Figure

3-1. Drawings of the system used to construct the CFD model to be discussed later provide a greater amount of detail and can be found in Appendix A.

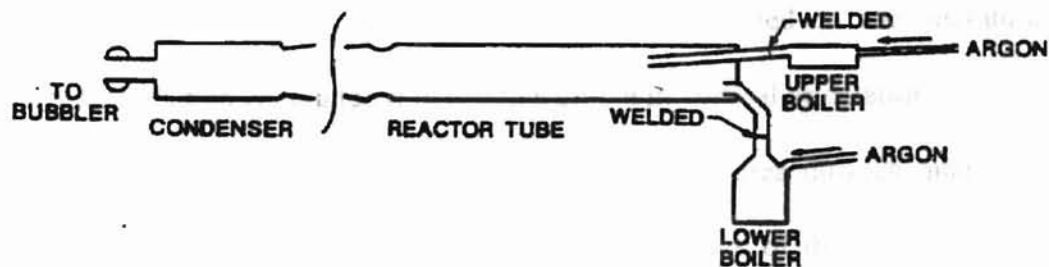


Figure 3-1. Current Eagle Picher Reactor (Ghajar et al., 1996)

All parts of the reactor configuration have been manufactured in house by Eagle-Picher personnel and are made from high quality commercial quartz glass obtained from Heraeus Amersil (1986). The choice of quartz for these types of processes is by no means a surprise. In fact, as discussed in the literature review, quartz is a material often used because of its stability at high temperatures and nonreactive nature with the source materials typically used in these processes. Other favorable characteristics of the quartz material include low thermal expansion, ease of construction when compared with other possible reactor materials, availability, and a transparent nature allowing visual inspection of certain process occurrences.

The reactor tube is 90 mm in diameter and approximately 1100 mm in length. The tube is also utilized in a horizontal configuration. It is not known with certainty why the horizontal setup was chosen, however, engineering insight and related information from the literature provide some possible explanation. It becomes immediately apparent

a vertical configuration may present difficulties involving lingering vapor species and inlet blockage. If the buoyant vapor species were maintained in close proximity to the inlets, they could react and nucleate on the inlets eventually causing an obstructed condition. The current design could have been created based on analogy with related crystal growth processes. It has been frequently presented in the literature that imperfections are often encountered in crystals grown in vertical orientations.

The vapor species are introduced into the reaction area through quartz transfer arms after they are vaporized in the boilers. By evaluation of the boiler structures, it becomes immediately apparent the process is carried out in batch form. Desired quantities of reactants have to be measured and loaded into each of the boilers. The boilers are then attached to the rest of the reactor configuration. There are no additional methods for adding reactants once the boilers have been attached and the process initiated. As can be seen in Figure 3-1, the usual orientation of the zinc (upper) boiler has been horizontal while that of the selenium (lower) boiler has been vertical. The possible reasons for the boiler orientations may be explained by considering characteristics of the quartz material and a comparison of the vapor pressures. The quartz utilized by Eagle-Picher has a maximum suggested working temperature between 950-1000 °C (1223.15-1273.15 K) for continuous use (Heraeus Amersil, 1986). Higher temperatures can be achieved with the material, however, this leads to a limited life especially when operated at temperatures above 1200 °C (1473.15 K) (Heraeus Amersil, 1986). The economic benefits for the repeated use of these chemical reactors are quite evident, though competing process considerations must also be evaluated. For effective mass transfer, the zinc reactant must be boiled to the highest temperature tolerated by the quartz material.

The temperature of the zinc boiler must be set to achieve maximum throughput of reactant with the selenium temperature set at a lower value to achieve the desired stoichiometric flow. These elements combine in a one-to-one stoichiometry to form the product powders, therefore careful attention must be paid to the specific boiling attributes of the reactants as well. Mass flow can be correlated to the vapor pressures of the constituent elements. To aid in process evaluation, tables of vapor pressures have been provided in Appendix B for comparison. Further analysis based on the vapor pressures is discussed in chapter VI.

Attached to the end of the chemical reactor by a slip joint connection is the condenser system. Liquid coolant circulates through the condenser at a much cooler temperature than that of the reactor to condense waste product or unreacted material. The outlet of the condenser is connected to a bubbler by latex tubing where remaining effluent is filtered out. The residual airborne particles then flow to a scrubber for further waste collection and processing.

The furnace and boiler heater system in use has also been specifically designed and built for use only for the production of II-VI compound powders. A good description of the physical makeup of the heating system can be found in the paper by Ghajar et al. (1996). The furnace is a three zone tube furnace approximately six inches in diameter. It has a center zone length of approximately twenty-four inches and front and rear zone lengths of approximately six inches. Each zone consists of a separate system of wire-wrapped tubular heating elements. The elements are packed in place within sculpted firebrick while the entire assembly is enclosed within a steel shell. Thermocouple wells are located in the center of each zone and are in contact with an interior mullite liner with

an approximate thickness of three-sixteenths of an inch. Located at the boiler end of the reactor are two boiler heaters. These heaters are easily moved and maneuvered into place around each respective boiler.

Temperature monitoring and control are possible due to a thermocouple system. Thermocouples located inside the wells on the furnace run to digital readouts and digital controllers. In turn, the controllers connect to a set of 240 volt, three phase, silicon controlled rectifiers. The boiler heaters also have thermocouples attached to them running to a digital thermometer. Boiler heater temperature control is usually achieved by operation of a ten-turn potentiometer connected to a 240 volt, three phase silicon controlled rectifier. Analog watt meters located on the furnace system provide an additional means of temperature control evaluation.

3.3 Reactor Operation Procedures

The entire II-VI synthesis process is tedious and time-consuming and only a modest amount of product is obtained in relation to the amount of resources utilized. Batch process execution usually requires a time period of three days. During any particular week, if an operator can overlap the end of one run with the beginning of another, it is possible to complete two production runs. Ghajar et al. (1996) have supplied a reasonable overview of the process steps and it will be presented here with added knowledge and insight from the author of the present work.

On day one, a clean quartz reactor tube is placed inside the furnace with the face of the boiler end of the reactor positioned flush with the front of the furnace. Using

quartz shims (cut pieces of quartz tubing), the reactor is carefully centered within the furnace. Stopcock grease is then applied to the male fitting on the end of the reactor tube. Next, the lower quartz boiler is loaded with a measured charge of selenium and is seated inside the tubular heater resting on a Lab-Jack lowering and raising mechanism. Adjustments are made until the outlet of the boiler is in alignment with the lower inlet of the reactor tube. A nylon supply tube is connected snugly to the back quartz extension tube and a slight flow of argon gas is initiated. A skilled operator then uses a hydrogen/oxygen welding torch to weld the lower boiler to the reactor tube. After an airtight connection has been made, the heater is adjusted so that it no longer supports the weight of the boiler. A single thermocouple is inserted through a side hole in the middle of the heater until contact is made with the side of the boiler. Attention is then turned towards the zinc boiler. A measured charge of zinc is placed within the boiler which is situated within a tubular heater resting on an adjustable rack. This rack is positioned until the outlet of the boiler is in alignment with the upper transfer arm located on the reactor. Next, a nylon supply tube is connected snugly to the back quartz extension tube and a flow of argon is established. Skilled personnel again use the hydrogen/oxygen welding torch to weld the boiler to the reactor tube. Following the welding procedure, the heater is adjusted until it no longer supports the weight of the boiler and a thermocouple is inserted through a side hole in the middle of the heater until contact is made with the boiler. At the exit of the condenser, a water bubbler is attached with latex tubing. A thorough check for leaks is then performed on the entire system. Afterwards, parts of the system are insulated with Fiberfrax and a blanket of the material is applied to the reactor tube exit where it connects with the condenser. Another piece of the blanket containing

cut slots is placed on the front of the reactor, with the slots necessary for positioning around the reactor transfer arms. Smaller pieces of the insulation are also packed around the lower boiler and transfer arm. The same process is then carried out for the upper boiler and transfer arm. The setup is finally left overnight with the argon flowing to purge the system of oxygen and contaminants detrimental to the process.

Beginning the second day, circulation of cooling fluid through the condenser is initiated. Power is also turned on to the three zone heaters of the furnace. The system is allowed to equilibrate for approximately two hours before the boiler heaters are activated by the adjustment of the ten-turn pots to achieve a predetermined heating rate. The boilers are separately brought to predetermined temperatures above the normal boiling points of 907 °C (1180 K) (Mathewson, 1959) and 685 °C (958 K) (Bailer et al., 1973) for zinc and selenium, respectively. Within the process, the vapor phase species are carried inside the reaction area with the aid of the argon carrier gas where they interact exothermically forming the product powder. The powder deposits primarily on the bottom of the reactor with smaller amounts coating other areas. The run is considered complete when a boiler is uncovered slightly and discovered to be empty. At the end of the process, the setup is allowed to cool the remainder of the day and evening to reach tolerable handling temperatures.

Day three begins with turning off the argon flow and removing the condenser. Any deposited material in the condenser is scraped out and collected as hazardous waste. The argon lines to the boilers are disconnected and the boiler heaters are carefully removed. The remaining reactor assembly, with boilers still attached, is removed from the furnace and placed in a specially manufactured rack. The operator then performs the

tedious task of scraping the product out from inside the reactor and placing it into containers. The collected product is weighed, catalogued, and stored. After the collection process is finished, the reactor assembly is taken to another part of the building where a water-cooled abrasive saw is used to remove the reactant boilers. Finally, extensive cleaning procedures involving the use of acids are carried out to prepare the components for the next process setup.

3.4 Initial Assessment of Process Operation

The inherent complexity of the process is quite evident. Adding to the complex nature of the reactor operation is the fact that the operators have each developed their own unique approach to the different synthesis processes. In the past, no two operators have executed the processes in exactly the same manner. Usually, 600 to 1200 grams of product were collected in a successful run, corresponding to theoretical yields of about 35-65% (on a zinc basis). However, these results were only reached when a successful run was completed and this varied between 30-80% of the time during the past, depending on the operator. The remaining waste materials have typically been collected, stored, and disposed of as hazardous waste. Premium prices have usually been paid by a measure of weight for disposal of the waste products. During operation, it has also been noted the reaction and mass transfer processes are extremely sensitive to changes. Therefore, this has caused the requirement for (or at least the attempt for) careful maintenance of process parameters once they have been attained. In addition, complex structures known as "wormholes" have been noted to form out of the product powder.

These were usually formed around the exit of the zinc (upper) inlet and ran a significant length of the reactor tube. These appeared to effectively reduce the residence time of the reactants and severely limit the amount of reactant interaction. Also, in the past, process completion had been routinely checked by physically removing insulation from around the reactant boilers and visually checking for any remaining material. If the process had not yet reached completion, this effectively altered the heat and mass transfer mechanisms for a period of time.

The described occurrences and characteristics have plagued reactor operations for many years. The processes have also seen many changes take place to the reactor and process operation protocol. With limited documentation available, it has been extremely difficult to assess the process characteristics. Indicated previously, the intent of this thesis, in collaboration with works from other researchers, is to aid in the understanding of the thermal and chemical processes while also providing suggestions and designs for more efficient operation. These actions should aid in the reduction of waste materials and thereby provide a higher profit margin for the desired products.

CHAPTER IV

FLUENT CFD SUITE

4.1 Background

Commercial CFD packages have evolved dramatically since their inception approximately twenty years ago. They began as tools of limited applicability and were often only utilized by professionals with specific skills related to numerical and computational techniques. Due to computing advances and the flexibility of the current CFD programs, they are commonly being used worldwide by many different industries for a wide array of problems.

In efforts to further CFD research and introduce future users to their line of products, companies have made it easier for some academic institutions to obtain these high technology tools. For instance, Fluent Inc. has provided their full working suite of software to Oklahoma State University with the benefit of a price discount. With the use of these programs in an academic environment, students have been able to acquire valuable experience with their fundamental operation and some have become quite skilled in their advanced operation and capabilities. Many employers, especially those heavily utilizing CFD, are often attracted to prospective employees even when they have only basic knowledge of these computational tools.

The objective of this chapter is to introduce the Fluent Suite of software programs to potential users and briefly summarize how they interact. It is also the intention to present some concerns, adopted from the Fluent literature, which generally must be addressed when developing a CFD model. In section two, a basic description of the entire Fluent Suite is presented. In the remaining sections, the specific components utilized for the current research are addressed in greater detail.

4.2 Suite Overview

This section presents the general components of the Fluent Suite and some of their interactions. Only brief mention is made of each of the components and their capabilities to provide exposure to the many different options available within the suite. It is emphasized, chiefly for the benefit of new users, other commercial CFD packages in current use also have similar options and computational characteristics. For further reading on the components discussed, manuals covering the individual programs should be referred to in the Fluent literature.

The entire Fluent Suite of programs contains the following components (Fluent Inc., 1996a):

- RAMPANT, FLUENT/UNS, FLUENT, and NEKTON, the solvers.
- PrePDF, the preprocessor for modeling PDF combustion in FLUENT/UNS.
- GeoMesh and preBFC, the preprocessors for geometry modeling, block-structured mesh generation, unstructured triangular-surface mesh generation, and 2-D unstructured mesh generation.

- Tgrid, the 2-D triangular and 3-D tetrahedral mesh generator.
- Grid filters for CAD/CAE packages such as I-DEAS surface and volume grid generators.

These individual components are often grouped together as packages based on their modeling capabilities (Fluent Inc., 1996a). The FLUENT package consists of two parts, the preprocessor GeoMesh and the main module FLUENT. GeoMesh is used to create the geometry and a structured quadrilateral/hexahedral grid. FLUENT is the general purpose finite volume program which then utilizes the structured grid to arrive at a computational solution. FLUENT is typically the desired program to employ when the geometries to be created are relatively simple. Potential interactions between FLUENT and other programs are shown in Figure 4-1. Further explanation of grid choices, particularly structured and unstructured, is considered in section 4.3.2.

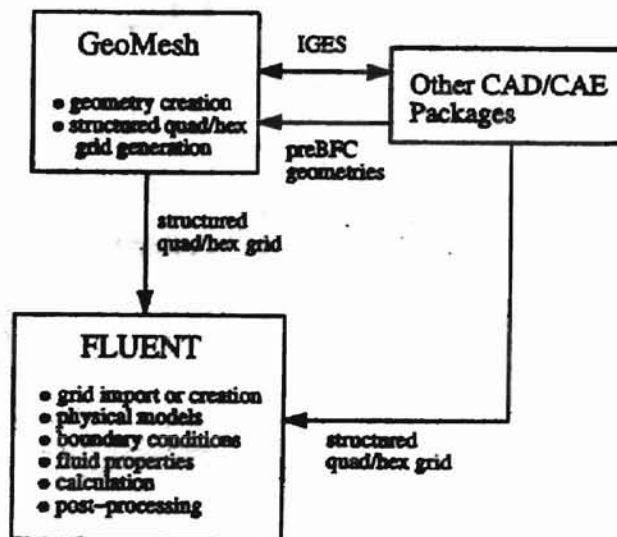


Figure 4-1. Program Interactions for FLUENT Software Package (Fluent Inc., 1996a)

Oklahoma State Univ. Library

The FLUENT/UNS and RAMPANT packages are comprised of three components. They each contain two preprocessors, GeoMesh and Tgrid, and the main module, FLUENT/UNS or RAMPANT. GeoMesh is again used to create the geometries and to generate grids. Within this package, structured or unstructured quadrilateral/hexahedral grids, 2-D triangular grids, or 3-D triangular surface grids can be utilized. Tgrid is accessed only when one wishes to generate 3-D tetrahedral grids. FLUENT/UNS is well suited for modeling incompressible/mildly compressible flows while RAMPANT is preferred for compressible/transonic/supersonic flows. Program interactions for these packages of programs are shown in Figure 4-2.

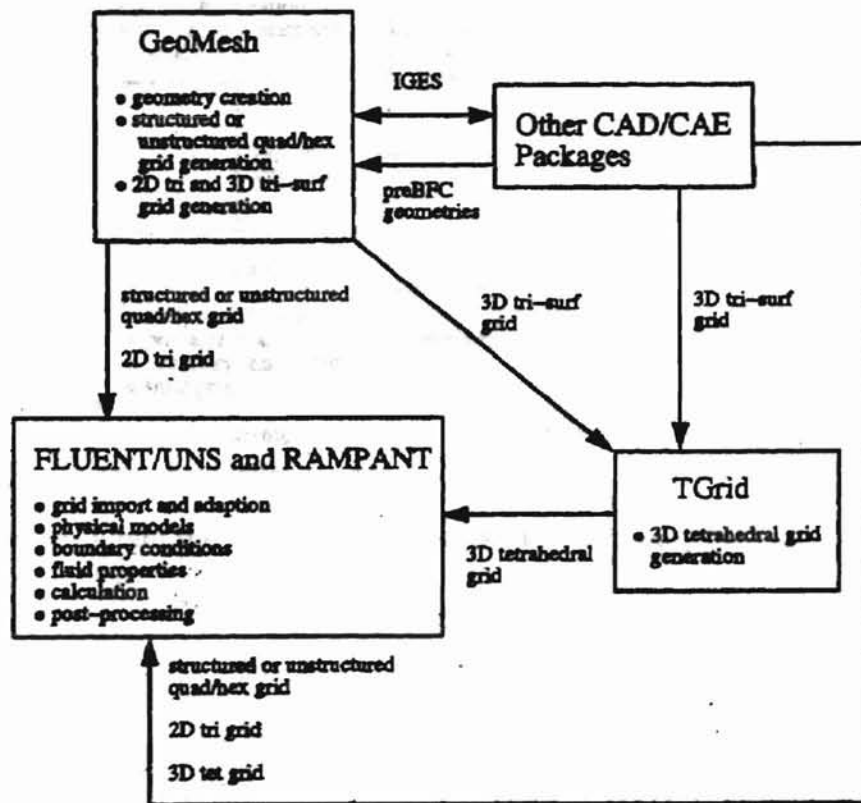


Figure 4-2. Program Interactions for FLUENT/UNS and RAMPANT Software Packages (Fluent Inc., 1996a)

Alabama State Univ. Library

NEKTON is a two piece package consisting of the preprocessor GeoMesh and the main module NEKTON. For this group of programs, GeoMesh is once again used to create the geometry. NEKTON limits the grids utilized to structured or unstructured quadrilateral/hexahedral grids and is the preferred program to use when modeling laminar flow and heat transfer in complex and/or deforming geometries. The related program interactions are shown in Figure 4-3. As indicated by all of the interaction diagrams, geometries can be created and imported from programs outside of the Fluent Suite as well.

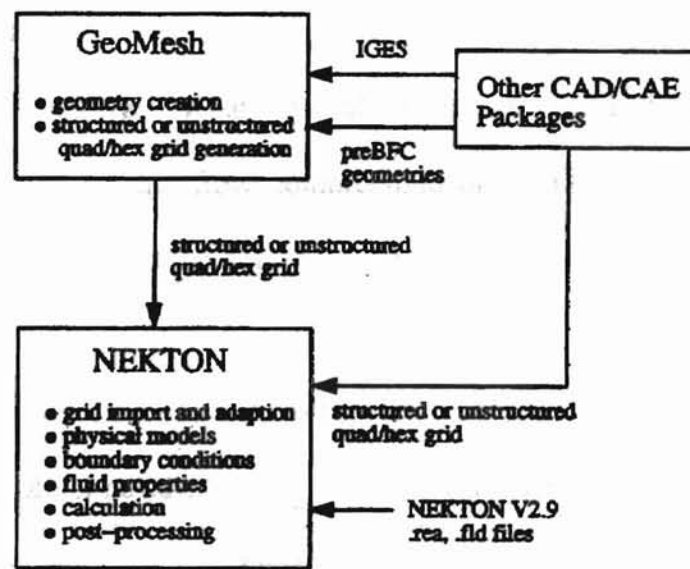


Figure 4-3. Program Interactions for the NEKTON Software Package (Fluent Inc., 1996a)

In addition to the software package descriptions, the Fluent Inc. (1996a) literature provides some important points to ponder before undertaking a CFD analysis, especially for the very first time. The points to consider are as follows:

Oklahoma State Univ. Library

- *Definition of the Modeling Goals:* What specific results are required from the CFD model, and how will they be used? What degree of accuracy is required from the model?
- *Choice of the Computational Model:* How will you isolate the area of interest from the complete physical system to be modeled? Where will the computational domain begin and end? What boundary conditions will be used at the boundaries of the model? Can the problem be modeled in two dimensions, or is a three-dimensional model required? Can one take advantage of symmetry or periodic boundaries to reduce the computational domain?
- *Choice of Solver:* What physical models are required? Is the flow laminar or turbulent? Is the flow compressible or incompressible? Is heat transfer important? Does the solver you choose have the necessary models for your problem?
- *Choice of Grid Type:* What type of grid (structured or unstructured, quadrilateral/hexahedral, or triangular/tetrahedral) is best suited for this problem? Is the geometry very complicated? Do large geometric scale discrepancies exist in the model? Does the solver chosen support the selected grid type?
- *Design Your Grid:* What degree of accuracy does one need in each region of the domain? Will the grid have to be adapted later? How many cells will be needed? Is there sufficient computer memory?

The majority of these issues should be evaluated in ample detail before considerable resources are committed to the actual CFD model creation.

4.3 GeoMesh

GeoMesh has already been presented as the program encompassing the geometry and grid creation tools for all of the Fluent Suite solvers. It is much more complex than has been indicated thus far. In fact, the program can be considered the central working area for CFD modeling within the Fluent Suite. Using the Session Manager of GeoMesh, shown in Figure 4-4, a wide array of choices are available. A user can select many

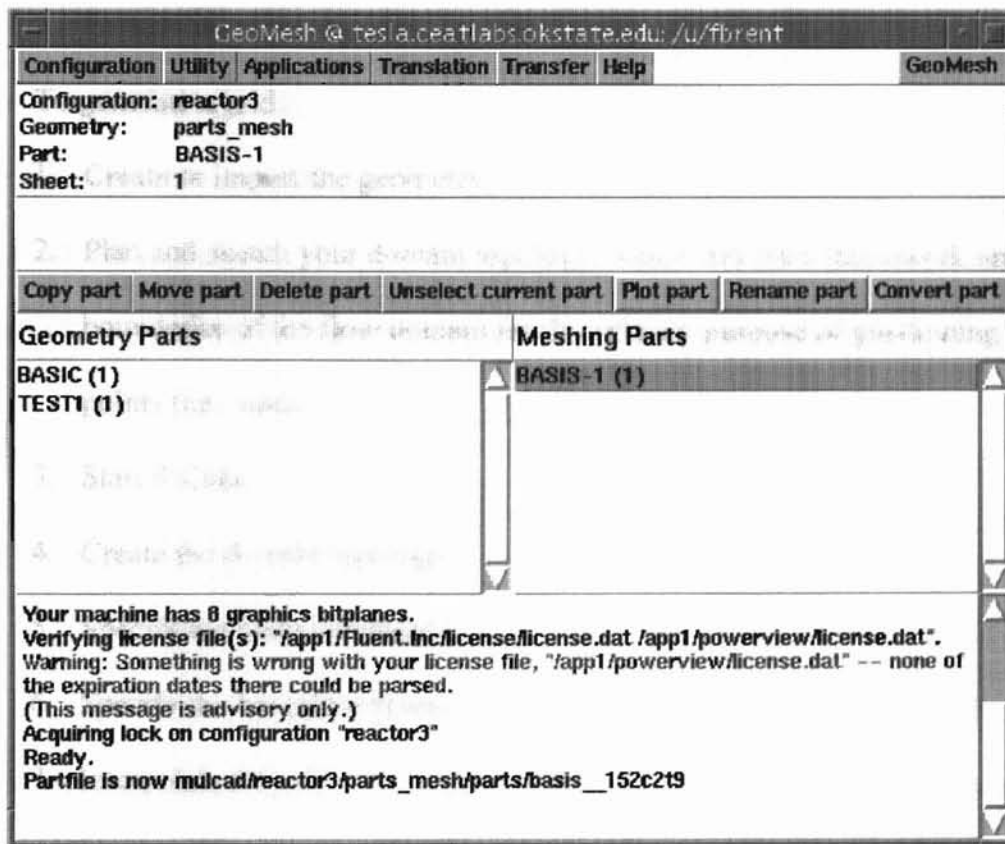


Figure 4-4. GeoMesh Session Manager Window

different menu options related to organizing files, importing and exporting files, and starting other subprograms to be discussed further, such as DDN, P-Cube, and Leo. The solver programs can also be initiated from within GeoMesh, but it is not necessary.

After the salient features of the model have been determined and a sound understanding of the Fluent Suite has been obtained, Fluent Inc. (1996a) recommends beginning with the following basic procedural steps for geometry and grid creation:

1. Start DDN.
2. Create points.
3. Create curves from the points.
4. Create surfaces from the curves, if needed.
5. Save the geometry file.
6. Exit DDN.

To generate a grid:

1. Create or import the geometry.
2. Plan and sketch your domain topology, which defines a framework on the boundaries of the flow domain for the primary purpose of positioning the grid points (i.e., nodes).
3. Start P-Cube.
4. Create the domain topology.
5. Specify the node distribution.
6. Specify the boundary types.
7. Interpolate the grid.

8. Exit P-Cube.

9. Export the grid file for the solver.

Often the creation and analysis can become quite complex and further modifications to the preprocessing steps mentioned above must be considered.

4.3.1 DDN

DDN is the geometry generation tool within GeoMesh. Geometries can be created and modified within DDN, or they may be imported from other compatible programs and then manipulated and modified. DDN is considered a surface modeler (as opposed to solids modeler), meaning the geometry is represented as a surface on a boundary (Fluent Inc., 1996a). Solid modelers usually represent geometries with interior spaces in addition to the surfaces. The typical strategy for geometry creation within DDN involves the creation of points, lines and curves from the points, and then surfaces from the lines and curves. Greater explanation of the commands and options available within DDN, as well as the other subprograms, can be found in Fluent's GeoMesh User's Guide (1996a).

4.3.2 P-Cube

P-Cube is known as the grid generation subprogram of GeoMesh. It uses the geometry created in DDN to form body-fitted grids. This is carried out by the user with a combination of the DDN geometry and the use of tracking tools which constrain the

placement of the topology, or the basic grid framework. Based on the topology, interconnected mesh areas can then be created. Within a 2-D geometry, "faces" are generally formed for the creation of quadrilateral or triangular grids. For hexahedral grids in 3-D, "blocks" are formed as precursors. In addition to the topology creation, P-Cube is the tool used for specifying node distributions, setting the boundary types, and interpolating the grids. Again, referring to the Fluent literature, a user can locate some specific strategies and become aware of possible problem areas.

Since this section covers the grid generation subprogram, it seems appropriate to consider a short explanation on the grid elements. While structured or unstructured grids are dictated ultimately by how domains are connected together, certain grid elements can usually be associated as structured or unstructured. Quadrilateral and hexahedral grids are often classified as structured while triangular and tetrahedral are considered unstructured. Structured grids are often applied to simple geometries containing as few curves and angles as possible. Unstructured grids experience their greatest applications within complicated geometries possibly containing many curves and angles. Additional grid morphologies can be created by the combination of the different grid elements and are called "hybrid" meshes.

4.3.3 Leo

Leo is a valuable diagnostic tool included with the Fluent Suite. Within this program, the grid can be viewed, grid quality information obtained, and the grid modified to improve the quality. Leo can also report skewness of grid elements, indicating

potential problem areas for the computational solution. As a general example for quadrilateral and hexahedral grids, Fluent indicates the skewness of elements should be less than 0.95 to obtain a reasonable solution. Other methods may be used to evaluate the grid quality within Leo and it can employ smoothing methods and node movement capabilities to improve the quality.

4.4 FLUENT/UNS

FLUENT/UNS is one of the Fluent Suite computational solvers. Its ability to handle fluid flow and heat transfer in complicated geometries has often made it the solver of choice. It is able to do this by allowing the user to choose between a structured or unstructured mesh comprised of the elements (triangular, tetrahedral, etc.) discussed previously. FLUENT/UNS has another desirable characteristic that allows solution adaptation from within the solver. This permits efficient use of resources by locally refining or coarsening the computational grid based on a previous execution of the program.

4.4.1 Governing Equations

Volume two of the FLUENT/UNS and RAMPANT User's Guide (Fluent Inc., 1996b) provides extensively detailed explanations of the governing equations. Considering all of the available options within the solver, these equations may take on many different forms. Therefore, in an effort to provide an overview of the material, only

the basic forms of the equations are discussed. It must be noted that axisymmetric forms of some of these equations are available within FLUENT/UNS; however, due to prevailing non-axisymmetric qualities with the model of interest, these equations could not be applied.

Mass Conservation Equation

In laminar flow the equation for conservation of mass (continuity equation) is:

$$\frac{\partial \rho}{\partial t} + \frac{\partial}{\partial x_i} (\rho u_i) = S_m \quad (4-1)$$

where ρ is the density, t is time, x is the spatial coordinate in the direction of indicator i , u is the velocity component in the direction of indicator i , and S_m is a source term. This is the basic form and is applicable to compressible and incompressible flows.

Momentum Conservation Equations

Conservation of momentum in laminar flow is given by:

$$\frac{\partial}{\partial t} (\rho u_i) + \frac{\partial}{\partial x_j} (\rho u_i u_j) = -\frac{\partial p}{\partial x_i} + \frac{\partial \tau_{ij}}{\partial x_j} + \rho g_i + F_i \quad (4-2)$$

where p is the static pressure, τ_{ij} is the stress tensor, ρg_i is the gravitational body force, and F_i contains all external body forces. The stress tensor mentioned above is given by:

$$\tau_{ij} = \left[\mu \left(\frac{\partial u_i}{\partial x_j} + \frac{\partial u_j}{\partial x_i} \right) \right] - \frac{2}{3} \mu \frac{\partial u_i}{\partial x_i} \delta_{ij} \quad (4-3)$$

where μ is the molecular viscosity and δ_{ij} is the Kronecker delta function.

Turbulence Equations

In FLUENT/UNS, turbulence modeling is offered by the use of two-equation turbulence models. The two choices given within FLUENT/UNS are the standard k-ε model and the Renormalization-Group (RNG) based k-ε model. The standard k-ε model has been the most frequently applied model within the past two decades and is considered more universal. This model is commonly employed in high Reynolds number problems. The RNG k-ε model is similar to the standard k-ε model, however, it has additional characteristics that make it quite desirable for certain kinds of flows. The major characteristic of concern related to the current research is its ability to better resolve transitional flow (between laminar and turbulent), when compared to the standard k-ε model. The physical system considered in this thesis appears to possess small turbulent regions within an otherwise laminar flow. Further detailed explanation about turbulence models can be found in the Fluent literature.

When the RNG k-ε model is applied, the momentum equations take the form:

$$\frac{\partial}{\partial t}(\rho u_i) + \frac{\partial}{\partial x_j}(\rho u_i u_j) = \frac{\partial}{\partial x_j} \left[\mu_{\text{eff}} \left(\frac{\partial u_i}{\partial x_j} + \frac{\partial u_j}{\partial x_i} \right) \right] - \frac{\partial p}{\partial x_i} \quad (4-4)$$

and μ_{eff} is defined below as:

$$\mu_{\text{eff}} = \mu_{\text{mol}} \left[1 + \sqrt{\frac{C_\mu}{\mu_{\text{mol}}} \frac{k}{\sqrt{\varepsilon}}} \right]^2 \quad (4-5)$$

where μ_{mol} is the molecular viscosity, C_μ is the statistically determined fixed constant 0.0845, k is the kinetic energy, and ε is the rate of dissipation. The RNG theory also characterizes the transport equations for k and ε as:

$$\frac{\partial}{\partial t}(\rho k) + \frac{\partial}{\partial x_i}(\rho u_i k) = \frac{\partial}{\partial x_i} \left(\alpha_k \mu_{eff} \frac{\partial k}{\partial x_i} \right) + \mu_t S^2 - \rho \varepsilon \quad (4-6)$$

and

$$\frac{\partial}{\partial t}(\rho \varepsilon) + \frac{\partial}{\partial x_i}(\rho u_i \varepsilon) = \frac{\partial}{\partial x_i} \left(\alpha_\varepsilon \mu_{eff} \frac{\partial \varepsilon}{\partial x_i} \right) + C_{1\varepsilon} \frac{\varepsilon}{k} \mu_t S^2 - C_{2\varepsilon} \rho \frac{\varepsilon^2}{k} - R \quad (4-7)$$

where μ_t is the turbulent viscosity and α_k and α_ε are the inverse effective Prandtl numbers for k and ε , respectively. The inverse Prandtl numbers are computed from the RNG analytically derived formula:

$$\left| \frac{\alpha - 1.3929}{\alpha_0 - 1.3929} \right|^{0.6321} \left| \frac{\alpha + 2.3929}{\alpha_0 + 2.3929} \right|^{0.3679} = \frac{\mu_{mol}}{\mu_{eff}} \quad (4-8)$$

where α_0 is equal to 1.0. S , in Equations (4-6) and (4-7), is defined as the modulus of the mean rate-of-strain tensor, S_{ij} , and is given as:

$$S \equiv \sqrt{2S_{ij}S_{ij}} \quad (4-9)$$

R in Equation (4-7) is given by:

$$R = \frac{C_\mu \rho \eta^3 \left(1 - \frac{\eta}{\eta_0} \right)}{1 + \beta \eta^3} \frac{\varepsilon^2}{k} \quad (4-10)$$

where $\eta = Sk/\varepsilon$, η_0 is approximately 4.38, and $\beta = 0.012$. Also, in Equation (4-7), $C_{1\varepsilon} = 1.42$ and $C_{2\varepsilon} = 1.68$ with both of these values analytically derived from RNG theory.

Heat Transfer Equations

The energy equation when defined in terms of sensible enthalpy is given as:

$$\frac{\partial}{\partial t}(\rho h) + \frac{\partial}{\partial x_i}(\rho u_i h) = \frac{\partial}{\partial x_i}(k + k_t) \frac{\partial T}{\partial x_i} - \frac{\partial}{\partial x_i} \sum_{j'} h_{j'} J_{j'} + \frac{Dp}{Dt} + (\tau_{ik})_{eff} \frac{\partial u_i}{\partial x_k} + S_h \quad (4-11)$$

where h is the sensible enthalpy, k is the molecular conductivity, k_t is the conductivity due to turbulent transport ($k_t = \mu_t/Pr_t$), $J_{j'}$ is the diffusion flux of species j' , and S_h is a source term which can include the heat of chemical reactions and other sources of energy. In the summation term above, it is pointed out that the effect of enthalpy transport due to species diffusion is taken into account. In addition, sensible enthalpy is described as:

$$h = \sum_{j'} m_{j'} h_{j'} \quad (4-12)$$

where $m_{j'}$ is the mass fraction of species j' and

$$h_{j'} = \int_{T_{ref}}^T c_{p,j'} dT \quad (4-13)$$

where c_p is the specific heat and T_{ref} is conveniently defined as 298.15 K. Energy sources are taken into account in the S_h term and contributions by chemical reaction are provided in the form:

$$S_{h, reaction} = \sum_{j'} \left[\frac{h_{j'}^0}{M_{j'}} + \int_{T_{ref}}^T c_{p,j'} dT \right] R_{j'} \quad (4-14)$$

where $h_{j'}^0$ is the enthalpy of formation of species j' , $M_{j'}$ is the molecular weight of species j' , and $R_{j'}$ is the volumetric rate of creation of species j' .

Heat transfer due to conduction was considered in the developed CFD model used in this research. The governing conduction equation is:

$$\frac{\partial}{\partial t} \rho h = \frac{\partial}{\partial x_i} \left(k \frac{\partial T}{\partial x_i} \right) + \dot{q}''' \quad (4-15)$$

where \dot{q}''' is defined as the volumetric heat source. Equations (4-11) and (4-15) are solved simultaneously to achieve a coupled heat transfer solution.

Chemical Species Transport and Reaction Equations

Two modeling options are available in FLUENT/UNS for describing chemical reactions, the generalized finite rate formulation and the mixture fraction/PDF formulation. The primary difference between the two is the chemical reactions must be specifically defined by the user in the finite rate form, while in the mixture fraction form reaction mechanisms are not explicitly defined, but are instead based upon chemical equilibrium calculations within the solver. The mixture fraction/PDF approach is chiefly used for combustion calculations and presented significant difficulties when considered for the current research. Therefore, the generalized finite formulation was used by default.

In chemically reacting flows, conservation equations for the reacting species are generally employed. FLUENT/UNS uses a convection-diffusion equation to characterize the processes and is presented in general form as:

$$\frac{\partial}{\partial t}(\rho m_i) + \frac{\partial}{\partial x_i}(\rho u_i m_i) = -\frac{\partial}{\partial x_i} J_{i,i} + R_i + S_i \quad (4-16)$$

where $J_{i,i}$ is the diffusion flux of species i , R_i is the mass rate of creation or depletion by chemical reaction, and S_i is the rate of creation by addition from the dispersed phase and user-defined sources. The dilute approximation is employed in FLUENT/UNS for mass diffusion modeling and for laminar flows, the diffusion flux is presented as:

Oklahoma State Univ. Library
Oklahoma State Univ. Library

$$J_{i,j} = -\rho D_{i,m} \frac{\partial m_{i'}}{\partial x_i} \quad (4-17)$$

where $D_{i,m}$ is considered the diffusion coefficient for species i' in the mixture. The turbulent form is also provided as:

$$J_{i,j} = -\left(\rho D_{i,m} + \frac{\mu_t}{Sc_t}\right) \frac{\partial m_{i'}}{\partial x_i} \quad (4-18)$$

where Sc_t is the turbulent Schmidt number defined as:

$$Sc_t = \frac{\mu_t}{\rho D_t} \quad (4-19)$$

FLUENT/UNS includes the transport of enthalpy in the energy equation due to multicomponent mixing flows by default. It can be represented by:

$$\nabla \cdot \left[\sum_{i'=1}^n (h_{i'}) \bar{J}_{i'} \right]$$

In reaction rate calculations, all chemical contributions to the source term in the energy equation, can be summarized by:

$$R_{i'} = \sum_k R_{i',k} \quad (4-20)$$

where $R_{i',k}$ is the rate of creation/destruction of species i' in reaction k . Additionally, the Arrhenius reaction rate formulation can be computed by:

$$R_{i',k} = \Gamma \left(\nu'_{i',k} M_{i'} T^{\beta_k} A_k \prod_{j' \text{ reactants+products}} C_{j'}^{\nu_{j',k}} \exp\left(-\frac{E_k}{RT}\right) \right) \quad (4-21)$$

where $\nu'_{i',k}$ is the molar stoichiometric coefficient for species i' in reaction k , $M_{i'}$ the molecular weight of species i' , β_k the temperature exponent, A_k the pre-exponential factor, $C_{j'}$ the molar concentration of each reactant or product species j' , $\nu_{j',k}$ the exponent

on the concentration of species j' in reaction k , E_k the activation energy for the reaction, and R the mixture gas constant. Further, Γ is defined by:

$$\Gamma = \sum_{j'=\text{all species}} C_{j'} \gamma_{j'k} \quad (4-22)$$

where $\gamma_{j'k}$ is the third-body efficiency of the j' th species in the k th reaction. FLUENT/UNS by default does not include the third-body efficiencies in the reaction rate calculations and the literature suggests using them only when specific values are available.

4.4.2 FLUENT/UNS Numerical Scheme

FLUENT/UNS is a finite volume application and solves all the governing differential equations in integral form using iterative techniques. Again, an extensive review of all equations, methods of application, and theory can be obtained from the Fluent literature (1996b). Substantial relevant portions of the manual are discussed within this section to supply an understanding of the methods exploited by the CFD program.

The governing equations are solved in order. Several iterations are often required to arrive at a final correct solution to the equations since they are “coupled,” or depend on one another. Fluent Inc. has provided a summary of the typical steps involved at each iteration along with a graphical representation shown in Figure 4-5. The steps are:

1. The u , v , and w momentum equations are each solved in turn using current values for pressure, in order to update the velocity field.

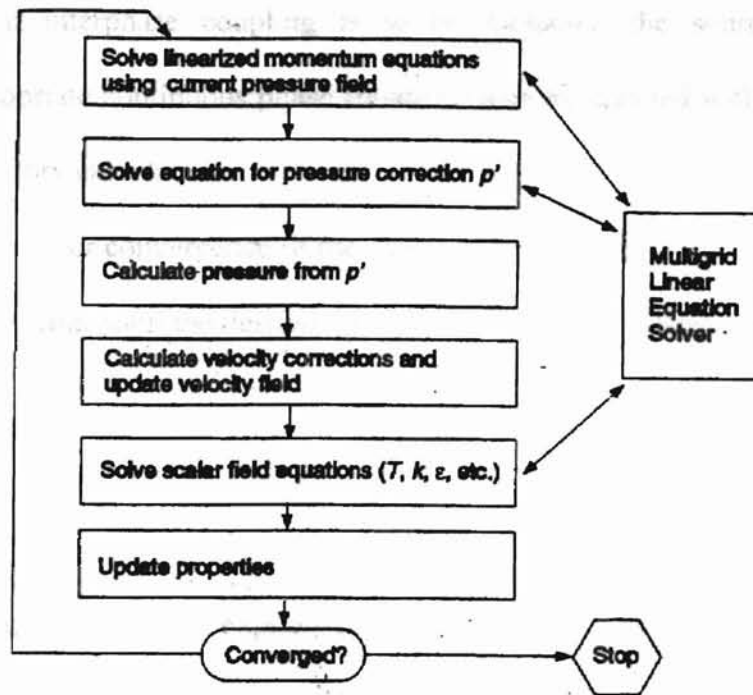


Figure 4-5. Overview of FLUENT/UNS Numerical Scheme (Fluent Inc., 1996b)

2. Locally, a “Poisson-type” equation for the pressure correction is derived from the continuity equation and the linearized momentum equations. This pressure correction equation is then solved to obtain the necessary corrections to the pressure and velocity fields such that continuity is achieved.
3. The k and ϵ equations are solved using the updated velocity field (for turbulent flow only).
4. Any auxiliary equations (e.g., energy, species conservation, and/or radiation) are solved using the previously updated values of the other variables.
5. Fluid properties are updated.

6. When interphase coupling is to be included, the source terms in the appropriate continuous phase equations may be updated with a discrete phase trajectory calculation.
7. A check for convergence of the equation set is made.

The iterations continue until the desired convergence criteria has been achieved.

Discretization

Providing a simplified explanation to the process, FLUENT/UNS applies its control volume techniques to convert the differential equations describing the processes to algebraic forms. These procedures are commonly referred to as “discretization.” In other words, the exact governing equations have been represented in such a way that discrete values can be used to describe portions of the processes. The example shown below illustrates the application of the techniques. A transport differential equation can be represented by:

$$\frac{\partial}{\partial x}(\rho u \phi) = \frac{\partial}{\partial x} \Gamma \frac{\partial \phi}{\partial x} + S_{\phi} \quad (4-23)$$

where ρ is the density, u is the velocity, ϕ is a scalar quantity, Γ is the diffusion coefficient, and S_{ϕ} is the source per unit volume of ϕ . This equation can be converted to a discretized form to yield:

$$J_e \phi_e - J_w \phi_w = \left(\Gamma_e \frac{\phi_E - \phi_P}{\Delta x_e} - \Gamma_w \frac{\phi_P - \phi_W}{\Delta x_w} \right) A + S_{\phi} \Delta V \quad (4-24)$$

where J is the mass flow rate, ΔV the volume, and A the cross-sectional area. A one-dimensional representation of a control volume showing the values of interest is

portrayed in Figure 4-6. It must be noted this is only a one-dimensional representation provided by Fluent Inc. for helping users to understand the underlying theory. More complicated forms of these algorithms are often applied to two and three-dimensional problems. Discrete values of ϕ are stored at the cell centers indicated by W, P, and E in Figure 4-6. Further complexity evolves when it is realized that face values of ϕ are needed for convective calculations. Interpolation procedures based on the cell center values are applied to acquire the needed face values.

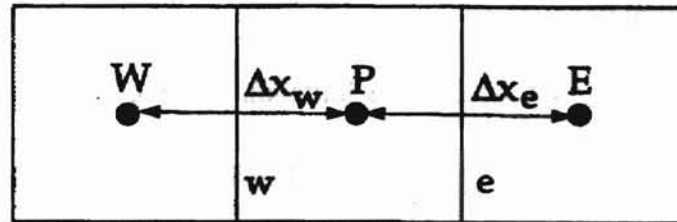


Figure 4-6. One-Dimensional Representation of Control Volume (Fluent Inc., 1996b)

Choices abound even for the interpolation procedures within FLUENT/UNS. Users can choose to apply a first-order upwind, power-law, or second-order upwind scheme. The diffusion terms in Equation (4-24) are central-differenced and thus always have second-order accuracy. For the remaining calculations, while power-law and second-order schemes are attractive for some applications, they were not primarily used or required in the current research and were not considered. The first-order upwind scheme was chosen based on its solution stability characteristics. The steady one-dimensional equation that describes the transport of ϕ is given by:

$$\frac{\partial}{\partial x}(\rho u \phi) = \frac{\partial}{\partial x} \Gamma \frac{\partial \phi}{\partial x} \quad (4-25)$$

where Γ and ρu are constant across the interval Δx . This equation can be integrated to yield the following solution which indicates the manner in which ϕ varies with x :

$$\frac{\phi(x) - \phi_0}{\phi_L - \phi_0} = \frac{\exp\left(Pe \frac{x}{L}\right) - 1}{\exp(Pe) - 1} \quad (4-26)$$

where ϕ_0 is ϕ evaluated at $x = 0$, ϕ_L is ϕ evaluated at $x = L$, and Pe is the Peclet number given by:

$$Pe = \frac{\rho u L}{\Gamma} \quad (4-27)$$

Based on the formulation presented in Equation (4-26), it is commonly shown that when large values of Pe are considered (indicating convection dominated flow), the value of ϕ is approximately equivalent to the upstream value.

Underrelaxation and overrelaxation methods are frequently used in numerical methods to aid in resolving difficulties encountered with nonlinear equations and to speed solution convergence. FLUENT/UNS allows underrelaxation to be applied and it can be represented by:

$$\phi_P = \phi_{P,old} + \alpha \Delta \phi_P \quad (4-28)$$

where ϕ_P is the new variable value, $\phi_{P,old}$ is the old variable value, and α the underrelaxation factor.

Applying many of the equations previously described allows the presentation of a conservation equation for the general variable ϕ at cell P:

$$a_P \phi_P = \sum_{nb} a_{nb} \phi_{nb} + b \quad (4-29)$$

where the subscript nb signifies neighbor cells. Forms of the equations are written for each cell in the grid. Algebraic schemes are then utilized in the solution of systems of equations. These are known as multigrid techniques and are further explained in the Fluent literature.

Pressure-Velocity Coupling

In numerical techniques, adequate consideration must be given to the coupling of pressure and velocity. The interdependence can be illustrated by the one-dimensional forms of the continuity and momentum equations:

$$\frac{\partial}{\partial x}(\rho u) = 0 \quad (4-30)$$

and

$$\frac{\partial}{\partial x}(\rho u u) = -\frac{\partial p}{\partial x} + \frac{\partial}{\partial x} \left[\mu \left(\frac{\partial u}{\partial x} \right) \right] + F \quad (4-31)$$

Without providing a detailed explanation, the Fluent literature indicates the above momentum and continuity equations can be represented numerically as:

$$a_p u_p = \sum_{nb} a_{nb} u_{nb} + (p_w - p_e)A + S \quad (4-32)$$

and

$$J_e - J_w = 0 \quad (4-33)$$

where J is the mass flow rate. In order to continue calculations, the face values of the velocities must be found. The interpolation techniques discussed previously, coupled

with averaging and weighting factors, are applied to find these velocity values. Utilizing these procedures, the face flow rate J_e can be defined as:

$$J_e = \hat{J}_e + d_e (p_p - p_w) \quad (4-34)$$

where \hat{J}_e encompasses the influence of neighboring velocities u_p and u_E , and d_e is defined by:

$$d_e = \frac{\rho_e A_e^2}{\bar{a}_p} \quad (4-35)$$

where \bar{a}_p is the average of the values of a_p for the cells P and E.

Equations (4-30) and (4-31) are coupled by nature, but when incompressible flow is encountered, some additional issues must be resolved. The density does not have definite ties to the pressure within these types of problems. To overcome these difficulties, a pressure-velocity coupling algorithm is employed.

Considering the current research, the Semi-Implicit Method for Pressure-Linked Equations (SIMPLE) method was found to work sufficiently. The Fluent literature briefly discusses the method which emphasizes relationships between velocity and pressure corrections that facilitates the conservation of mass and the attainment of the pressure field. Using the method, the face flux J_e^* can be acquired from:

$$J_e^* = \hat{J}_e^* + d_e (p_p^* - p_w^*) \quad (4-36)$$

If the value found does not satisfy the continuity equation, a correction J_e' is added to the face flow rate J_e^* . The corrected face flow rate then satisfies continuity and becomes:

$$J_e = J_e^* + J_e' \quad (4-37)$$

In addition, the use of the SIMPLE algorithm requires that J_e' be defined as:

$$J'_e = d_e (p'_P - p'_W) \quad (4-38)$$

where p' is the cell pressure correction. The formulations described are applied at discrete points to arrive at the equation (illustrated for a point P):

$$a_P p'_P = \sum_{nb} a_{nb} p'_{nb} + b \quad (4-39)$$

where b is then defined as:

$$b = J_w^* - J_e^* \quad (4-40)$$

After a solution is achieved for each iteration, the cell pressure and face flow rate are corrected by:

$$p_e = p_e^* + \alpha_p p'_e \quad (4-41)$$

and

$$J_e = J_e^* + d_e (p'_P - p'_W) \quad (4-42)$$

where α_p is the underrelaxation factor for pressure.

Residuals and Convergence

Residuals are frequently used within FLUENT/UNS to judge convergence of a solution. Consider the conservation equation for variable ϕ at cell P:

$$a_P \phi_P = \sum_{nb} a_{nb} \phi_{nb} + b \quad (4-43)$$

where a_P is the center coefficient, a_{nb} are the influence coefficients for the neighboring cells, and b is the contribution of the constant part of the source term S_c in $S = S_c + S_{P\phi}$ and of the boundary conditions. In Equation (4-43), a_P is defined by:

$$a_p = \sum_{nb} a_{nb} - S_p \quad (4-44)$$

The residual R^ϕ used within FLUENT/UNS is equal to the amount of inequality in Equation (4-43) summed over all of the computational cells P. This basic form is considered the “unscaled” residual and is shown to be:

$$R^\phi = \sum_{cells P} \left| \sum_{nb} a_{nb} \phi_{nb} + b - a_p \phi_p \right| \quad (4-45)$$

Often the convergence is difficult to judge based on the unscaled residuals. Therefore, a scaling process is usually adopted. The form applicable to the momentum equations is:

$$R^\phi = \frac{\sum_{cells P} \left| \sum_{nb} a_{nb} \phi_{nb} + b - a_p \phi_p \right|}{\sum_{cells P} |a_p \phi_p|} \quad (4-46)$$

Fluent Inc. (1996b) indicates this is the more appropriate convergence evaluation criterion for the majority of problems handled by the solver. Similar techniques are applied to remaining equations (including continuity). Coupled with experience and other evaluation techniques, inspection of the residual values allows users to decide whether or not adequate solution convergence has been achieved.

CHAPTER V

FLUENT/UNS 2-D MODEL DEVELOPMENT

5.1 Introduction

The FLUENT/UNS software program was utilized to develop a descriptive 2-D computational model of the reactor system. Initially, a substantial amount of time was spent learning the basic operation of the GeoMesh subprograms and the FLUENT/UNS solver. As operational skills improved and a better understanding of the computational techniques was attained, more features were added to the basic model. Primarily, through trial and error procedures, the final definitive model was obtained. The information presented in this chapter describes the thought processes and techniques exercised for the development of this computational model. The first topic discussed is an evaluation of the physical process before initiation of the CFD analysis. Following is an explanation of how the model was developed and correlated to the experimental data (with the computational data located in Appendix F). In addition, the assumptions and simplifications of the 2-D model are considered. In closing, consideration is given to convergence and model feasibility issues followed by an evaluation of the results provided by the computational model.

5.2 Pre-CFD Process Assessment

Before construction of the computational model was pursued, characteristics of the system under consideration had to be determined. Material thermophysical properties were collected, and in the current research, some were determined by the use of theoretical formulations. A compilation of the material properties can be found in Appendix E. System boundary conditions were also calculated based on the experimental process data. After all of the important process properties were determined, further insight was pursued by dimensional analysis.

By analysis of the experimental data, many of the basic process characteristics were more fully understood. Estimation of mass flow rates showed the process proceeds relatively slowly. The primary controlling factor appears to be the boiling rate of the reactants. In addition to the process being carried out at slow speeds when compared with other industrial processes, very high temperatures (higher than 1100 K) were maintained. Additional analysis of the reaction kinetics and thermocouple data also indicated that when the reactants were in contact with one another, the reaction rate proceeded somewhat rapidly.

Dimensional analysis often provides a means of comparison from one process to the next and allows a researcher to gauge the relative importance of various phenomena within a given system. The following discusses evaluation of some dimensionless parameters. After the discussion, a summary of the values considered are provided in Table 5-1.

One value of importance frequently used is the Reynolds number, indicating the ratio of inertial to viscous forces, and is defined as:

$$\text{Re} = \frac{\rho V D}{\mu} \quad (5-1)$$

Using a mass-weighted combined flow calculation on the main reactor tube and involving only the gas phase reactants and carrier gas evaluated at 1200 K, a value of approximately 24 was determined. This value is considerably less than the critical value (Re_{cr}) of 2300 for internal flow, and indicates the propensity of the flow to remain laminar. The properties used in this calculation and the others to follow can be found in Appendix E.

The Prandtl number is another value often used in engineering analysis. It provides important information about the ratio of molecular momentum to the thermal diffusivity. It is defined as:

$$\text{Pr} = \frac{\mu c_p}{k} = \frac{\nu}{\alpha} \quad (5-2)$$

Again using a mass weighted property evaluation at 1200 K, a value of 0.70 was obtained. This value is characteristic of gas phase flows and indicates the importance of the thermal diffusion.

In gas phase flowing systems, it is not surprising that heat transfer by convection can generally be expected to be more dominant than by conduction. The Peclet number, or ratio of convection to conduction, gives this indication and is defined as:

$$\text{Pe} = \text{Re Pr} = \frac{\rho c_p V D}{k} \quad (5-3)$$

Based on property evaluation as before, the value obtained was 17, making evident the expected role of convection in the heat transfer processes. This was another

Schmidt numbers were also calculated based on:

$$Sc = \frac{v}{D_y} \quad (5-4)$$

These values signify the importance of molecular momentum to mass diffusivity and were figured based on properties evaluated at 1200 K and diffusion coefficients of the reactants in the argon carrier gas. The values obtained were 0.31 and 0.55 for selenium (diatomic) and zinc, respectively. In the low velocity flowing system, these indicate the needed influence of diffusion.

Another value of interest was the product of density and specific heat, otherwise known as the volumetric heat capacity (ρc_p). Evaluation of this parameter at 1200 K provided a value of 503 J/m³-K. Incropera and Dewitt (1990) indicate materials with values below 1000 J/m³-K store thermal energy poorly. Having this low value for the volumetric heat capacity suggests that the flowing system may have difficulty possessing substantial amounts of thermal energy and would attempt to quickly distribute the energy it possesses. From analysis of the CFD model, this effect is noticeable.

Table 5-1. Summary of Representative Parameters

Re	24
Pr	0.70
Pe	17
Sc_{Se_2}	0.31
Sc_{Zn}	0.55
ρc_p (J/m ³ -K)	503

With sufficient understanding of the process flowing and heating attributes, focus was turned toward the development of an initial CFD modeling plan. This was another primary facet of the overall investigation that had to be addressed before significant resources were committed to the modeling efforts. Consideration was given to the significant amounts of time needed to learn the programs, timetable for results, and the available computational and storage resources. Based on these, it was concluded the 2-D model discussed in the next section, while neglecting the powder deposition, could still provide critical insight into the overall process behaviors.

5.3 FLUENT/UNS 2-D CFD Model Development

This section covers the development of the 2-D model used in the analysis of the Eagle-Picher chemical reactor. In providing a basis for future model development of similar systems, it was imperative to document in detail the steps carried out to arrive at a feasible model. The range of topics discussed encompass an overview on the creation of the geometry to more in-depth evaluation of the choices for the various flow and chemical models employed. Only brief descriptions of the modeling tools are given to show their order of involvement and application. More detail on these tools can be found in Fluent Inc. (1996a). More discussion focusing on the application to the current research is presented in Appendix E.

After verified physical system dimensions and specific modeling goals were developed, creation of the model geometry was initiated. This was accomplished by the use of the DDN subprogram within GeoMesh. In realizing the geometry was ultimately

only a means to an end, care was taken to minimize the number of entities created. Within the DDN geometry tool, the zinc inlet structure was effectively shortened by approximately 35 mm when compared with the measurements in Appendix A. This was carried out to avoid over-restricting the flow exiting from the selenium nozzle within the 2-D model. The final DDN geometry was then imported into P-Cube where the system of faces that make up the topology were developed. P-Cube was also used to specify the many settings for the boundary conditions, assign the node distribution, and generate the grid.

It was apparent boundary conditions had to be resolved earlier to afford the initial process analysis. With respect to the computational model, the boundary conditions were not needed until the grid had been generated. Presentation of the boundary conditions acquired from the experimental system can be found in Appendix D.

The RNG k - ϵ turbulence model was utilized to arrive at the final computational solution. The Fluent literature (1996b) indicates the appropriateness of the model for low Reynolds number flows when localized areas of turbulence may develop in the otherwise laminar flow. Even though the Reynolds number was quite low, the use of the turbulence model appeared to be a favorable choice due to the flow behavior around the front of the reactor, especially in the vicinity of the inlets. In addition, due to significant temperature gradients encountered in the front of the reactor, the possibility existed for the development of secondary flow (or swirling) behavior. Further discussion with a Fluent representative indicated that the inclusion of a turbulence model is ultimately decided by the user based on evaluation of how well the model resolves the flow characteristics. Computational runs were carried out to evaluate the differences between the laminar and

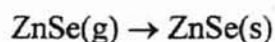
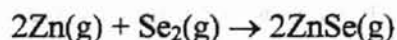
turbulent models. The results were somewhat surprising. Comparison of the calculated numerical results and the graphical output showed no major differences. The computed yields were extremely close and the graphical outputs were almost identical. Due to becoming familiar with the model and noting it caused no noticeable increase in solution time or data file size, the model was kept within the solution.

The Arrhenius rate expression was used to characterize the chemical reaction. The form used by the solver can be represented by Equation 4-21, however for purposes of developing the reaction mechanism, a simplified and more familiar version is:

$$k(T) = k_0 e^{-\frac{E_a}{RT}} \quad (5-5)$$

The desired unknown variables within the expression are the activation energy (E_a) and the pre-exponential factor (k_0). A comprehensive review of the available literature by the research group produced little information providing adequate insight to the kinetics of the reaction mechanism. Therefore, estimation was used to arrive at a descriptive process activation energy and an iterative process utilizing the experimental data was exercised to develop the pre-exponential factor.

The reaction mechanism, for the range of temperatures encountered in the current research, appears to take the form:



Many authors such as Sha et al. (1995) and Berkowitz and Chupka (1966), with most of the work pertaining to crystal preparation, have shown the reactants to exist primarily in the forms shown in the reaction. The ZnSe(g) species is known to be very unstable and quickly forms the solid species. In fact, the overall reaction is commonly represented as

the two gas phase reactants combining to form the solid product. As may be concluded, the first reaction step is endothermic while the second is quite exothermic. Using the HSC Chemistry program output in Appendix C by Outokumpu Research Oy (1997), typical ΔH values evaluated at 1000 °C (1273 K) were 66.52 kJ (15.89 kcal) and -379.3 kJ (-90.60 kcal) per mole of written reaction, respectively. For the purposes of the current research, the first reaction mechanism was chosen for modeling. Again, due to lack of relevant information, a second order rate form was assumed and is presented as:

$$r = k[\text{Zn}]^1[\text{Se}_2]^1 \quad (5-6)$$

In finding the activation energy, an interesting method was developed. Energy changes take place during a chemical reaction and a representation of these can be seen in Figure 5-1. From the figure, it can be noted a certain amount of energy must be supplied to the reactants to achieve the transition state. Once this has been reached the forward reaction occurs developing the products. Based on transition state theory, Tinoco et al. (1995) provide a correlation between the enthalpy of reaction and activation energy. This is shown to be:

$$\Delta H_{\text{react}} = E_a - RT \approx E_a \quad (5-7)$$

Often the contribution of the RT product is negligible (as in this application) and the enthalpy of reaction can be directly related to the activation energy as shown above. In finding the activation energy, the transition state was assumed to occur with the first reaction mechanism step. The change in enthalpy at a representative temperature of 1000°C (1273 K) was chosen from the output provided by the computer program HSC Chemistry (Outokumpu Research Oy, 1997). This choice appears reasonable since the

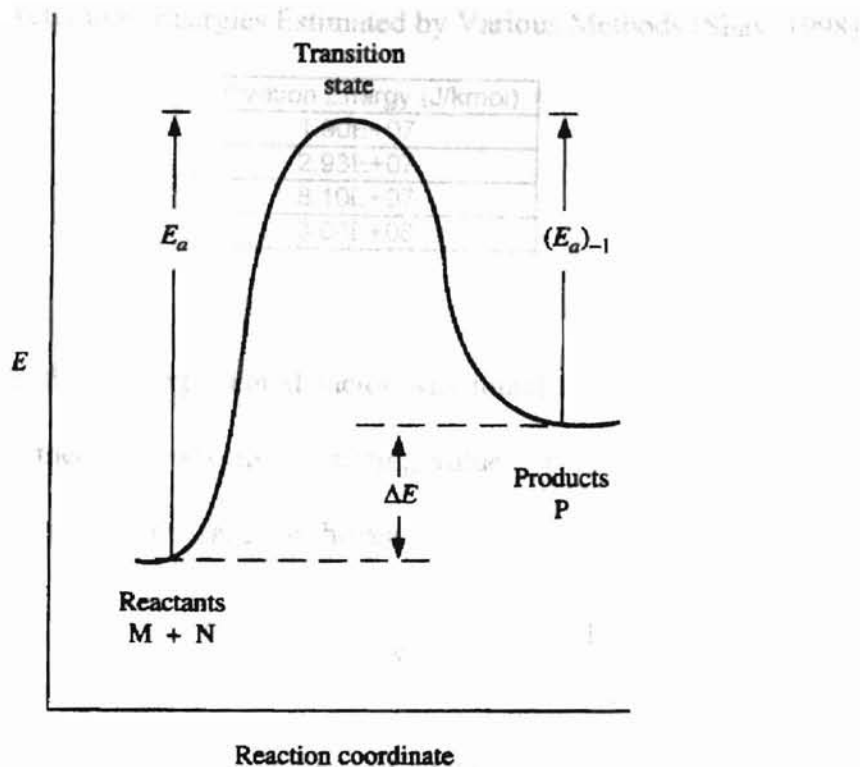


Figure 5-1. Energy Changes Occurring in a Hypothetical Reaction (Tinoco et al., 1995)

zinc and selenium reactant streams come into the reactor at approximate temperatures of 1300 K and 1000 K, respectively, with the reactor temperatures ordinarily around 1200-1300 K. The value obtained, after appropriate unit conversions, was 6.65×10^7 J/kmol (corresponding to 15.887 kcal per mole of written reaction in Table C-1 by Outokumpu Research Oy, 1997). Similar supporting thermochemical data can also be found in the work by Barin et al. (1977). From the data shown in Appendix C, there is little variation of the values over the observed temperature range. This value can be compared to those estimated and compiled in Table 5-2. They were calculated for the same reaction by colleagues using various methods and aid in supplying bounds to other derived values. For further information, the reader is referred to Shay (1998).

Table 5-2. Activation Energies Estimated by Various Methods (Shay, 1998)

Activation Energy (J/kmol)
1.90E+07
2.93E+07
8.10E+07
3.00E+08

Even though the pre-exponential factor was found by iterative methods, it was beneficial to utilize theory to develop a starting value. This was found based on the formulation by Levenspiel (1972) and for the reaction of interest it can be shown as:

$$k_o = \left(\frac{\sigma_{Zn} + \sigma_{Se_2}}{2} \right)^2 \frac{N}{10^3} \sqrt{8\pi\kappa T \left(\frac{1}{M_{Zn}} + \frac{1}{M_{Se_2}} \right)} \quad (5-8)$$

Using molecular diameters of 2.76×10^{-10} m and 4.68×10^{-10} m for the zinc and selenium molecules respectively, an initial value of 1.803×10^8 m³/kmol-s was calculated. This calculation was performed using the metallic radius for zinc (Mathewson, 1959) and the atomic radius for selenium (Bailer et al., 1973). Actual molecular sizes for both of these species are expected to be less than the values used. In addition, Levenspiel (1972) indicates the actual value for the pre-exponential factor is usually much lower than predicted. The theoretical formulation assumes every collision results in product development and does not take into account the effects due to an inert gas.

5.4 Correlation of Computational Model

In the previous section, core components of the computational model were developed and discussed. With each step carried out, the model came closer to realizing its final form. The goal of this section is to bring closure to the model development by

determining a realistic value for the remaining unknown, the pre-exponential factor, while correlating to the results obtained from the physical system in use by Eagle-Picher.

First and foremost was the development of the connection between the physical system and the computational model. This can best be explained by an example of the approach taken. Within the physical system, the reactants were brought together and allowed to interact over a period of time. The batch results were then collected and evaluated. Two experimental production runs were chosen from the limited amount of quality data collected. The cases were selected based on their inherent successful operation and limited amount of complications encountered. In addition, these cases afforded temperature data which was used to more closely recreate the temperature boundary conditions in the computational model. The case runs can be found in Appendix D. These are identified by their lot number based on an Eagle-Picher naming convention. The two cases utilized are designated as cases BA97202 and BA97195.

For the physical system, the yields can be expressed in terms of a formulation presented by Schmidt (1998):

$$Y = \frac{\text{Desired product formed}}{\text{Reactant fed}} \times 100 \quad (5-9)$$

Based on this definition, values of 63.1 % and 56.9 % were calculated for cases BA97202 and BA97195, respectively. Values and results for these calculations are shown in Table 5-3.

For the computational model, it was decided to develop a relationship to the physical system based on the output collected at the reactor exit. This actually afforded one of the only readily apparent methods. In the steady-state model, since the process worked with only gas phase species, there was no product accumulation. Therefore,

Table 5-3. Reactant Loadings and Yields

Case	Zinc Reactant Loading (g)	Selenium Reactant Loading (g)	Recovered Product (g)	Yield (%)
BA97202	500.0	684.7	747.3	63.1
BA97195	500.7	684.5	674.7	56.9

using the principle of conservation of mass and the definition of yield from Equation (5-9), the following formulation to gauge yield was developed for the computational model:

$$Y = \frac{\dot{m}_{o,ZnSe}}{\dot{m}_{o,ZnSe} + \dot{m}_{o,Zn} + \dot{m}_{o,Se_2}} \times 100 \quad (5-10)$$

As complete conversion was attained, the calculated value approached 100 %. Within FLUENT/UNS, appropriate exit mass flow values were obtained using flow rate options based on mass fractions at the exit.

The final step for the complete model determination involved the resolution of an appropriate pre-exponential factor. Using the definition for yield and the boundary conditions for Case BA97202, a trial and error process was adopted with the results shown in Table 5-4. Using knowledge gained from the work of colleagues (Shay, 1998 and Morrison, 1998) an estimated value of $2.0 \times 10^4 \text{ m}^3/\text{kmol}\cdot\text{s}$ was used as a starting point. A similar procedure was applied to case BA97195 with its associated yield of 56.9 %. The results of these iterations can be found in Table 5-5.

Table 5-4. Pre-exponential Factor Iteration for Case BA97202

Case Descriptor	Pre-exponential Factor ($\text{m}^3/\text{kmol}\cdot\text{s}$)	Yield (%)	Difference From Actual Yield (%)
k1-1	2.00E+04	46.1	-26.9
k1-2	4.00E+04	59.6	-5.6
k1-3	5.00E+04	64.2	1.7

Table 5-5. Pre-exponential Factor Iteration for Case BA97195

Case Descriptor	Pre-exponential Factor (m ³ /kmol-s)	Yield (%)	Difference From Actual Yield (%)
k2-1	5.00E+04	68.1	19.6
k2-2	2.50E+04	55.6	-2.4

To lessen the potential for error in determination of the pre-exponential factor, an average of the two final results was taken to arrive at a value which minimized the difference in yields for each case. The results are shown in Table 5-6. The final value of 3.75×10^4 m³/kmol-s was used for the remainder of the process evaluation models with case corr1-1 used as the basis against which all other models were evaluated.

Table 5-6. Determination of Final Pre-exponential Factor

Case Descriptor	Case	Pre-exponential Factor (m ³ /kmol-s)	Yield (%)	Difference From Actual Yield (%)
corr1-1	BA97202	3.75E+04	58.3	-7.6
corr2-1	BA97195	3.75E+04	61.6	8.3

5.5 Model Simplifications and Assumptions

Simplified models are often used to characterize complex systems. Important insight into some processes may be gained by the use of some basic descriptive equations commonly found in engineering texts. Classical calculation techniques proved inadequate for the degree of knowledge necessary for this research. Therefore, the CFD approach was employed. It is expected with these models that some degree of

simplification is still unavoidable. The list of simplifications and assumptions applicable for the first level model created in this research includes the following:

1. Two-dimensional
2. Steady-state
3. Non-axisymmetric
4. Radiant heat transfer neglected
5. Pressure effects neglected
6. All species are gas phase
7. Product accumulation neglected

5.6 Convergence and Model Feasibility Considerations

Evaluation of proper solution convergence is a significant concern with computational techniques. Various forms of iterative algorithms are widely used in computer codes (commercial and otherwise). Proper attention must be given to the signals provided by the codes indicating a reasonable solution has been reached.

FLUENT/UNS afforded some useful options allowing for the evaluation of computational solutions. The primary indicator of convergence, apparently used by the majority of the solvers within the Fluent Suite, was the scaled residuals. These residuals are an indicator of a rate of change for each of the primary equations. Once these values fall below the preset criteria, the solution stops iterating. The Fluent literature indicates the default values for the termination criteria within FLUENT/UNS are deemed adequate

for the vast majority of computational cases considered (Fluent Inc., 1996b). These values are shown in Table 5-7 with other usual parameter settings.

Table 5-7. Typical Residual Termination Criteria

Residual	Monitor	Check Convergence	Convergence Criterion
continuity	yes	yes	1.00E-03
x-velocity	yes	yes	1.00E-03
y-velocity	yes	yes	1.00E-03
k	yes	yes	1.00E-03
epsilon	yes	yes	1.00E-03
energy	yes	yes	1.00E-06
zn	yes	yes	1.00E-03
se2	yes	yes	1.00E-03
znse	yes	yes	1.00E-03

The Fluent literature (1996b) further indicates special consideration must be given to flows where gravity is included in the model and buoyant effects are deemed important. Often the residual reduction criteria shown in Table 5-7 must be increased by at least an order of magnitude or other means must be used to signal proper solution convergence (Fluent Inc., 1996b).

A useful calculation, which indicates the importance of including the buoyancy forces in computations, is given by the ratio of the Grashof number to the square of the Reynolds number:

$$\frac{Gr}{Re^2} = \frac{\beta g \Delta T D}{V^2} \quad (5-9)$$

When this number approaches or exceeds unity, buoyancy contributions are quite significant (Fluent Inc., 1996b). The Reynolds number was retained from previous calculations and the Grashof number was obtained from:

$$Gr = \frac{g\beta(T_w - T_b)D^3}{\nu^2} \quad (5-10)$$

where the viscosity was calculated using a mass-weighted formulation evaluated at 1200 K. Values of 1273 K and 1185 K were used for the wall and bulk temperatures, respectively. The ideal gas formulation for β was applied using the bulk temperature. Evaluation of the Grashof number provided a value of 3.4×10^5 resulting in a value of 590 for the Gr/Re^2 ratio. This indicated buoyant forces were very important in the development of this model. Consideration of the graphical results presented by the final model supports this conclusion. Based on this result, the Fluent literature as well as a customer support representative from the company were consulted. They both indicated a final steady-state solution may not exist for some laminar high-buoyancy flows. These complications proved formidable in the development of the final model.

Adequate solution convergence was strongly coupled to the grid development (as would be expected for many solutions). In the beginning stages, a moderately rough grid of approximately 3000 nodes was utilized to compute the solution. However, it was quickly learned inadequate solution stability was a problem. The node density was improved to 5009 nodes with an appreciable difference noted in the convergence and solution stability. With a normal case (on a well developed grid), which did not include the effects of gravity, the residuals decreased steadily to the convergence criteria. As an example, running the case currently considered without gravity resulted in complete convergence in 130 iterations. However, with the gravitational effects added, the residuals behave in the manner shown in Figure 5-2. It can be seen there is a point reached where the solution oscillated in a behaved steady manner. For all cases considered in this study, this occurred at approximately 150-200 iterations. Additional

investigative case runs were made allowing the solution to continue out to as much as 1000 iterations to insure that any surprising behavior would not be encountered. Since the solution never reached the convergence criteria, acceptable solution feasibility was a concern. The residuals typically encountered in the steady oscillatory solution were as shown in Table 5-8.

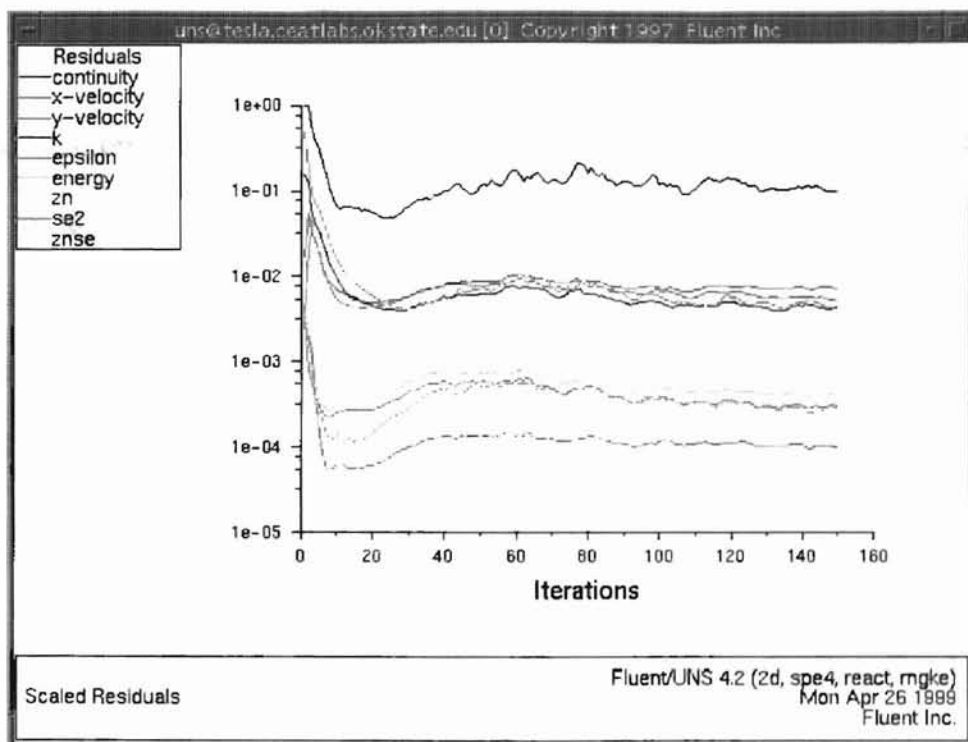


Figure 5-2. Typical Residual Behavior for Solution Considering Gravity

The first step for checking solution convergence was the evaluation of the graphical output based on the results. Underdeveloped solutions frequently displayed strange behavior. An example would be achieving a temperature distribution in a region which did not seem reasonable. The biggest indicator of solution stability was the computation of the desired output, the yield. Once the model had achieved a steady

Table 5-8. Typical Residual Values for Baseline Model

Residual	Typical Solution Value
continuity	9.9082E-02
x-velocity	7.0561E-03
y-velocity	5.2666E-03
k	4.4194E-03
epsilon	4.6125E-03
energy	1.0435E-04
zn	4.3362E-04
se2	3.1561E-04
znse	3.0107E-04

solution, additional iterations were performed to investigate the stability of the results and to gain insight into the degree of accuracy. For the baseline model (case corr1-1 in Appendix F), the results are shown in Table 5-9. An additional significant figure was included to illustrate the small amount of variation. The results obtained were quite good and well within the experimental deviation of the somewhat unpredictable physical system. Turning the gravity option off and running the solution to convergence (case

Table 5-9. Evaluation of Variability of Process Solution for Case Corr1-1

Iterations (150+)	Yield (%)
10	58.29
20	57.35
30	58.52
40	58.53
50	58.82
60	59.02
70	59.25
80	58.96
90	58.75
100	58.32

Mean	Standard Deviation
58.58	0.53

nograv in Appendix F) resulted in a yield of 58.7 %, differing from the previous solution (at 150 iterations) by only 0.69%. Even though the yields for both solutions compared quite well, the results obtained with the model considering gravity appeared to more accurately present predicted flow patterns.

Within this section, the computational model was developed, tested, and its feasibility confirmed. This model was used as the basis for process investigation cases considered in the next chapter. It is noted that some degree of solution convergence variability was encountered in a few of the process solutions. In computational work this is to be expected. For a few of the more deviant cases, this was remedied by producing a mesh with a greater node density. However, all of the cases followed the general characteristic pattern of the baseline model solution. Further, all of the results of the investigative study in the next chapter followed expected trends and appeared to be well within the experimental variability of the physical process. This provided an additional degree of validity to the computational model.

5.7 Presentation and Evaluation of Results

The results from the output of FLUENT/UNS proved invaluable in the analysis of the system. Besides providing numerical means for evaluation, the program also allowed effortless development of graphical representations.

Expected complex flow patterns can be observed in Figure 5-3. Due to the two-dimensional nature of the model, the regions of stagnant flow are probably over predicted. However, past system analyses support the occurrence of these phenomena to

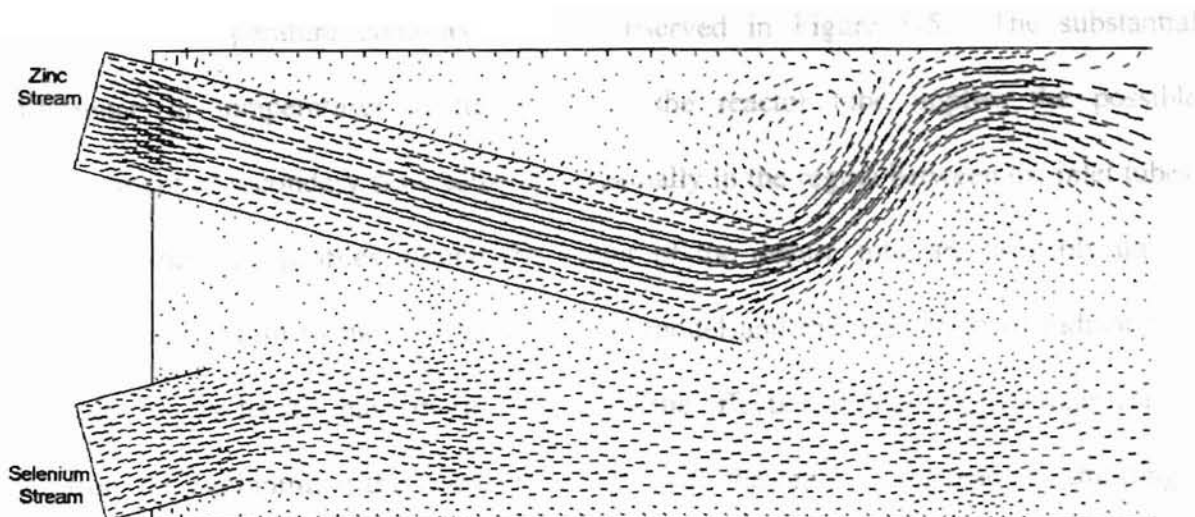


Figure 5-3. Velocity Vectors at Front of Chemical Reactor

a degree. The $Zn(g)$ species can be observed exiting the upper outlet and quickly overcoming gravity effects in traveling towards the top of the reactor. Swirling behavior appears to occur above the $Zn(g)$ outlet due to the upward movement of the gas. With the rising of the gas immediately upon exit, the potential for product nucleation and growth on the lower portion of the $Zn(g)$ outlet becomes evident. While most of the $Se_2(g)$ appears to remain along the bottom of the reactor, the velocity vectors indicate the possibility of the $Se_2(g)$ traveling inside the bottom portion of the $Zn(g)$ outlet. If the flow rates are not substantial enough, the nucleation and growth of the product could cause plugging of the outlet, a problem frequently encountered in past operation. It must be noted that while cases neglecting gravity produced quite similar yields, they did not show the flow patterns and species distributions adequately. Figure 5-4 shows an additional view of the velocity behavior for the entire reactor. It indicates the moving $Zn(g)$ stream continues to some degree along the top of the reactor tube. As gases expand in the reactor, the lighter species also proceed upward.

The temperature contours can be observed in Figure 5-5. The substantial difference in temperatures at the front of the reactor tube implies the possible development of secondary flow behavior, especially in the region between the inlet tubes. While temperature profiles around the center of the reactor tube are probably under-predicted, due again to the 2-D nature of the model and the neglect of radiant heat transfer, the results still have merit. It appears the effects from the $\text{Se}_2(\text{g})$ stream can be felt from the beginning of the reactor to the exit with the center of the reactor exhibiting a tendency to stay a few degrees cooler than the areas closest to the walls.

Other useful insight is provided by observing the concentration contours of the species. In Figure 5-6, the buoyant nature of the $\text{Zn}(\text{g})$ species again becomes clear. The highest concentrations of this species remain towards the top of the reactor tube. Figure 5-7 shows the less buoyant nature of the $\text{Se}_2(\text{g})$ species with its concentrations staying highest along the bottom of the reactor. It becomes obvious that the streams stay partially segregated with this reactor configuration. Of particular interest was the behavior around the $\text{Zn}(\text{g})$ outlet. The $\text{Se}_2(\text{g})$ species can be observed attempting to intrude inside the outlet. The behavior of the $\text{ZnSe}(\text{g})$ species is represented in Figure 5-8. Significant formation can be observed not far from the $\text{Zn}(\text{g})$ outlet. The proximity of the $\text{ZnSe}(\text{g})$ initial product formation tends to indicate the potential for a possible plugging problem. This phenomenon was not as strongly observed in the case neglecting the effects of gravity. The results re-emphasize the necessity for adequate flow rates to prevent this occurrence. A variational study is considered in the next chapter to address some of these problems.

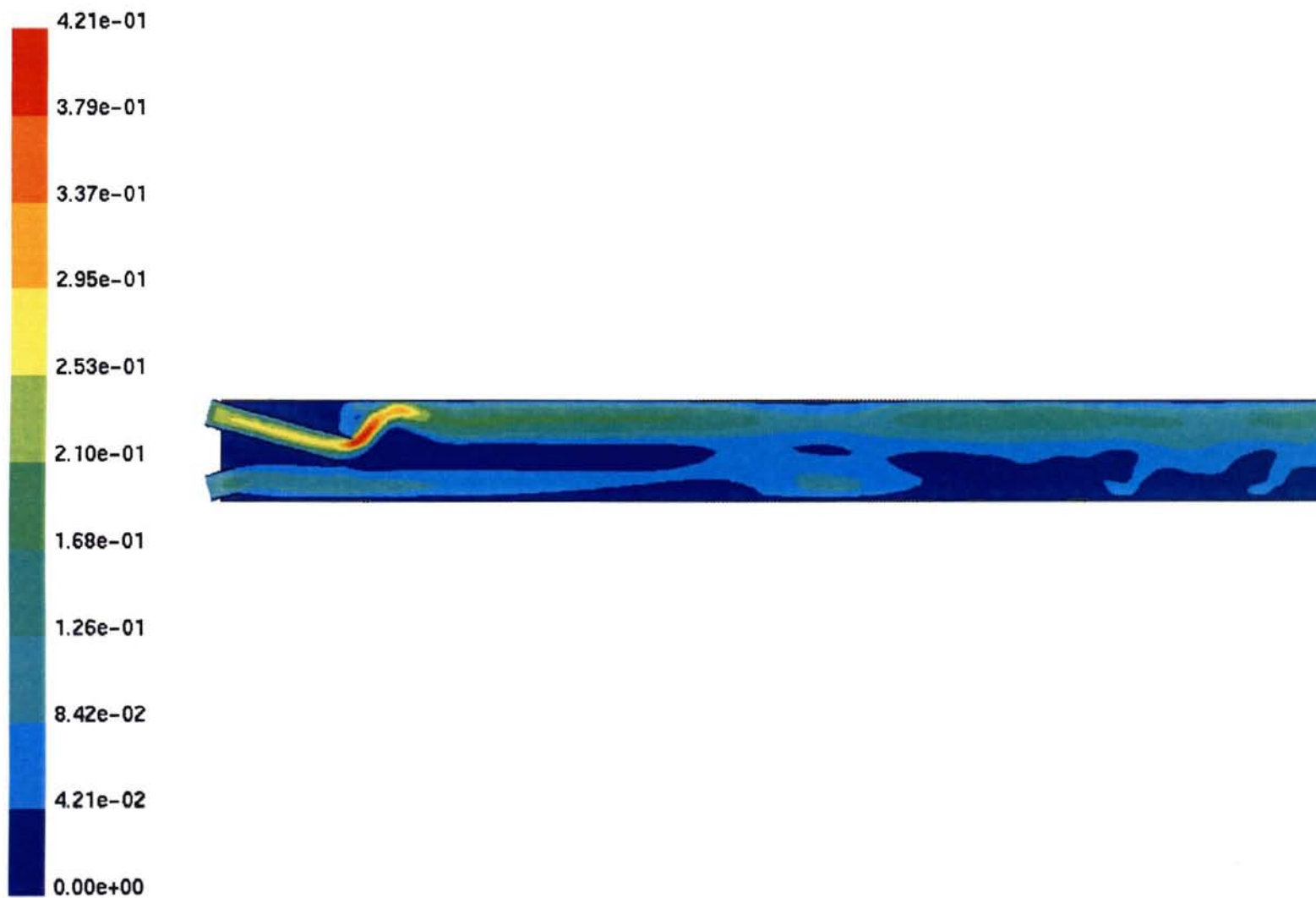


Figure 5-4. Contours of Velocity Magnitude (m/s)

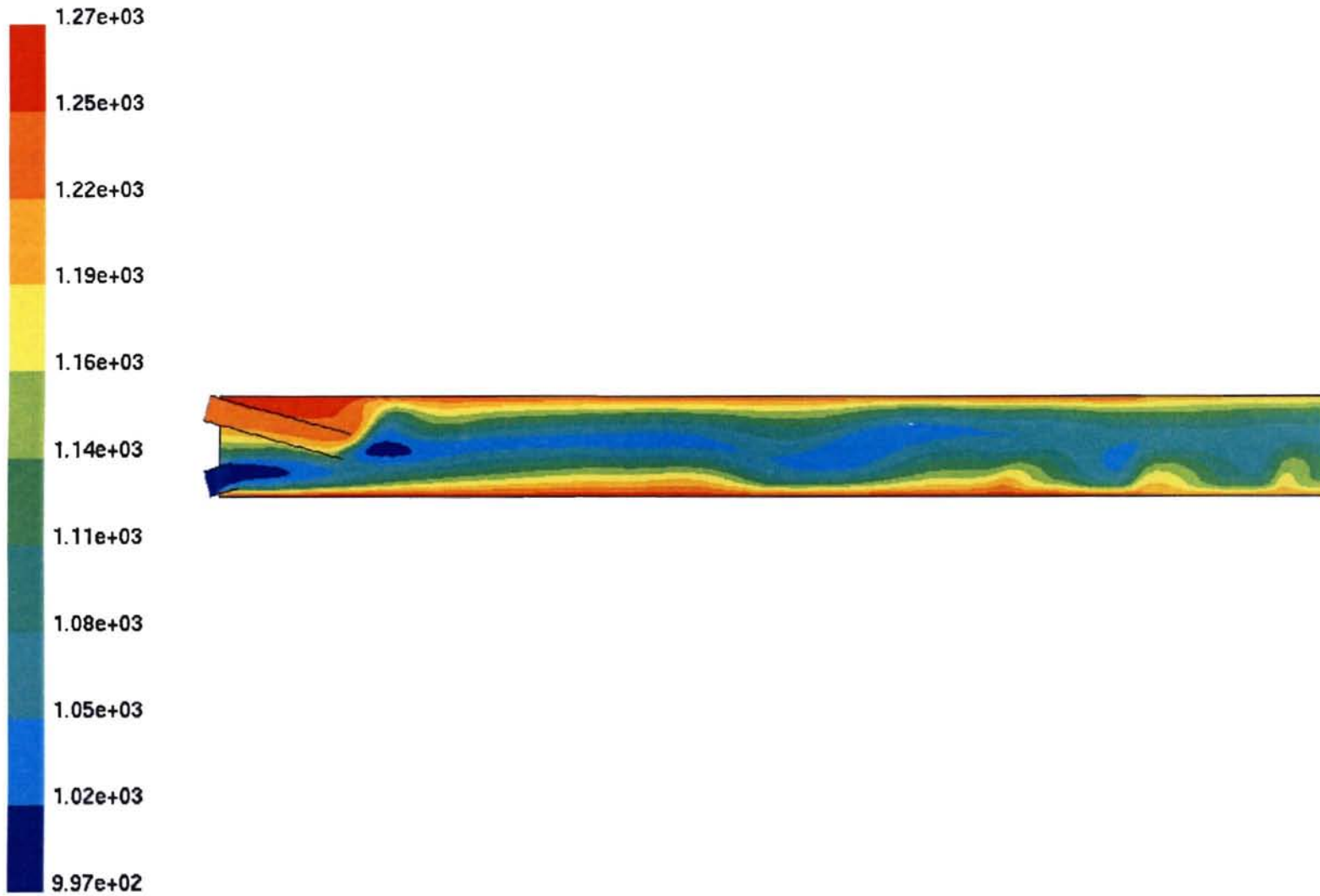


Figure 5-5. Contours of Static Temperature (K)

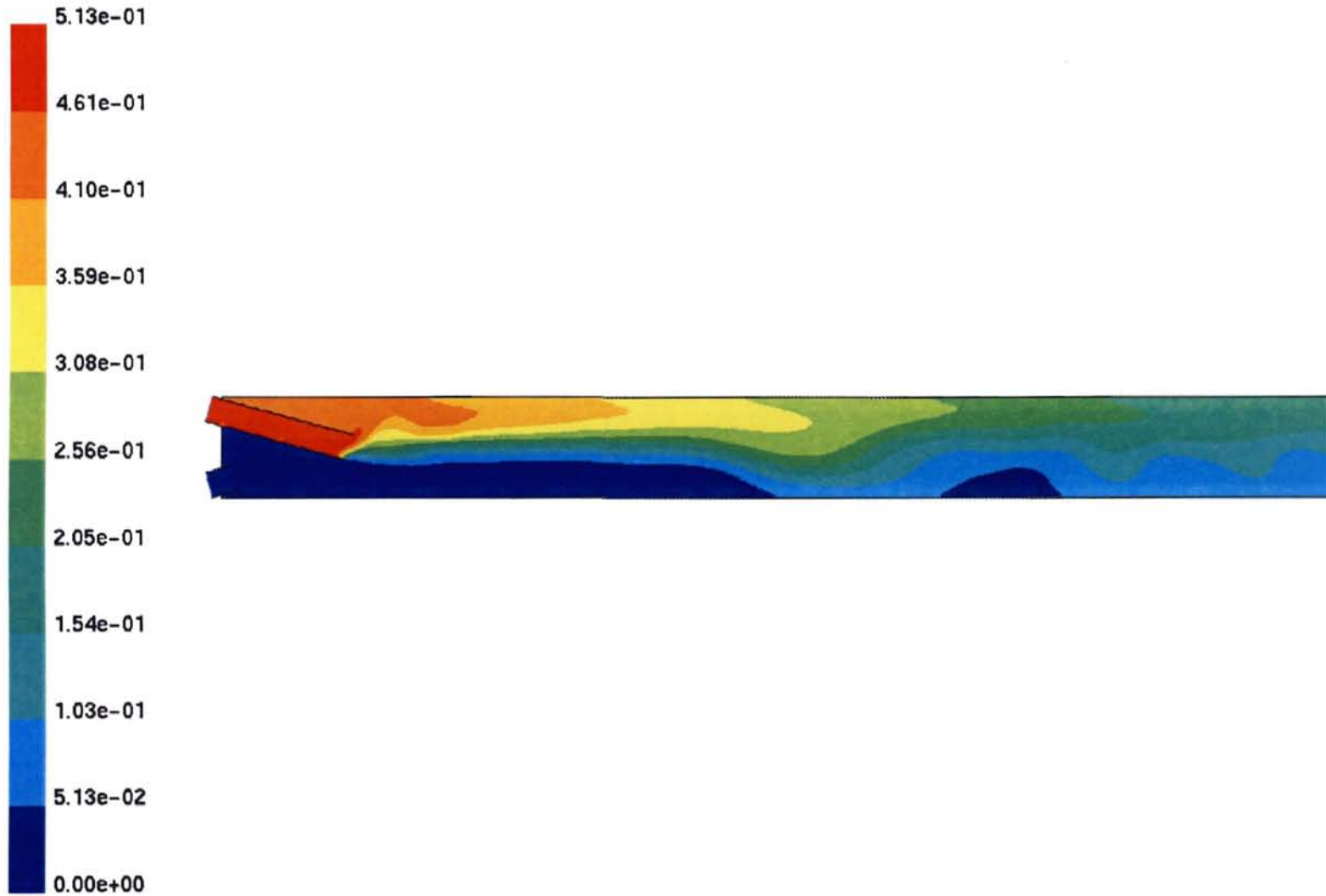


Figure 5-6. Contours of Zn Concentration (kg/m³)

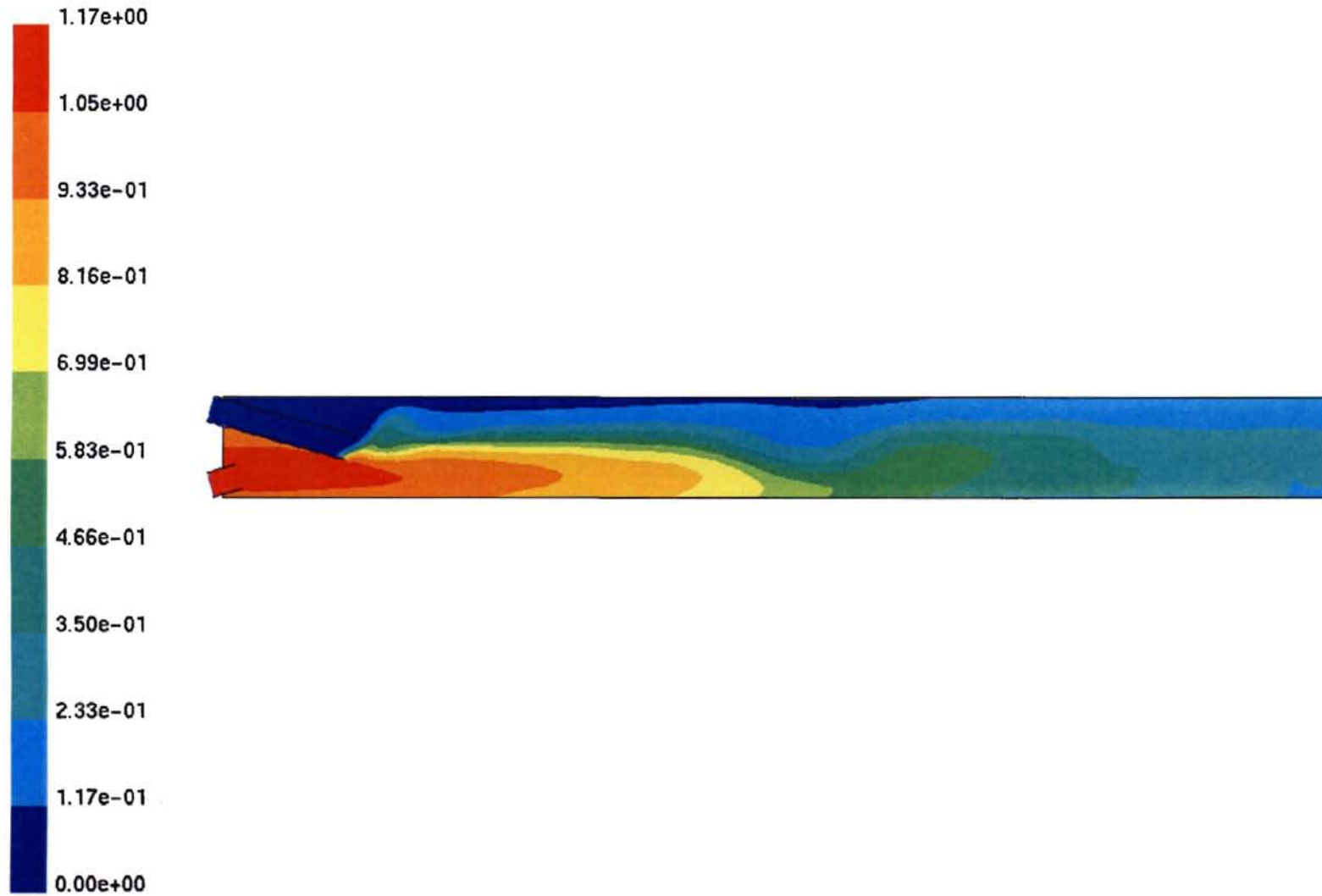


Figure 5-7. Contours of Se₂ Concentration (kg/m³)

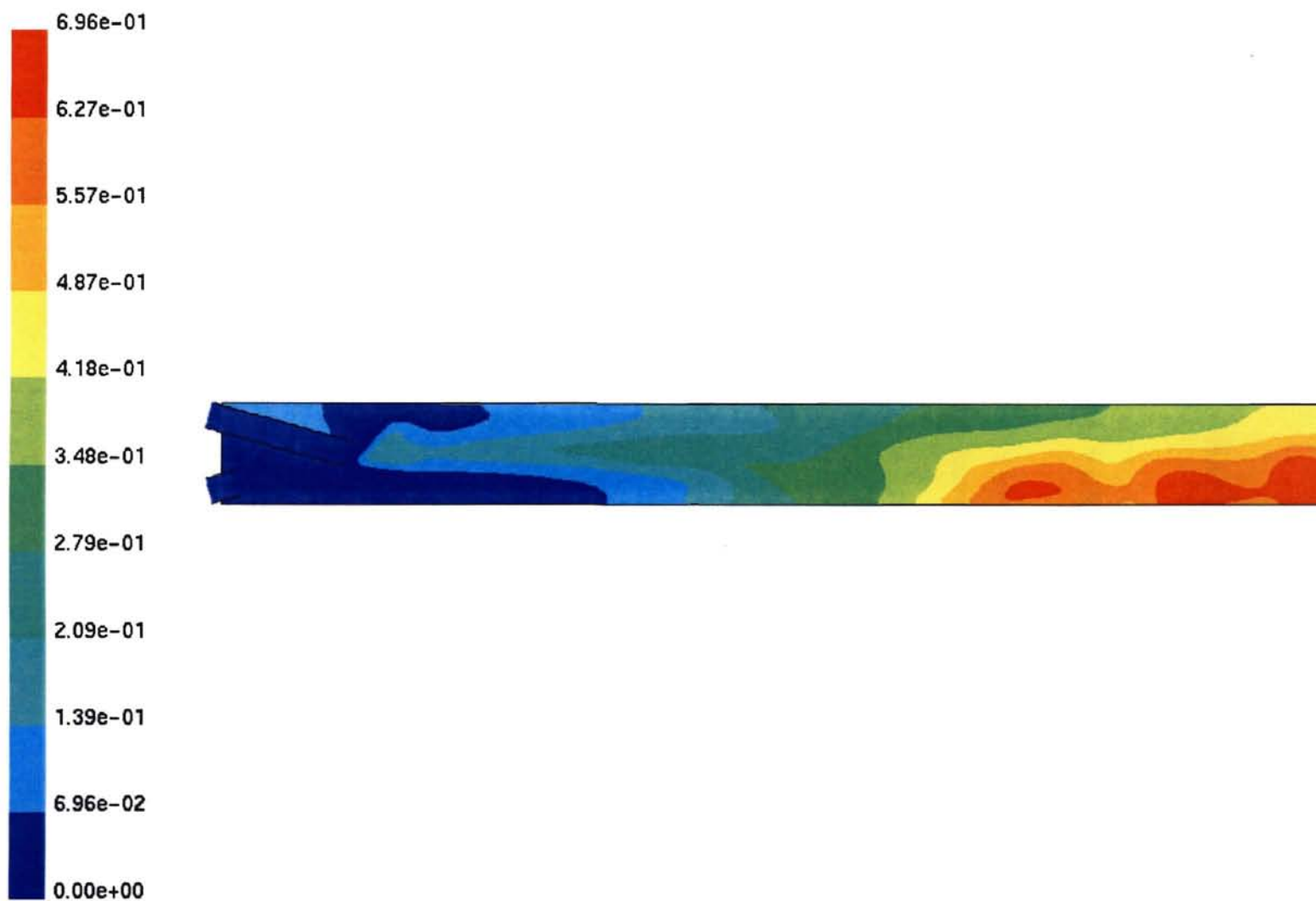


Figure 5-8. Contours of ZnSe Concentration (kg/m^3)

There are a multitude of parameters to be considered in the current study conducted within this

CHAPTER VI

PROCESS PARAMETER VARIATIONAL INVESTIGATION

6.1 Introduction

This chapter showcases FLUENT/UNS as a useful and valuable tool in process evaluation and optimization. Process parameter variations were considered for the current Eagle-Picher reactor configuration. Physical changes to the reactor were not considered in this first level investigation. The primary goal of the study was to develop computational results that could provide dramatic insight into the process in its current state. It was felt this would allow some comparison to the large amounts of data collected in the past. In addition, it would offer a firm footing for more aggressive configurational changes without the potential of compromising process performance. While the results of the study were feasible and resided well within chemistry and engineering reason, it is felt more extensive sensitivity analyses need to be performed on the physical system. The results could then be more closely analyzed and compared to those obtained in the computational study. It is not recommended to devote significant resources toward these efforts until more reliable process control is applied.

In an extensive evaluation, there are a multitude of parameters to be considered. For the current Eagle-Picher reactor, the variational study conducted within this chapter considered the following:

1. Front zone (approximately first six inches of reactor) temperatures
2. Middle zone (approximately middle twenty-four inches of reactor) temperatures
3. Rear zone (approximately last six inches of reactor) temperatures
4. Argon flow rates associated with the zinc inlet
5. Argon flow rates associated with the selenium inlet
6. Zinc reactant flow rates
7. Selenium reactant flow rates
8. Stoichiometric reactant flow rates

In future investigations, the listing of parameters to consider for the Eagle-Picher reactor could also include the following:

1. Reactant and argon carrier gas inlet diameters
2. Reactant and argon carrier gas inlet lengths
3. Reactant and argon carrier gas inlet locations
4. Two-phase flow (interaction with the product powder)
5. Reactor tube sizes
6. Flow obstructions (could be used to invoke greater turbulent mixing)
7. Reactor lengths
8. Other carrier gases

All of these considerations would be important in achieving more efficient operation of the chemical reactor.

This chapter initially considers the effects of reactor zone temperature variations on the product yield. Argon carrier gas effects on each of the reactant streams is then evaluated. Following are considerations of reactant flow rates and reactant flow rates under stoichiometric conditions. Lastly, based on the results of the parametric study, a reactor process is presented utilizing the indicated optimal conditions. A more comprehensive listing of the data presented in this chapter can be found in Appendix F.

6.2 Reactor Temperature Zones

Front Zone

For the front zone, temperature variations were considered from 1200 K to 1400 K. The rationale for the lower temperature of 1200 K was based on the normal boiling point of 1180 K for the zinc species. The upper bound value was based on the maximum recommended working temperatures for the quartz material. The maximum working temperature was somewhat higher, but it was assumed the reactor tubes would be used repeatedly and minimum material degradation (that accompanies continual use at high temperatures) was desired.

The results for the front zone temperature variational study are shown in Table 6-1. It is observed in this region of the reactor tube, as long as reasonable temperature settings were utilized, the results did not differ significantly. The collected data indicated

expected results. Due to the extensive length of the zinc inlet, minimal reactant mixing was achieved in this zone and subsequently showed the temperature variations in the front zone as having little effect. There was, however, a noticeable trend with increased yields appearing at the higher temperatures. These results were in line with that expected from theoretical calculations based on the Arrhenius rate expression. While these effects may seem somewhat minimal, the increase in yield at higher temperatures within process operations over an extended period of time cannot be disregarded and would have beneficial economic impact.

Table 6-1. Front Zone Temperature Variation Effects on Yield

Case Descriptor	Temperature (K)	Yield (%)
temp1-1	1400	60.7
temp1-2	1350	59.5
temp1-3	1300	59.3
temp1-4	1250	58.1
temp1-5	1200	57.9

Middle Zone

The effects associated with the middle zone temperature variations appear to be more pronounced, as shown in Table 6-2. The reasons for this are quite understandable. The middle region is much larger (approximately twenty-four inches in length) than the other two (each approximately six inches in length) as outlined in Chapter II and it is the area where the reactants achieve their greatest contact. Again, the noticeable trend is higher yields as temperature is increased.

Table 6-2. Middle Zone Temperature Variation Effects on Yield

Case Descriptor	Temperature (K)	Yield (%)
temp2-1	1400	64.7
temp2-2	1350	62.3
temp2-3	1300	60.0
temp2-4	1250	58.4
temp2-5	1200	55.1

Rear Zone

Rear zone temperature variation effects were similar to those encountered within the front zone with minimal variation across the temperature range. These results are shown in Table 6-3. Again, higher temperatures appear to result in higher yields. The primary reason for the small variation is more than likely due to the predominant reactant mixing and reaction within the larger middle zone. In addition, by the time the flow reaches this zone, reactant concentrations have decreased and the flow is considerably laminar, lessening the opportunities for further reactant to product conversion.

Table 6-3. Rear Zone Temperature Variation Effects on Yield

Case Descriptor	Temperature (K)	Yield (%)
temp3-1	1400	60.8
temp3-2	1350	59.9
temp3-3	1300	59.3
temp3-4	1250	58.9
temp3-5	1200	58.2

6.3 Reactant Stream Argon Flow Rates

Argon carrier gas flow variations were evaluated for each of the inlet streams. Using the baseline model as a starting point, the carrier gas flow rates were reduced or increased by a percentage of the observed for each individual stream.

Zinc Inlet Argon Flow Rates

Two variations above and below the baseline model were considered with the results shown in Table 6-4. As indicated by the data, lower argon flow rates produced higher yields. These results are quite credible based on collision theory. It is desirable for the zinc and selenium species to interact as frequently as possible. When additional species are introduced and deemed non-essential to the progression of the reaction, the collision frequency of the reactants is effectively reduced and subsequently the yield. While the results show desired lower argon flow rates, graphical output from FLUENT/UNS indicated the potential for zinc inlet plugging under the lower argon flow rate conditions. This tendency was initially addressed in Chapter V and can be observed in Figure 5-8. Due to the limited amount of experimental data obtained from the physical system and the inability to perform more follow-up experiments for further investigation, extensive insight into this problem was not pursued in this thesis. Other colleagues have attempted to resolve this problem and their considerations can be found in Morrison (1998) and Shay (1998).

Table 6-4. Zinc Inlet Argon Flow Rate Effects on Yield

Case Descriptor	Description	Yield (%)
arzn1	Ar (Zn) Flow Rate -50% of BM	64.0
arzn2	Ar (Zn) Flow Rate -25% of BM	59.7
corr1-1	Baseline Model (BM)	58.3
arzn3	Ar (Zn) Flow Rate +25% of BM	56.5
arzn4	Ar (Zn) Flow Rate +50% of BM	55.1

Selenium Inlet Argon Flow Rates

Once again, higher yields can be found due to the reduction of argon flow into the reactor, this time through the selenium inlet. The results are presented in Table 6-5 and are once more in line with those expected from collision theory. Reducing the selenium stream argon flow rates produced no recognizable problems (based on observations within the graphical outputs supplied by FLUENT/UNS) with plugging at the zinc or selenium inlets. All experimental data was obtained with the selenium inlet argon flow rate approximately equal to or slightly higher than the zinc inlet argon flow rate. This provided minimal insight into the effects of unbalanced argon flow rates. While the exact underlying reasons for the nearly equal argon flow rates are essentially unknown, maintaining these rates is perceived to aid in the prevention of plugging at the selenium inlet. While minimal product appears to be produced within the front zone, nozzle plugging due to the product accumulation is deemed a possibility. It is also conjectured that the higher selenium inlet argon flow rates aid in reducing product accumulation on the outside of the zinc inlet exit. These effects, expectedly, were not adequately resolved within the CFD model and need to be further addressed utilizing experimental procedures.

Table 6-5. Selenium Inlet Argon Flow Rate Effects on Yield

Case Descriptor	Description	Yield (%)
arse1	Ar (Se ₂) Flow Rate -50% of BM	61.4
arse2	Ar (Se ₂) Flow Rate -25% of BM	59.3
corr1-1	Baseline Model (BM)	58.3
arse3	Ar (Se ₂) Flow Rate +25% of BM	56.6
arse4	Ar (Se ₂) Flow Rate +50% of BM	55.1

6.4 Reactant Flow Rates

The effects on yield due to reactant stream variations were investigated in this section. The baseline model (case corr1-1) presented in Chapter V was again utilized as the basis for the flow rate variations.

For the case runs developed, a novel approach was applied to correlate inlet temperatures to the boiling induced reactant flow rates. Since each of the reactant boilers were operated under similar conditions (approximately equal argon flow rates), the flow rates were linked to their respective vapor pressures. The functions used to calculate the vapor pressures along with tables of values are located in Appendix B. To illustrate the correlation, the baseline model was considered. Observing the data presented for case BA97202 in Appendix D, the vapor pressure for each reactant stream was evaluated at its respective assumed combined temperature (ACT). When it was desired to increase the flow rate of a reactant with respect to the baseline model, the temperature was iteratively changed until the vapor pressure had increased by a desired percentage. The flow rate was then projected to have increased by an equal amount. While this did not provide an exact representation, it did allow better resolution of the boundary conditions when

compared to the method of changing the reactant flow rates while maintaining the same inlet temperatures.

Zinc Reacant Flow Rates

The zinc inlet stream was the only reactant stream varied while keeping all other parameters at the values specified in the baseline model. Table 6-6 summarizes the data obtained from the investigation. This provided the needed insight into non-stoichiometric flow effects. One interesting result revealed was the large drop in yields associated with excess selenium. There was a significant difference when compared with the excess zinc results. It is known the production process has commonly been used in the past with an excess of selenium reactant. This has apparently been a primary contributor to the characteristic lower yields. In addition, from the trends, it can be observed yields decreased across the range of variations as flows deviated from stoichiometry. Also, from the graphical output, as the zinc flow rates were decreased, potential plugging problems again materialized around the exit of the zinc inlet. This effect can be observed in Figure 6-1 in Section 6.6. Since the figure is associated with an aggressive pursuit of optimal operating conditions, it involved a reduction of the zinc flow rate. As mentioned previously, it was felt more involved experimental endeavors must be pursued and compared with the computational results to resolve the extent of applicability of the computational model to predict this phenomenon.

Table 6-6. Zinc Reactant Flow Rate Effects on Yield

Case Descriptor	Description	Yield (%)
zn1	Zn Flow Rate -50% of BM	50.5
zn2	Zn Flow Rate -25% of BM	56.7
corr1-1	Baseline Model (BM)	58.3
zn3	Zn Flow Rate +25% of BM	57.5
zn4	Zn Flow Rate +50% of BM	55.7

Stoichiometric Reactant Flow Rates

Having determined from the previous study that stoichiometric flows produced higher yields, an investigation was performed on the effects of higher and lower stoichiometric flows. The data is furnished in Table 6-7. For this study, the zinc stream argon mass flow rate was increased to match that of the selenium stream. From the observed data it became obvious that lower stoichiometric flows produced the highest yields. However, as may be anticipated, plugging at the zinc inlet became a problem with the lower flow rates based on the FLUENT/UNS graphical outputs. Some consideration is given to this problem in Section 6.6.

Table 6-7. Stoichiometric Reactant Flow Rate Effects on Yield

Case Descriptor	Description	Yield (%)
stoich1	Stoichiometric Flow -50%	69.6
stoich2	Stoichiometric Flow -25%	63.1
stoich3	Stoichiometric Flow	57.4
stoich4	Stoichiometric Flow +25%	54.0
stoich5	Stoichiometric Flow +50%	50.6

6.5 Comparison of Results

After the completion of the computational investigations, it was perceived that a comparison of results to those obtained by my colleagues would be beneficial. Morrison (1998) performed some data and basic CFD analyses while Shay (1998) carried out interaction analyses on the available experimental data and performed a detailed computational study for a new reactor design. Both utilized a 2-D FLUENT/UNS model. Many of the conclusions arrived at in this chapter and in the works of Morrison (1998) and Shay (1998) are in close agreement with the experimental data (contained within the Eagle-Picher ZnSe synthesis logbooks). Even though limited experimental data was collected, many of the process effects due to the different parameter settings outlined within this chapter were realized within the experimental results.

Analysis of the data contained in this thesis suggests the use of higher zone temperatures to aid in increasing yields. Understandably, the kinetic energies of the molecules would be increased and should result in greater collision efficiency. It is granted however, that operating the reactor at higher temperatures would potentially increase secondary flow behavior due to larger temperature gradients, especially within the front zone of the reactor. Based on the analysis of the limited experimental data, Shay (1998) conjectured that lower furnace temperatures decreased the likelihood of complex body formations (wormholes). It is suggested that more experimental work be carried out to resolve the benefits and disadvantages of utilizing the higher furnace temperatures. Clearly, from the computational data, temperatures have the potential for producing a significant impact on the product yields.

Not surprisingly, Shay (1998) arrived at the same conclusions when compared to those in this thesis on the argon carrier gas flow rates. The lower flow rates produced a noticeable increase in the yields. In addition, his work addressed the complexities encountered with the inlet plugging and complex structure formations. Based on analysis of the experimental data, research group recommendations included a slight increase in the rates currently used to aid in prevention of plugging.

Reactant flow rates, the obvious controlling factors of the overall process, were other facets of the research where agreement was found. Morrison (1998) provided some discussion of the benefits of low stoichiometric flows. He also concluded yields drop off noticeably as flows deviate from stoichiometry. Shay (1998) presented similar conclusions in his work.

6.6 Optimized Model

After completing the computational study and acquiring confidence in the results, a final model was pursued encompassing the determined optimal parameters. While the underlying desired values were quite evident, special attention was given to the location of ZnSe(g) product within the reactor. An iterative process was developed to arrive at a set of conditions conducive to the maximization of yield while considering the potential for plugging. Some of the initial cases showed very favorable yields, however, the graphical output presented evidence of significant ZnSe(g) development within the exit of the zinc inlet. Case runs were continued until substantial intrusion was no longer evident, with the final results shown in Table 6-8. Somewhat conservative temperatures

were used for the zones based on the desired repeated use of the reactor tubes. The final form of the ZnSe(g) concentration contours can be seen in Figure 6-1. The established yield of 66.2 % was a significant improvement over the baseline case (actual percentage improvement of 13.6 %). If improvements such as the ones presented in this section are effectively applied, increased product yields could be realized, subsequently leading to a reduction in hazardous material storage and disposal costs.

Depending on further testing and correlation to the physical system, some interesting potential guidelines can be obtained and process characteristics evaluated. Of particular interest in this research has been the difficulty of accurately predicting the conditions corresponding to the onset of zinc inlet plugging. The current developed computational model shows process tendencies for this occurrence and is consistent with the results obtained from the evaluation of the experimental data. Morrison (1998) considers minimum inlet velocities associated with the plugging phenomena based on the

Table 6-8. Characteristic Values for Optimal Case Opt1

Case Descriptor	opt1
Zone 1 Temperature (K)	1350
Zone 2 Temperature (K)	1350
Zone 3 Temperature (K)	1300
Zn Inlet Temperature (K)	1231
Zn Reactant Flow Rate (kg/s)	3.768E-05
Ar (Zn) Flow Rate (kg/s)	7.891E-06
Zn Inlet Velocity (m/s)	1.881E-01
Se ₂ Inlet Temperature (K)	986
Se ₂ Reactant Flow Rate (kg/s)	4.551E-05
Ar (Se ₂) Flow Rate (kg/s)	7.891E-06
Se ₂ Inlet Velocity (m/s)	9.459E-02
Yield (%)	66.2

experimental data. He arrived at an estimated range of minimum velocities (0.2 to 0.4 m/s) for which probable product nucleation occurs on the exit of the zinc inlet. He also mentions there is unavoidable uncertainty in the determination of these values. Nonetheless, his results are consistent with those obtained with the current computational model. The calculated inlet velocity for the zinc inlet for the optimized case presented was 0.188 m/s (under the lower end of the range). Admittedly, an aggressive approach was utilized with respect to product formation within the reactor as is evident in Figure 6-1. However, the goal was to present an optimal model which provided some initial starting points for much more involved process experimentation.

Research by its very nature is a continual process. Arriving at this final optimal model, exploration was continued to improve the efficiency of the computational model and to provide more verification for the case runs completed. Using the optimal model, a combination of underrelaxation factors were discovered which provided an additional approach to solution convergence. Using the previous procedure, the mesh density was significantly increased in an iterative fashion to aid in obtaining the desired solution convergence and stability. Adjusting the underrelaxation factors to 0.3 for momentum and 0.9 for temperature resulted in favorable convergence based on increasing the default convergence criterion by an order of magnitude. While not investigated, it is probable the new combination of underrelaxation factors would effectively allow a decreased grid density to obtain an adequate solution. The results obtained from this adjusted procedure provided more verification of the current results. The yield obtained by utilizing this procedure was 64.6 % (case opt1mod in Appendix F), providing a percentage difference in yields of -2.42 %. In addition, a completely converged solution using the default

convergence criterion was carried out for the same case disregarding gravity. This (case opt1ng in Appendix F) produced a yield of 65.5 %, providing a difference of only -1.06 %. These results again provided further validation to the computational procedures utilized.

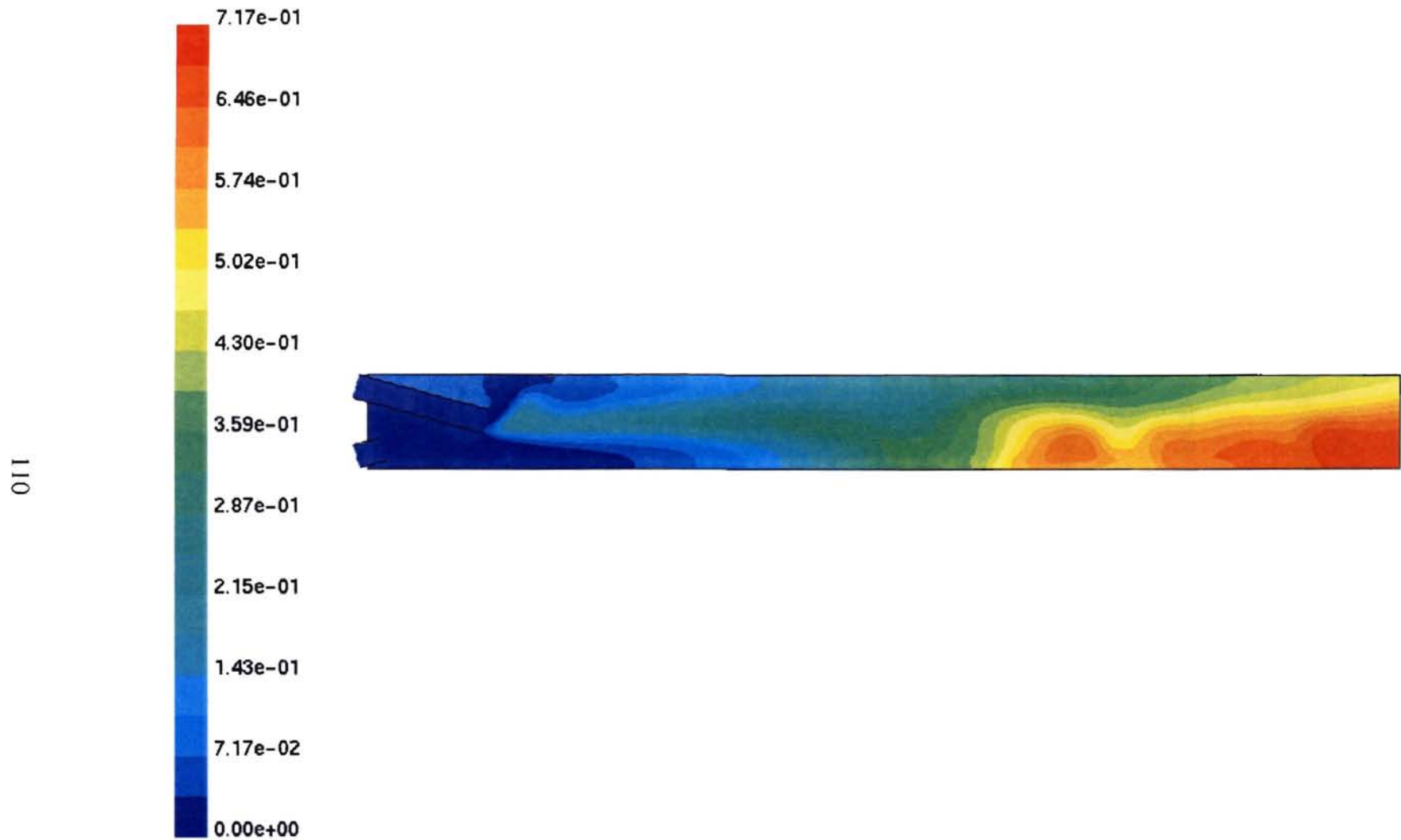


Figure 6-1. Contours of ZnSe Concentration for Optimum Case (kg/m^3)

CHAPTER VII

SUMMARY, CONCLUSIONS, AND RECOMMENDATIONS

7.1 Scope and Purpose Summary

Eagle-Picher, Inc. has developed a unique proprietary process for the production of II-VI compound powders. The current methods of production involve the utilization of a batch-type aerosol reactor that has historically produced erratic and often inadequate results. One of the primary contributors to the problems encountered has been presented as poor process control (primarily with the mass flow). A secondary process inhibitor, as a result of the mass flow control problem, has been the development of plugging difficulties encountered at the exit of the zinc inlet. The past combination of poor process control and the relatively unknown internal effects encountered within the reactor by process adjustment has made it difficult to analyze and optimize production results. Research was performed and documented within this thesis to address many of these issues. The remaining portions of this chapter detail the conclusions and recommendations that emerged during the latter stages of this work.

7.2 Conclusions

The Eagle-Picher process has been optimized throughout its operational history by relying on analysis of historical data and operator's intuition and desire to experiment. However, as alluded to in the previous section, a significant amount of variability was still inherent due to insufficient process control. This made it difficult to assess isolated process parameter effects and to ascertain accurate numerical process quantities (such as mass flow rates).

The 2-D Fluent/UNS computational model was created (with an extensive amount of the information located in Appendix E) and shown to adequately represent the physical reactor configuration. Application of the model, coupled with information from the available literature, allowed a first-level determination of the characteristic kinetic parameters. Based on a second order rate form, values of 6.65×10^7 J/kmol and 3.75×10^4 m³/kmol-s were found for the activation energy and pre-exponential factor, respectively. This model was then applied in a variational study to ascertain optimal operating conditions. The trends indicated higher temperatures coupled with lower reactant and carrier gas flows produced the highest yields. The higher temperatures were associated with increased kinetic energies that subsequently enhanced the molecular collision frequencies. The lower flow rates were associated with longer reactor residence times. Additionally, a graphical relationship between zinc stream mass flow rates and plugging at the exit of the zinc inlet nozzle was developed. Lower flow rates tended to result in a higher likelihood of product nucleation and deposition near the exit of the inlet. Pursuing an aggressive approach based on the results indicated by the variational study

and taking into consideration the location of product near the exit of the zinc inlet, a set of suggested optimal operating values were proposed. These values are summarized in Table 6-8.

7.3 Recommendations

Due to the difficulties encountered with the process parameter evaluations (primarily the mass flow rates and pressures) it is strongly recommended Eagle-Picher update their process control systems and implement many of the improvements proposed in the works by Morrison (1998) and Shay (1998). Once the process enhancements have been made, Eagle-Picher should apply and evaluate the suggested operating conditions summarized in Table 6-8.

Many aspects of the computational model could be improved in future endeavors. At the completion of this thesis, a few additional computational efforts were undertaken to assess possible improvements to the model. A combination of factors contributed to the improvement of solution convergence. They included the choice of a pressure outlet boundary condition at the exit coupled with the adjustment of the momentum and temperature underrelaxation factors to 0.3 and 0.9, respectively. The change in the outlet boundary condition alone did not result in improved convergence when considering the solution scaled residuals. In addition, the boundary condition change tended to provide a slight backflow phenomenon, the likelihood of which remains undetermined in the physical system. Using these changes, coupled with a slightly modified yield calculation procedure, a selection of the process runs was executed again and produced identical

results with respect to the trends. Furthermore, for the optimum case presented in Chapter VI, the product contours around the front of the reactor were nearly identical. All of these results, in addition to those mentioned in Chapters V and VI, strongly support the previous determination that the model effectively provided results well within the variability limits of the physical process. For future analyses, it is suggested more information be obtained from the physical system better resolving inlet flow rates and pressures in addition to possible flow patterns near the exit of the reactor. This would aid in the determination of appropriate geometry considerations and boundary conditions at the entrances and exit of the computational reactor model.

While the applicability of the 2-D model has been presented, further 3-D modeling efforts should be pursued to provide greater insight into the effects of the secondary and transverse flows within the reactor. Work related to these concerns is forthcoming by Nikolic (In progress). Additional computational work could also attempt to address radiation heat transfer and two-phase flow effects. Inclusion of a radiation heat transfer model would increase the heat transfer efficiency throughout the reactor. Application of a radiation model may prove formidable, however, as an initial literature search provided very few radiation thermophysical properties for the materials considered in this thesis. Estimation techniques and formulations will more than likely be required to obtain these properties in the absence of documented values. For two-phase flow issues, gas-solid interactions and subsequent particle deposition could be investigated more thoroughly with advanced models as well. Using the work contained in this thesis as a foundation, these options (as well as others) are available for further exploration.

REFERENCES

- Abid, C. and F. Papini (1997). "Thermal Instabilities in a Mixed Convection Phenomenon: Nonlinear Dynamics," Physical Review E, Vol. 56, No. 6, pp. 6735-6744.
- Abou-Ellail, M. M. M. and S. M. Morcos (1983). "Buoyancy Effects in the Entrance Region of Horizontal Rectangular Channels," Journal of Heat Transfer, Vol. 105, pp.924-928.
- Angermeier, D., R. Monna, A. Slaoui, and J. C. Muller (1997). "Modeling and Analysis of the Silicon Epitaxial Growth with SiHCl_3 in a Horizontal Rapid Thermal Chemical Vapor Deposition Reactor," Journal of the Electrochemical Society, Vol. 144, No. 9, pp. 3256-3261.
- Aoki, T., M. Morita, S. Wickramanayaka, Y. Nakanishi, and Y. Hatanaka (1996). "Growth of ZnSe Thin Films by Radical Assisted MOCVD Method," Applied Surface Science, Vol. 92, pp. 132-137.
- Aven, M. and J. S. Prener (1967). Physics and Chemistry of II-VI Compounds, John Wiley and Sons, New York.
- Bailer, J. C., H. J. Emeleus, R. Nyholm, and A. F. Trotman-Dickenson (Editors) (1973). Comprehensive Inorganic Chemistry, Vol. 2, First Edition, Pergamon, Oxford.
- Barin, I., O. Knacke, and O. Kubaschewski (1977). Thermochemical Properties of Inorganic Substances, Supplement, Springer-Verlag, New York.
- Beiser, A. (1986). Physics, Fourth Edition, Benjamin/Cummings, Menlo Park, California.
- Berkowitz, J. and W. A. Chupka (1966). "Equilibrium Composition of Selenium Vapor; the Thermodynamics of the Vaporization of HgSe, CdSe, and SrSe," Journal of Chemical Physics, Vol. 45, No. 11, pp. 4289-4302.
- Bird, R. B., W. E. Stewart, and E. N. Lightfoot (1960). Transport Phenomena, John Wiley and Sons, New York.

- Bottcher, K. and H. Hartmann (1995). "Zinc Selenide Single Crystal Growth by Chemical Transport Reactions," Journal of Crystal Growth, Vol. 146, pp. 53-58.
- Bottcher, K., H. Hartmann, and R. Rostel (1996). "Influence of Convection on Zinc Selenide Single Crystal Growth by Chemical Vapour Transport," Journal of Crystal Growth, Vol. 159, pp. 161-166.
- Brown, T. L., H. E. LeMay, and B. E. Bursten (1994). Chemistry: The Central Science, Sixth Edition, Prentice Hall, Englewood Cliffs, New Jersey.
- Chang, R. (1991). Chemistry, Fourth Edition, McGraw-Hill, New York.
- Chase, M. W., C. A. Davies, J. R. Downey, D. J. Frurip, R. A. McDonald, and A. N. Syverud (1985). JANAF Thermochemical Tables, Supplement No. 1, Vol. 14, Third Edition, American Chemical Society and American Institute of Physics, New York.
- Chen, Q. (1996). "Rigorous Kinetic Modeling of High-Temperature Reactions," Chemtech, Vol. 26, No. 9, pp. 29-35.
- Collins, D. J., A. J. Strojwas, and D. D. White (1994). "A CFD Model for the PECVD of Silicon Nitride," IEEE Transactions on Semiconductor Manufacturing, Vol. 7, No. 2, pp.176-183.
- Cussler, E. L. (1997). Diffusion: Mass Transfer in Fluid Systems, Second Edition, Cambridge University Press, New York.
- Fluent Inc. (1996a). Fluent GeoMesh Release 3.0 User's Guide, January 12, 1996, Lebanon, New Hampshire.
- Fluent Inc. (1996b). FLUENT/UNS and RAMPANT Release 4.0 User's Guide, Vol. 2, March 28, 1996, Lebanon, New Hampshire.
- Fotiadis, D. I., M. Boekholt, K. F. Jensen, and W. Richter (1990a). "Flow and Heat Transfer in CVD Reactors: Comparison of Raman Temperature Measurements and Finite Model Predictions," Journal of Crystal Growth, Vol. 100, pp. 577-599.
- Fotiadis, D. I., S. Kieda, and K. F. Jensen (1990b). "Transport Phenomena in Vertical Reactors for Metalorganic Vapor Phase Epitaxy," Journal of Crystal Growth, Vol. 102, pp. 441-470.
- Friedlander, S. K. (1977). Smoke, Dust, and Haze: Fundamentals of Aerosol Behavior, John Wiley and Sons, New York.

- Fukuda, T., K. Umetsu, P. Rudolph, H. J. Koh, S. Iida, H. Uchiki, and N. Tsuboi (1996). "Growth and Characterization of Twin-Free ZnSe Single Crystals by the Vertical Bridgman Method," Journal of Crystal Growth, Vol. 161, pp. 45-50.
- Ghajar, A. J., A. H. Johannes, G. L. Foutch, and T. M. Potts (1996). "Proposal: Synthesis Reactor Design for Cadmium and Zinc Selenides," OCAST Applied Research Project AR6-068.
- Giridharan, M. G., S. Lowry, and A. Krishnan (1995). "Coupled Conductive-Convective-Radiative Conjugate Heat Transfer Model for Complex Applications," ASME Paper No. 95-WA/HT-5, Presented at the 1995 ASME International Mechanical Engineering Congress and Exposition, San Francisco, California - November 12-17.
- Gobbert, M. K., T. P. Merchant, L. J. Borucki, and T. S. Cale (1997). "A Multiscale Simulator for Low Pressure Chemical Vapor Deposition," Journal of the Electrochemical Society, Vol. 144, No. 11, pp. 3945-3951.
- Hamill, N. (1996). "CFD Comes of Age in the CPI," Chemical Engineering, Vol. 103, No. 12, pp. 68-72.
- Harris, C. K., D. Roekaerts, F. J. J. Rosendal, F. G. J. Buitendijk, Ph. Daskopoulos, A. J. N. Vreenegoor, and H. Wang (1996). "Computational Fluid Dynamics for Chemical Reactor Engineering," Chemical Engineering Science, Vol. 51, No. 10, pp. 1569-1594.
- Hatanakata, Y., T. Aoki, M. Morita, and Y. Nakanishi (1996). "ZnSe Crystal Growth by Radical Assisted MOCVD," Applied Surface Science, Vol. 100-101, pp. 621-624.
- Heraeus Amersil (1986). "Price List: Fused Silica, Fused Quartz," Heraeus Amersil Incorporated, Sayreville, New Jersey.
- Incropera, F. P. and D. P. DeWitt (1990). Introduction to Heat Transfer, Second Edition, John Wiley and Sons, New York.
- Ishigaki, H. (1997). "The Effect of Buoyancy on Laminar Flow and Heat Transfer in Pipes," JSME International Journal, Series B, Vol. 40, No. 2, pp. 273-280.
- Jensen, K. F. (1989). "Transport Phenomena and Chemical Reaction Issues in OMVPE of Compound Semiconductors," Journal of Crystal Growth, Vol. 98, pp. 148-166.
- Jones, E. R. and R. L. Childers (1990). Contemporary College Physics, Addison-Wesley, Reading, Massachusetts.
- Kaldis, E. (Editor) (1982). Current Topics in Materials Science, Vol. 9, North Holland, Amsterdam.

- Kikuma, I. and T. Shiohara (1996). "Seeded Melt Growth of ZnSe Crystals Under Zn Partial Pressure," Journal of Crystal Growth, Vol. 161, pp. 60-63.
- Kodas, T. T. and S. K. Friedlander (1988). "Design of Tubular Flow Reactors for Monodisperse Aerosol Production," AIChE Journal, Vol. 34, No. 4, pp. 551-557.
- Korostelin, Y. V., V. I. Kozlovsky, A. S. Nasibov, and P. V. Shapkin (1996a). "Vapour Growth of II-VI Solid Solution Single Crystals," Journal of Crystal Growth, Vol. 159, pp.181-185.
- Korostelin, Y. V., V. I. Kozlovsky, A. S. Nasibov, and P. V. Shapkin (1996b). "Vapour Growth and Characterization of Bulk ZnSe Single Crystals," Journal of Crystal Growth, Vol. 161, pp.51-59.
- Kruis, F. E. and L. Falk (1996). "Mixing and Reaction in a Tubular Jet Reactor: A Comparison of Experiments With a Model Based on a Prescribed PDF." Chemical Engineering Science, Vol. 51, No. 10, pp. 2439-2448.
- Kulakov, M. P. and A. V. Fadeev (1981). "Stoichiometry of Zinc Selenide Crystals Obtained From the Melt," Inorganic Materials, Vol. 17, pp. 1156-1160.
- Kyomen, S., T. Usui, M. Fukawa, and M. Ohmi (1996). "Combined Free and Forced Convection for Laminar Steady Flow in Horizontal Tubes," JSME International Journal, Series B, Vol. 39, No. 1, pp. 44-50.
- Levenspiel, O. (1972). Chemical Reaction Engineering, Second Edition, John Wiley and Sons, New York.
- Mathewson, C. H. (1959). Zinc: The Science and Technology of the Metal, Its Alloys and Compounds, Reinhold, New York.
- Morrison, D. R. (1998). "Analysis and Design of a Laminar Flow Reactor for the Production of ZnSe Powders," M. S. Thesis, Department of Chemical Engineering, Oklahoma State University, Stillwater, Oklahoma.
- Morrison, D. R., Z. Nikolic, and C. D. Shay (1997). OCAST Project Summer 1997 Report, Eagle-Picher Inc. internal company correspondence.
- Muranoi, T., T. Shiohara, A. Sotokawa, H. Yoshida, S. Isobe, and N. Kanbe (1995). "Gas Effect on Transport Rates of ZnSe in Closed Ampoules," Journal of Crystal Growth, Vol. 146, pp. 49-52.
- Narusawa, U. (1995). "Buoyancy-Induced Laminar Convective Rolls in Rectangular Geometry," Numerical Heat Transfer, Part A, Vol. 28, pp. 195-213.

- Nikolic, Z. (In Progress). M. S. Thesis, Department of Mechanical and Aerospace Engineering, Oklahoma State University, Stillwater, Oklahoma.
- Outokumpu Research Oy (1997). HSC Chemistry for Windows, Version 3.0, Pori, Finland.
- Perry, R. H. and D. W. Green (1997). Perry's Chemical Engineers' Handbook, Seventh Edition, McGraw-Hill, New York.
- Pratsinis, S. E. (1988). "An Overview of Material Synthesis by Aerosol Processes," AIChE Symposium Series: Fluidization and Fluid-Particle Systems – Fundamentals and Applications, Vol. 85, No. 270, pp. 57-68.
- Pratsinis, S. E., T. T. Kodas, M. P. Dudukovic, and S. K. Friedlander (1986a). "Aerosol Reactor Design: Effect of Reactor Geometry on Powder Production and Vapor Deposition," Powder Technology, Vol. 47, pp. 17-23.
- Pratsinis, S. E., T. T. Kodas, M. P. Dudukovic, and S. K. Friedlander (1986b). "Aerosol Reactor Design: Effect of Reactor Type and Process Parameters on Product Aerosol Characteristics," Industrial and Engineering Chemistry Design and Development, Vol. 25, pp. 634-642.
- Pratsinis, S. E., T. T. Kodas, M. P. Dudukovic, and S. K. Friedlander (1986c). "The Effect of Aerosol Reactor Residence Time Distribution on Product Aerosol Characteristics," Chemical Engineering Science, Vol. 41, No. 4, pp. 693-700.
- Pratsinis, S. E. and S. Vemury (1996). "Particle Formation in Gases: A Review," Powder Technology, Vol. 88, pp. 267-273.
- Ranade, V. V. (1997). "Improve Reactors via CFD," Chemical Engineering, Vol. 104, No.5, pp. 96-102.
- Rau, H. (1978). "Nonstoichiometry of ZnSe and CdSe," Journal of Physics and Chemistry of Solids, Vol. 39, pp. 879-882.
- Rudolph, P., N. Schafer, and T. Fukuda (1995). "Crystal Growth of ZnSe From the Melt," Materials Science and Engineering – Reports: A Review Journal, Vol. R15, No. 3, pp. 85-133.
- Sadakata, M., Y. B. Xu, and A. Harano (1996). "A Systematic Approach for the Design of Aerosol Reactors," Powder Technology, Vol. 88, pp. 261-266.
- Scheele, G. F. and T. J. Hanratty (1963). "Effect of Natural Convection Instabilities on Rates of Heat Transfer at Low Reynolds Numbers," AIChE Journal, Vol. 9, No. 2, pp. 183-185.

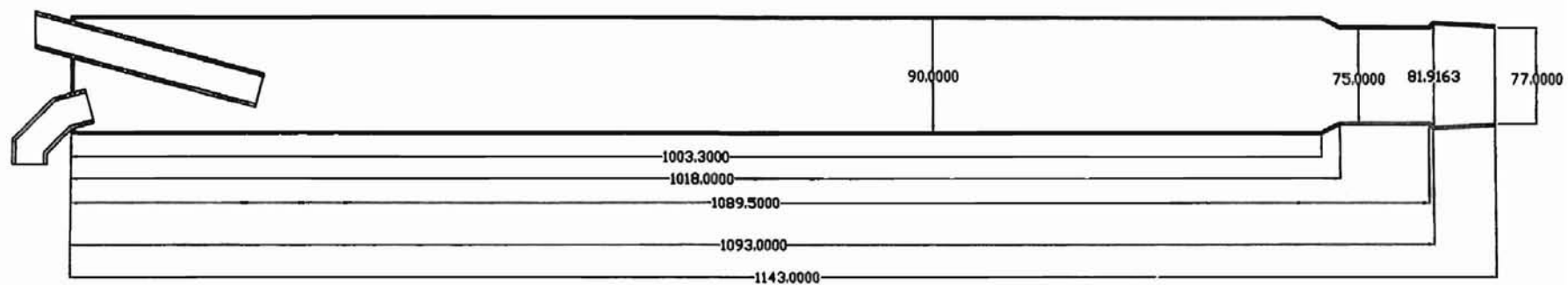
- Schmidt, L. D. (1998). Engineering of Chemical Reactions, Oxford University Press, New York.
- Sha, Y., C. Su, W. Palosz, M. P. Volz, D. C. Gillies, F. R. Szofran, S. L. Lehoczky, H. Liu, and R. F. Brebrick (1995). "Mass Flux of ZnSe by Physical Vapor Transport," Journal of Crystal Growth, Vol. 146, pp. 42-48.
- Shanley, A. (1996). "Pushing the Limits of CFD," Chemical Engineering, Vol. 103, No. 12, pp. 66-67.
- Shay, C. D. (1998). "Design and Optimization of a High Temperature Reactor for the Production of II-VI Compounds via Computer Models and Statistical Experimentation," M. S. Thesis, Department of Chemical Engineering, Oklahoma State University, Stillwater, Oklahoma.
- Sitter, H. (1995). "Hot-Wall Beam Epitaxy and Atomic-Layer Epitaxy of II-VI Compounds for Electronics," Proceedings of the SPIE – The International Society for Optical Engineering, Vol. 2373, pp. 31-38.
- Stamatakis, P., C. A. Natalie, B. R. Palmer, and W. A. Yuill (1991). "Research Needs in Aerosol Processing," Aerosol Science and Technology, Vol. 14, pp. 316-321.
- Su, C. (1987). "Growth Rate of CdS by Vapor Transport in a Closed Ampoule," Journal of Crystal Growth, Vol. 80, pp. 333-342.
- Tinoco, I. T., K. Sauer, and J. C. Wang (1995). Physical Chemistry: Principles and Applications in Biological Sciences, Third Edition, Prentice Hall, Upper Saddle River, New Jersey.
- Touloukian, Y. S., P. E. Liley, and S. C. Saxena (1970a). Thermophysical Properties of Matter: Thermal Conductivity-Nonmetallic Liquids and Gases, Vol. 3, IFI/Plenum, New York.
- Touloukian, Y. S. and T. Makita (1970b). Thermophysical Properties of Matter: Specific Heat-Nonmetallic Liquids and Gases, Vol. 6, IFI/Plenum, New York.
- Touloukian, Y. S., S. C. Saxena, and P. Hestermans (1970c). Thermophysical Properties of Matter: Viscosity, Vol. 11, IFI/Plenum, New York.
- Triboulet, R. (1975). "The Scope of the Low Temperature Growth of Bulk II-VI Compounds," Proceedings of SPIE – The International Society for Optical Engineering, Vol. 2373, pp. 24-30.
- Van Vlack, L. H. (1989). Elements of Materials Science and Engineering, Sixth Edition, Addison-Wesley, Reading, Massachusetts.

- Wilck, M. and F. Stratmann (1997). "A 2-D Multicomponent Modal Aerosol Model and its Application to Laminar Flow Reactors," Journal of Aerosol Science, Vol. 28, No. 6, pp. 959-972.
- Wu, J. J., H. V. Nguyen, and R. C. Flagan (1986). "Synthesis of Fine Powders in Aerosol Reactors," Aerosols: Formation and Reactivity: Proceedings of the Second International Aerosol Conference, Berlin, pp. 910-913.
- Wu, J. J., H. V. Nguyen, R. C. Flagan, K. Okuyama, and Y. Kousaka (1988). "Evaluation and Control of Particle Properties in Aerosol Reactors," AIChE Journal, Vol. 34, No. 8, pp. 1249-1256.
- Xiong, Y. and S. E. Pratsinis (1991). "Gas Phase Production of Particles in Reactive Turbulent Flows," Journal of Aerosol Science, Vol. 22, No. 5, pp. 637-655.
- Yaws, C. L. (1995). Handbook of Vapor Pressure: Inorganic Compounds and Elements, Vol. 4, Gulf, Houston, Texas.

APPENDIX A

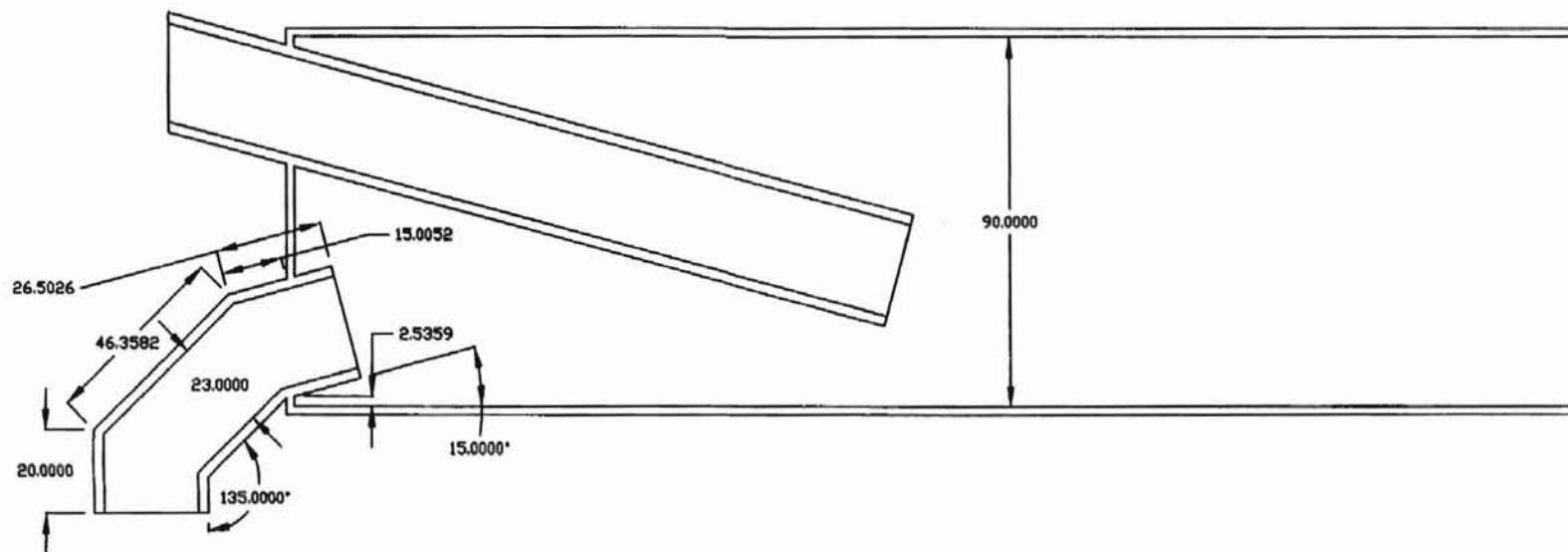
REACTOR AND BOILER DIMENSIONS

This Appendix contains two-dimensional drawings of the general reactor system used during experimental observations. All reactor components (i.e., reactor tube and reactant inlets) are circular in nature with dimensions given at their largest respective cross sections. These dimensions have also been utilized for the computer modeling efforts with minor adaptations.



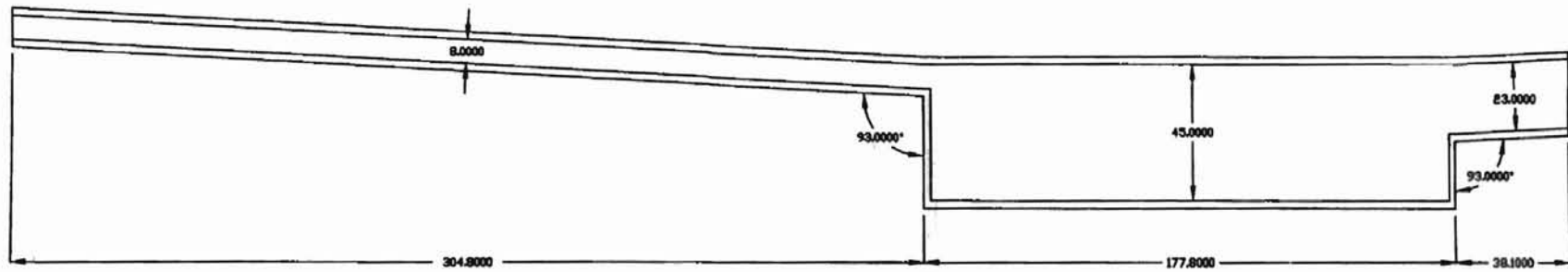
- Notes: (1) All dimensions are in millimeters
(2) The zinc and selenium transfer arm wall thicknesses are 2.5 mm
(3) All other wall thicknesses are 2.0 mm
(4) All tubing entrances and exits are cut parallel to the vertical or horizontal except for the transfer arm exits

Figure A-1. Reactor Tube Dimensions



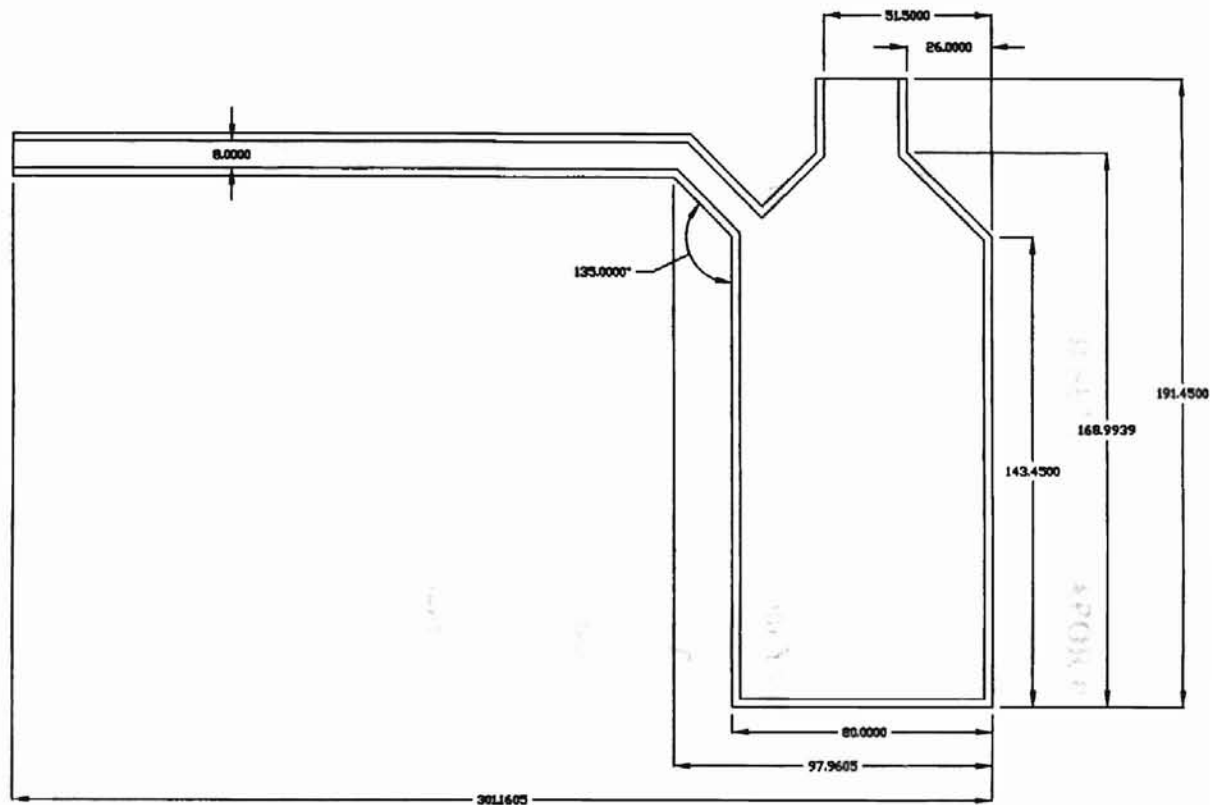
- Notes:
- (1) All dimensions are in millimeters
 - (2) The zinc and selenium transfer arm wall thicknesses are 2.5 mm
 - (3) All other wall thicknesses are 2.0 mm
 - (4) All tubing entrances and exits are cut parallel to the vertical or horizontal except for the transfer arm exits

Figure A-3. Selenium Transfer Arm Dimensions



- Notes:
- (1) All dimensions are in millimeters
 - (2) All wall thicknesses are 2.5 mm
 - (3) All tubing entrances and exits are cut parallel to the vertical or horizontal

Figure A-4. Zinc Boiler Dimensions



- Notes:
- (1) All dimensions are in millimeters
 - (2) All wall thicknesses are 2.5 mm
 - (3) All tubing entrances and exits are cut parallel to the vertical or horizontal

Figure A-5. Selenium Boiler Dimensions

APPENDIX B

ZINC AND SELENIUM VAPOR PRESSURE DATA

Vapor pressure functions and data for the primary materials of research interest are contained within this appendix. Both zinc and selenium vapor pressure functions were evaluated using the following equation from Yaws (1995):

$$\log_{10} P = A + \frac{B}{T} + C \log_{10} T + DT + ET^2 \quad (\text{B-1})$$

where P is for pressure (in mm Hg) and T is for temperature (in K). The coefficients and temperature ranges of applicability are shown below in Table B-1 with numerical data shown in Tables B-2 and B-3 for zinc and selenium, respectively. Please note for some numerical analyses performed within the thesis (Chapter VI) it was necessary to develop vapor pressure data beyond the applicable temperature range for selenium. The obtained results did not appear to deviate from expected results. Vapor pressure estimation techniques, while not included in the thesis, provided an additional means for evaluating the adequacy of the extension beyond the applicable temperature range.

Table B-1. Coefficients and Temperature Ranges for Vapor Pressure Functions (Yaws, 1995)

		Zinc	Selenium
Coefficients	A	-2.0314E+01	9.9457E+02
	B	-4.6362E+03	-4.3994E+04
	C	1.0073E+01	-3.7357E+02
	D	-3.8085E-03	2.2452E-01
	E	4.8860E-07	-5.1145E-05
T _{min} (K)		692.70	397.00
T _{max} (K)		3170.00	930.00

Table B-2. Vapor Pressure of Zinc at Various Temperatures

Temperature (K)	Temperature (°F)	Vapor Pressure (mmHg)	Vapor Pressure (psia)	Vapor Pressure (Pa)
700	800.33	1.97103E-01	3.81134E-03	2.62783E+01
725	845.33	3.96994E-01	7.67658E-03	5.29282E+01
750	890.33	7.63932E-01	1.47720E-02	1.01849E+02
775	935.33	1.41033E+00	2.72712E-02	1.88028E+02
800	980.33	2.50714E+00	4.84801E-02	3.34258E+02
825	1025.33	4.30571E+00	8.32586E-02	5.74048E+02
850	1070.33	7.16428E+00	1.38534E-01	9.55158E+02
875	1115.33	1.15792E+01	2.23905E-01	1.54377E+03
900	1160.33	1.82208E+01	3.52332E-01	2.42924E+03
925	1205.33	2.79726E+01	5.40901E-01	3.72938E+03
950	1250.33	4.19745E+01	8.11652E-01	5.59614E+03
975	1295.33	6.16672E+01	1.19245E+00	8.22162E+03
1000	1340.33	8.88383E+01	1.71785E+00	1.18441E+04
1025	1385.33	1.25667E+02	2.43000E+00	1.67543E+04
1050	1430.33	1.74770E+02	3.37949E+00	2.33008E+04
1075	1475.33	2.39240E+02	4.62613E+00	3.18961E+04
1100	1520.33	3.22684E+02	6.23967E+00	4.30210E+04
1125	1565.33	4.29254E+02	8.30039E+00	5.72292E+04
1150	1610.33	5.63676E+02	1.08997E+01	7.51506E+04
1175	1655.33	7.31266E+02	1.41403E+01	9.74941E+04
1200	1700.33	9.37944E+02	1.81368E+01	1.25049E+05
1225	1745.33	1.19024E+03	2.30154E+01	1.58686E+05
1250	1790.33	1.49530E+03	2.89142E+01	1.99356E+05
1275	1835.33	1.86085E+03	3.59829E+01	2.48093E+05
1300	1880.33	2.29524E+03	4.43825E+01	3.06007E+05
1325	1925.33	2.80736E+03	5.42852E+01	3.74283E+05
1350	1970.33	3.40666E+03	6.58737E+01	4.54183E+05
1375	2015.33	4.10311E+03	7.93409E+01	5.47036E+05
1400	2060.33	4.90718E+03	9.48891E+01	6.54237E+05
1425	2105.33	5.82981E+03	1.12730E+02	7.77244E+05
1450	2150.33	6.88236E+03	1.33083E+02	9.17572E+05
1475	2195.33	8.07660E+03	1.56175E+02	1.07679E+06
1500	2240.33	9.42469E+03	1.82243E+02	1.25652E+06

Table B-3. Vapor Pressure of Selenium at Various Temperatures

Temperature (K)	Temperature (°F)	Vapor Pressure (mmHg)	Vapor Pressure (psia)	Vapor Pressure (Pa)
400	260.33	1.44128E-06	2.78698E-08	1.92155E-04
425	305.33	2.24330E-05	4.33782E-07	2.99082E-03
450	350.33	2.10181E-04	4.06423E-06	2.80219E-02
475	395.33	1.33823E-03	2.58770E-05	1.78416E-01
500	440.33	6.33907E-03	1.22577E-04	8.45140E-01
525	485.33	2.39141E-02	4.62421E-04	3.18828E+00
550	530.33	7.56409E-02	1.46265E-03	1.00846E+01
575	575.33	2.08575E-01	4.03318E-03	2.78078E+01
600	620.33	5.16421E-01	9.98592E-03	6.88505E+01
625	665.33	1.17405E+00	2.27023E-02	1.56527E+02
650	710.33	2.49240E+00	4.81950E-02	3.32293E+02
675	755.33	5.00326E+00	9.67468E-02	6.67046E+02
700	800.33	9.58526E+00	1.85348E-01	1.27793E+03
725	845.33	1.76425E+01	3.41150E-01	2.35214E+03
750	890.33	3.13426E+01	6.06064E-01	4.17867E+03
775	935.33	5.39071E+01	1.04239E+00	7.18702E+03
800	980.33	8.99236E+01	1.73883E+00	1.19888E+04
825	1025.33	1.45604E+02	2.81550E+00	1.94122E+04
850	1070.33	2.28856E+02	4.42534E+00	3.05116E+04
875	1115.33	3.48983E+02	6.74820E+00	4.65272E+04
900	1160.33	5.15767E+02	9.97327E+00	6.87633E+04
925	1205.33	7.37753E+02	1.42658E+01	9.83590E+04

* Note: Validated temperature range of applicability for vapor pressure function is 397 - 930 K

950	1250.33	1.01966E+03	1.97170E+01	1.35944E+05
975	1295.33	1.35919E+03	2.62823E+01	1.81210E+05
1000	1340.33	1.74381E+03	3.37197E+01	2.32489E+05
1025	1385.33	2.14879E+03	4.15507E+01	2.86482E+05
1050	1430.33	2.53748E+03	4.90668E+01	3.38303E+05
1075	1475.33	2.86516E+03	5.54029E+01	3.81989E+05
1100	1520.33	3.08631E+03	5.96792E+01	4.11474E+05

Fig. C.1. The effect of temperature for Reaction (1) $(\text{ZnS}(\text{s}) + \text{O}_2(\text{g}) \rightarrow \text{Zn}(\text{s}) + \text{SO}_2(\text{g}))$
Data from Research Oy, 1997

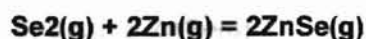
Fig. C.1. The effect of temperature for Reaction (1)

APPENDIX C

HSC CHEMISTRY DATA

Outputs from HSC Chemistry (Outokumpu Research Oy, 1997) are contained in this appendix. This data was used in process evaluation and characterization in Chapter V and Appendix E. Within the provided output, T stands for temperature, ΔH for change in enthalpy, ΔS for the change in entropy, ΔG for the change in Gibbs free energy, and K for the equilibrium constant.

Table C-1. Thermochemical Data for Reaction $\text{Se}_2(\text{g}) + 2\text{Zn}(\text{g}) = 2\text{ZnSe}(\text{g})$
(Outokumpu Research Oy, 1997)



T C	ΔH kcal	ΔS cal	ΔG kcal	K	
0.000	18.094	-16.209	22.522	9.523E-19	
100.000	17.850	-16.970	24.183	6.845E-15	
200.000	17.609	-17.542	25.909	1.075E-12	
300.000	17.373	-17.995	27.687	2.765E-11	
400.000	17.143	-18.366	29.506	2.629E-10	
500.000	16.918	-18.677	31.358	1.365E-09	
600.000	16.699	-18.943	33.239	4.781E-09	
700.000	16.487	-19.173	35.145	1.278E-08	
800.000	16.281	-19.375	37.073	2.814E-08	
900.000	16.081	-19.553	39.020	5.374E-08	
1000.000	15.887	-19.712	40.983	9.210E-08	
1100.000	15.700	-19.853	42.961	1.451E-07	
1200.000	15.519	-19.980	44.953	2.140E-07	
1300.000	15.345	-20.095	46.957	2.992E-07	
1400.000	15.177	-20.199	48.972	4.006E-07	
1500.000	15.015	-20.292	50.996	5.175E-07	
1600.000	14.860	-20.378	53.030	6.489E-07	
1700.000	14.711	-20.455	55.072	7.937E-07	
1800.000	14.568	-20.526	57.121	9.503E-07	
1900.000	14.432	-20.590	59.177	1.117E-06	
2000.000	14.302	-20.648	61.239	1.294E-06	
Se2(g)		Extrapolated from		2000.000 K	
Zn(g)		Extrapolated from		2000.000 K	
ZnSe(g)		Extrapolated from		2000.000 K	
Formula	FM	Conc.	Amount	Amount	Volume
	g/mol	wt-%	mol	g	l or ml
Se2(g)	157.920	54.704	1.000	157.920	22.414 l
Zn(g)	65.380	45.296	2.000	130.760	44.827 l
	g/mol	wt-%	mol	g	l or ml
ZnSe(g)	144.340	100.000	2.000	288.680	44.827 l

Table C-2. Thermochemical Data for Reaction $\text{ZnSe(g)} = \text{ZnSe(s)}$
(Outokumpu Research Oy, 1997)

ZnSe(g) = ZnSe(s)

T C	ΔH kcal	ΔS cal	ΔG kcal	K	
0.000	-94.794	-43.266	-82.976	2.486E+66	
100.000	-94.419	-42.095	-78.711	1.271E+46	
200.000	-94.040	-41.197	-74.548	2.735E+34	
300.000	-93.653	-40.455	-70.467	7.449E+26	
400.000	-93.255	-39.815	-66.454	3.777E+21	
500.000	-92.845	-39.247	-62.501	4.666E+17	
600.000	-92.423	-38.733	-58.603	4.672E+14	
700.000	-91.987	-38.261	-54.753	1.984E+12	
800.000	-91.538	-37.822	-50.949	2.381E+10	
900.000	-91.076	-37.411	-47.188	6.187E+08	
1000.000	-90.600	-37.022	-43.466	2.898E+07	
1100.000	-90.111	-36.652	-39.783	2.150E+06	
1200.000	-89.609	-36.298	-36.136	2.298E+05	
1300.000	-89.092	-35.959	-32.523	3.301E+04	
1400.000	-88.562	-35.633	-28.943	6.038E+03	
1500.000	-88.019	-35.317	-25.396	1.350E+03	
1600.000	-87.462	-35.012	-21.879	3.573E+02	
1700.000	-86.891	-34.715	-18.393	1.090E+02	
1800.000	-86.306	-34.426	-14.936	3.756E+01	
1900.000	-85.708	-34.144	-11.508	1.437E+01	
2000.000	-85.096	-33.869	-8.107	6.019E+00	
ZnSe(g)		Extrapolated from		2000.000	K
ZnSe(s)		Extrapolated from		1300.000	K
Formula	FM	Conc.	Amount	Amount	Volume
	g/mol	wt-%	mol	g	l or ml
ZnSe(g)	144.340	100.000	1.000	144.340	22.414 l
	g/mol	wt-%	mol	g	l or ml
ZnSe(s)	144.340	100.000	1.000	144.340	26.631 ml

Table C-3. Thermochemical Data for Reaction $\text{Zn(s)} + \text{Se(s)} = \text{ZnSe(s)}$
(Outokumpu Research Oy, 1997)



T C	ΔH kcal	ΔS cal	ΔG kcal	K	
0.000	-38.008	-3.280	-37.113	4.973E+29	
100.000	-37.998	-3.242	-36.788	3.534E+21	
200.000	-38.056	-3.376	-36.458	6.946E+16	
300.000	-39.659	-6.602	-35.875	4.796E+13	
400.000	-39.902	-6.991	-35.195	2.678E+11	
500.000	-41.934	-9.909	-34.273	4.885E+09	
600.000	-42.211	-10.246	-33.265	2.123E+08	
700.000	-42.475	-10.532	-32.225	1.729E+07	
800.000	-42.725	-10.777	-31.160	2.220E+06	
900.000	-42.961	-10.987	-30.071	4.004E+05	
1000.000	-43.183	-11.169	-28.963	9.381E+04	
Zn(s)		Extrapolated from		1180.000	K
Se(s)		Extrapolated from		958.000	K
Formula	FM g/mol	Conc. wt-%	Amount mol	Amount g	Volume l or ml
Zn(s)	65.380	45.296	1.000	65.380	9.157 ml
Se(s)	78.960	54.704	1.000	78.960	16.416 ml
ZnSe(s)	g/mol	wt-%	mol	g	l or ml
ZnSe(s)	144.340	100.000	1.000	144.340	26.631 ml

APPENDIX D

CASE PROCESS CHARACTERISTICS

This appendix contains the detailed data used for the correlation of the computational model in Chapter V. These two cases afforded reasonable resolution of boundary conditions and represented favorable results with the experimental system. The temperature setpoints correspond to Eagle-Picher settings for desired reactor zone temperatures. Using an experimental calibrated thermocouple setup, accurate temperature data was obtained for the temperature zones. These were represented as corrected temperatures in the tables. More discussion on the experimental thermocouple setup can be found in Nikolic (In progress). Yields were calculated based on the formulation provided by Schmidt (1998), as presented in Chapter V. As mentioned in the main body of this thesis, there was significant difficulty encountered in resolving mass flow rates. These were estimated using drops in boiler power output readings to estimate the end of the reaction process. More information related to this estimation technique can be found in Morrison (1998). Additional needed information was taken from the outputs provided by the process control systems. All gray fields in the tables represent needed inputs retrieved or estimated from the experimental system while the remaining fields were calculated based on those values. The primary chemical process data is located

within Eagle-Picher ZnSe PVT synthesis logbooks while the presented temperature data can be found in Morrison et al. (1997). Additional discussion is included in Morrison (1998) and Shay (1998).

Vapor pressure data, using the correlation found in Appendix B, was also included for the cases. Under similar conditions, these values provided insight into the mass flow of the reactants. It is desired for the reactants to flow and react in a one to one stoichiometry when considering the reactants as elemental species. Since the inlet mass flow rates were under similar conditions (approximately equal argon mass flow rates), the ratios of the elemental vapor pressures at their respective process temperatures were computed. Values less than one indicated a possible deficiency in zinc as the elements were boiled. Considering the computation for Case BA97202 in Table D-1, a ratio of 0.7284 was obtained, indicating the potential for more selenium reactant to enter the reactor than zinc. This provided interesting results and gave a means of comparison to the conclusion drawn by Morrison (1998). In his work, he performed more involved mass flow analyses and concluded the selenium supply typically ran out when approximately only three-quarters of the zinc supply had been used. The results indicate the necessity for more effective resolution and control of the process mass flow rates.

Table D-1a. Case BA97202 Process Characteristics

Experiment Description		
Run Date	Exp. No./Run No.	Product Lot No.
7/21/97	7/4	BA97202

Yield Data	
Product Collected	Yield
kg	%
0.7473	63.1

Furnace Zone and Time Data						
Front Zone Temperature Setpoint	Front Zone Corrected Temperature	Center Zone Temperature Setpoint	Center Zone Corrected Temperature	Rear Zone Temperature Setpoint	Rear Zone Corrected Temperature	Estimated Run Time
K	K	K	K	K	K	s
1248.15	1273.15	1248.15	1263.15	1198.15	1223.15	13500

Ar (Zn) Stream Properties						
Inlet Temperature	Inlet Flow Meter Reading	Inlet Volumetric Flow Rate	Inlet Volumetric Flow Rate	Density at Inlet Temperature	Mass Flow Rate	Molar Flow Rate
K		mL/min	m ³ /s	kg/m ³	kg/s	kmol/s
298.15	15	303.44	5.0574E-06	1.8329	8.2583E-06	2.0673E-07

Zn Stream Properties			
Inlet Temperature	Initial Charge	Mass Flow Rate	Molar Flow Rate
K	kg	kg/s	kmol/s
1229.15	0.5000	3.7037E-05	5.6640E-07

Ar-Zn Combined Stream Properties						
Combined Mass Flow Rate	Ar Mass Fraction	Zn Mass Fraction	Assumed Combined Temperature (ACT1)	Ar Density at ACT1	Ar Volumetric Flow Rate at ACT1	Zn Density at ACT1
kg/s			K	kg/m ³	m ³ /s	kg/m ³
4.5295E-05	0.1823	0.8177	1229.15	0.3961	2.0850E-05	0.6484

Zn Volumetric Flow Rate at ACT1	Combined Volumetric Flow Rate at ACT1	Inlet Diameter	Cross-Sectional Area	Combined Average Velocity
m ³ /s	m ³ /s	m	m ²	m/s
5.7125E-05	7.7974E-05	0.0230	4.1548E-04	1.8767E-01

Table D-1b. Case BA97202 Process Characteristics

Ar (Se ₂) Stream Properties						
Inlet Temperature	Inlet Flow Meter Reading	Inlet Volumetric Flow Rate	Inlet Volumetric Flow Rate	Density at Inlet Temperature	Mass Flow Rate	Molar Flow Rate
K		mL/min	m ³ /s	kg/m ³	kg/s	kmol/s
298.15	16	305.21	5.0868E-06	1.6329	8.3063E-06	2.0793E-07

Se ₂ Stream Properties			
Inlet Temperature	Initial Charge	Mass Flow Rate	Molar Flow Rate
K	kg	kg/s	kmol/s
997.15	0.6847	5.0719E-05	3.2117E-07

Ar-Se ₂ Combined Stream Properties						
Combined Mass Flow Rate	Ar Mass Fraction	Se ₂ Mass Fraction	Assumed Combined Temperature (ACT2)	Ar Density at ACT2	Ar Volumetric Flow Rate at ACT2	Se ₂ Density at ACT2
kg/s			K	kg/m ³	m ³ /s	kg/m ³
5.9025E-05	0.1407	0.8593	997.15	0.4882	1.7013E-05	1.9301

Se ₂ Volumetric Flow Rate at ACT2	Combined Volumetric Flow Rate at ACT2	Inlet Diameter	Cross-Sectional Area	Combined Average Velocity
m ³ /s	m ³ /s	m	m ²	m/s
2.6277E-05	4.3290E-05	0.0230	4.1548E-04	1.0419E-01

Vapor Pressure Data				
Zn Vapor Pressure at ACT1	Zn Vapor Pressure at ACT1	Se Vapor Pressure at ACT2	Se Vapor Pressure at ACT2	Vapor Pressure Ratio (Zn/Se)
mm Hg	Pa	mm Hg	Pa	
1237.03	164923.30	1698.36	226429.62	0.7284

Notes:

- (1) Argon (Zn) calibration curve used from 7/9/97 in ZnSe PVT synthesis logbooks
- (2) Argon (Se₂) calibration curve used from 7/2/97 in ZnSe PVT synthesis logbooks

Table D-2a. Case BA97195 Process Characteristics

Experiment Description		
Run Date	Exp. No./Run No.	Product Lot No.
7/14/97	4/5	BA97195

Yield Data	
Product Collected	Yield
kg	%
0.6747	56.9

Furnace Zone and Time Data						
Front Zone Temperature Setpoint	Front Zone Corrected Temperature	Center Zone Temperature Setpoint	Center Zone Corrected Temperature	Rear Zone Temperature Setpoint	Rear Zone Corrected Temperature	Estimated Run Time
K	K	K	K	K	K	s
1348.15	1373.15	1348.15	1368.15	1198.15	1293.15	10800

Ar (Zn) Stream Properties						
Inlet Temperature	Inlet Flow Meter Reading	Inlet Volumetric Flow Rate	Inlet Volumetric Flow Rate	Density at Inlet Temperature	Mass Flow Rate	Molar Flow Rate
K		mL/min	m ³ /s	kg/m ³	kg/s	kmol/s
298.15	11	218.68	3.6447E-06	1.6329	5.9514E-06	1.4898E-07

Zn Stream Properties			
Inlet Temperature	Initial Charge	Mass Flow Rate	Molar Flow Rate
K	kg	kg/s	kmol/s
1223.15	0.5007	4.6361E-05	7.0899E-07

Ar-Zn Combined Stream Properties						
Combined Mass Flow Rate	Ar Mass Fraction	Zn Mass Fraction	Assumed Combined Temperature (ACT1)	Ar Density at ACT1	Ar Volumetric Flow Rate at ACT1	Zn Density at ACT1
kg/s			K	kg/m ³	m ³ /s	kg/m ³
5.2313E-05	0.1138	0.8862	1223.15	0.3980	1.4952E-05	0.6515

Zn Volumetric Flow Rate at ACT1	Combined Volumetric Flow Rate at ACT1	Inlet Diameter	Cross-Sectional Area	Combined Average Velocity
m ³ /s	m ³ /s	m	m ²	m/s
7.1157E-05	8.6109E-05	0.0230	4.1548E-04	2.0725E-01

Table D-2b. Case BA97195 Process Characteristics

Ar (Se ₂) Stream Properties						
Inlet Temperature	Inlet Flow Meter Reading	Inlet Volumetric Flow Rate	Inlet Volumetric Flow Rate	Density at Inlet Temperature	Mass Flow Rate	Molar Flow Rate
K		mL/min	m ³ /s	kg/m ³	kg/s	kmol/s
298.15	12	224.96	3.7494E-06	1.6329	6.1225E-06	1.5326E-07

Se ₂ Stream Properties			
Inlet Temperature	Initial Charge	Mass Flow Rate	Molar Flow Rate
K	kg	kg/s	kmol/s
991.15	0.6845	6.33796E-05	4.0134E-07

Ar-Se ₂ Combined Stream Properties						
Combined Mass Flow Rate	Ar Mass Fraction	Se ₂ Mass Fraction	Assumed Combined Temperature (ACT2)	Ar Density at ACT2	Ar Volumetric Flow Rate at ACT2	Se ₂ Density at ACT2
kg/s			K	kg/m ³	m ³ /s	kg/m ³
6.9502E-05	0.0881	0.9119	991.15	0.4912	1.2464E-05	1.9418

Se ₂ Volumetric Flow Rate at ACT2	Volumetric Flow Rate at ACT2	Inlet Diameter	Cross-Sectional Area	Combined Average Velocity
m ³ /s	m ³ /s	m	m ²	m/s
3.2640E-05	4.5104E-05	0.0230	4.1548E-04	1.0856E-01

Vapor Pressure Data				
Zn Vapor Pressure at ACT1	Zn Vapor Pressure at ACT1	Se Vapor Pressure at ACT2	Se Vapor Pressure at ACT2	Vapor Pressure Ratio (Zn/Se)
mm Hg	Pa	mm Hg	Pa	
1169.85	155967.68	1603.78	213819.92	0.7294

Notes:

- (1) Argon (Zn) calibration curve used from 7/9/97 in ZnSe PVT synthesis logbooks
- (2) Argon (Se₂) calibration curve used from 7/2/97 in ZnSe PVT synthesis logbooks

APPENDIX E

FLUENT/UNS CFD MODEL DOCUMENTATION

This appendix chronicles the general approach used for the creation and utilization of the FLUENT/UNS computational model used in this research. Due to the breadth of information considered and the somewhat overwhelming nature of the FLUENT/UNS package documentation, it was not feasible to cover every aspect in detail. Instead, this appendix emphasizes important information and steps critical to efficient model generation. An additional objective was to provide a basic background for future model developments involving similar types of investigations.

Material coverage is separated into topics based on the individual programs included in the FLUENT/UNS package. At the end of the appendix, all properties used in the computational model have been included in tables and the sources indicated.

E.1 DDN

DDN was used to generate the geometry of the 2-D reactor representation. Emphasized in Chapter IV, the geometry is only a means to an end and is eventually discarded once the grid has been generated. Therefore, the geometry was kept simple and the number of entities created minimized. A rendering of the geometry created in DDN

is shown in Figure E-1. The locations of important points within the model have been provided in Table E-1 with enlarged views of the geometry shown in Figures E-2 and E-3. The node numbers provided in Table E-1 correspond to the numbered points in Figures E-2 and E-3. The units used were millimeters. As can be noted on the geometry, there are extra points created that appear to serve no outstanding useful purpose. Indeed, these points are important and when utilized within P-Cube, they indicated the importance of a well-planned CFD analysis.

DDN presents the look and feel of a typical CAD program. It also is operated in similar fashion. More documentation on understanding its capabilities can be found in Fluent Inc. (1996a).

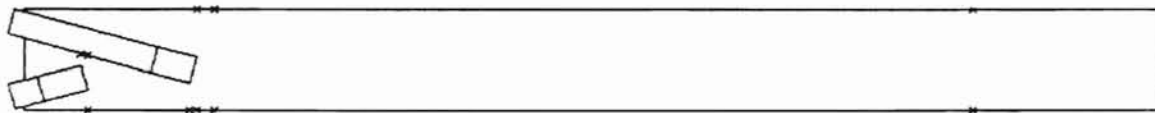


Figure E-1. DDN Model Representation

Table E-1. DDN Geometry Coordinates

Node Number	DDN Coordinates
1	(-9.03 , 89.89)
2	(-14.98 , 67.67)
3	(-14.49 , 22.46)
4	(-8.54 , 0.25)
5	(0.00 , 90.00)
6	(0.00 , 87.47)
7	(0.00 , 63.66)
8	(0.00 , 26.35)
9	(0.00 , 2.54)
10	(0.00 , 0.00)
11	(11.10 , 29.32)
12	(17.06 , 7.11)
13	(49.74 , 50.33)
14	(49.74 , 39.67)
15	(55.69 , 48.73)

Node Number	DDN Coordinates
16	(55.69 , 17.46)
17	(55.69 , 0.00)
18	(117.77 , 55.91)
19	(111.82 , 33.69)
20	(145.63 , 24.64)
21	(145.63 , 0.00)
22	(151.58 , 90.00)
23	(151.58 , 46.85)
24	(151.58 , 0.00)
25	(167.30 , 90.00)
26	(167.30 , 0.00)
27	(836.48 , 90.00)
28	(836.48 , 0.00)
29	(1002.82 , 90.00)
30	(1002.82 , 0.00)

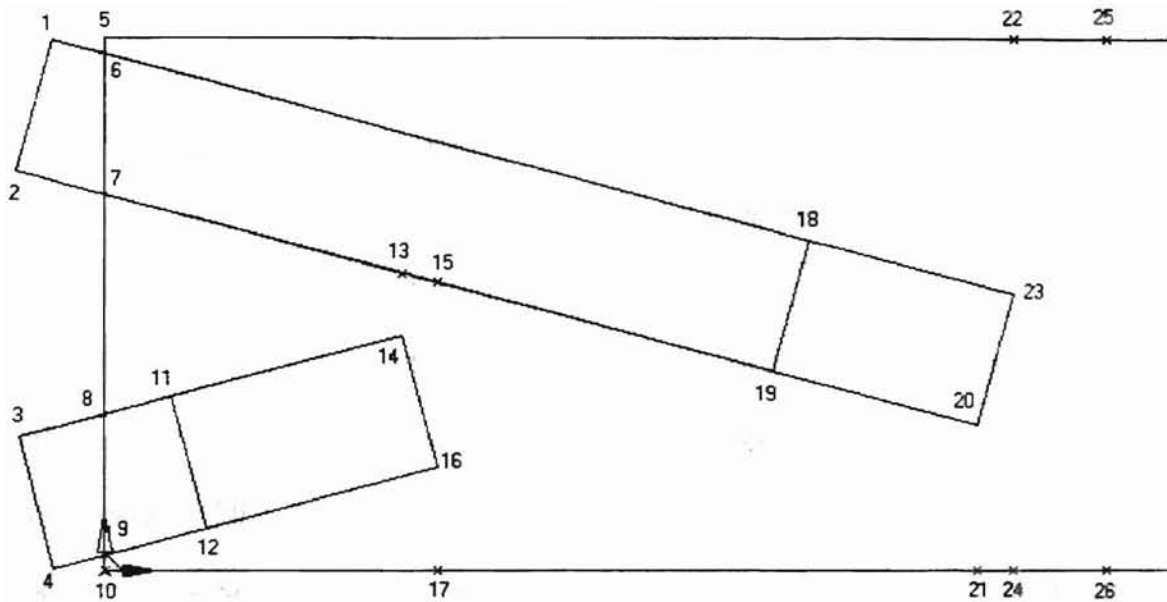


Figure E-2. DDN Geometry – Front of Reactor

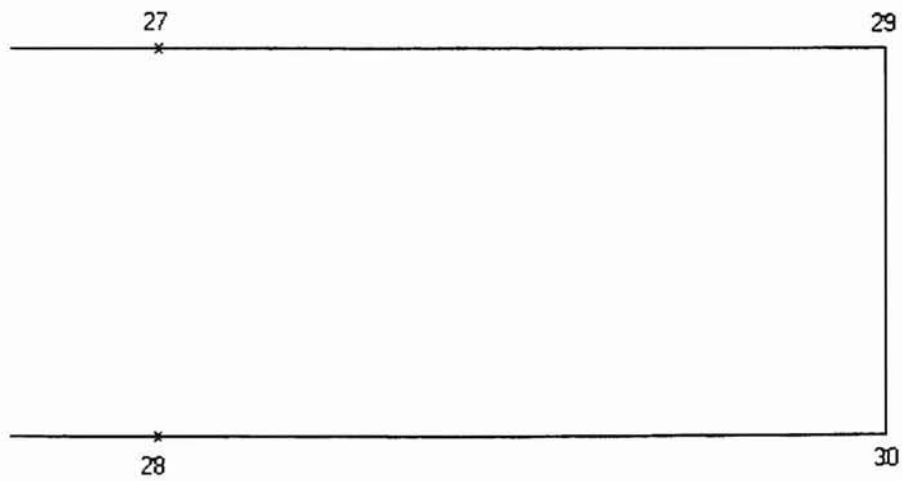


Figure E-3. DDN Geometry – Rear of Reactor

E.2 P-Cube

P-Cube played a critical role in the development of the final CFD model. Within this program, the faces were created, boundary conditions set, node density for the grid specified, and the grid generated.

Utilizing the points and lines provided from DDN, the system of faces were overlaid on the geometry. The result can be seen in Figure E-4. Noticeably, the extra points created in DDN served their purpose. In combination with the tracking tools in P-Cube, they allowed precise alignment of face boundaries around the front of the reactor.

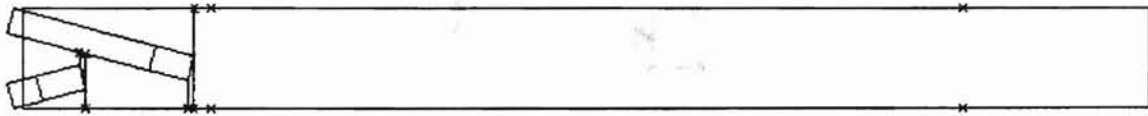


Figure E-4. P-Cube Model Representation

Next, using the panel shown in Figure E-5, boundary conditions for the edges and faces were specified. This panel was accessed from the **B Cond** (in bold to indicate menu choice) pull-down menu. Using procedures outlined in Fluent Inc. (1996a), all edges and faces were designated as shown in Figures E-6 and E-7. The specification system was adopted by the author and indicates the assignments carried out within P-Cube. W1 indicates a wall specification with a zone number of 1. Additionally, VI stood for velocity-inlet and OF for outflow. For the faces, all of the zones were designated as fluid and were indicated by the Z assignment. For example, Z1 refers to fluid zone 1. The reasons for the different zone number specifications encompass the inclusion of

differing boundary conditions and the desire for acquiring numerical information at certain locations or areas within the solver.

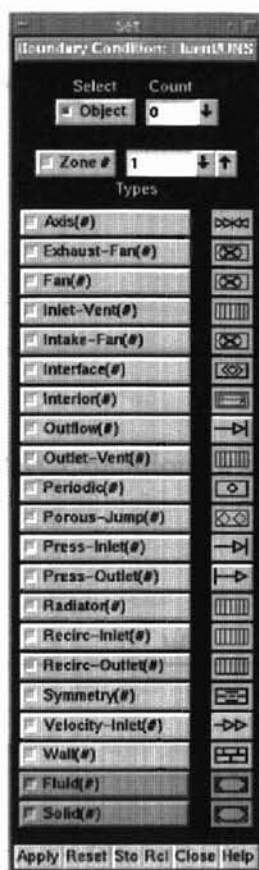


Figure E-5. Boundary Condition Specification Panel

With the boundary conditions panel active and all zones specified, the front of the reactor resembled that shown in Figure E-8. Initially, by default, all edges were wall boundaries indicated by the brick pattern overlaid on top. Note within Figures E-6 and E-8, inlet tube exits and interior edge entities were designated as having no boundary specifications (thus no brick pattern overlaid on them in Figure E-8), indicating their somewhat invisible nature with respect to the solver.

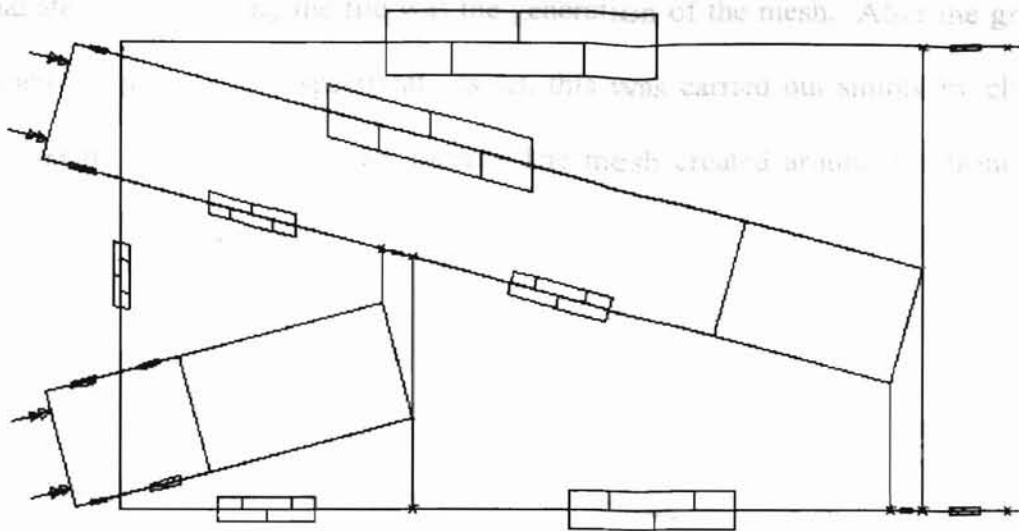


Figure E-8. Rendering of Boundary Conditions in P-Cube

Specifying the node distribution was the next task carried out. The node distributions for each edge of the topology (based on triangular grid elements) was set by use of the panel shown in Figure E-9. It was accessed from the **Bunch** pull-down menu by picking **Bunch (Tri, Tri-Surf) Set**. Each edge of the geometry was selected and the desired number of nodes applied. The final node distribution around the front of the reactor is presented in Figure E-10.



Figure E-9. Bunch Node Distribution Panel

The final step before saving the file was the generation of the mesh. After the grid was determined adequate and all specifications set, this was carried out simply by choosing **Mesh: Create** from the pull-down menu. The mesh created around the front of the reactor is shown in Figure E-11.

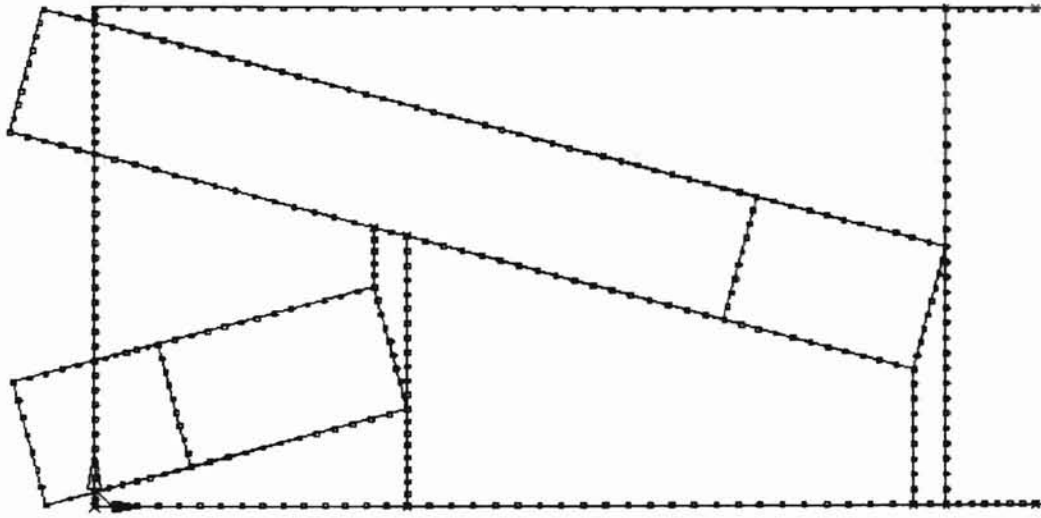


Figure E-10. P-Cube Node Distribution – Front of Reactor

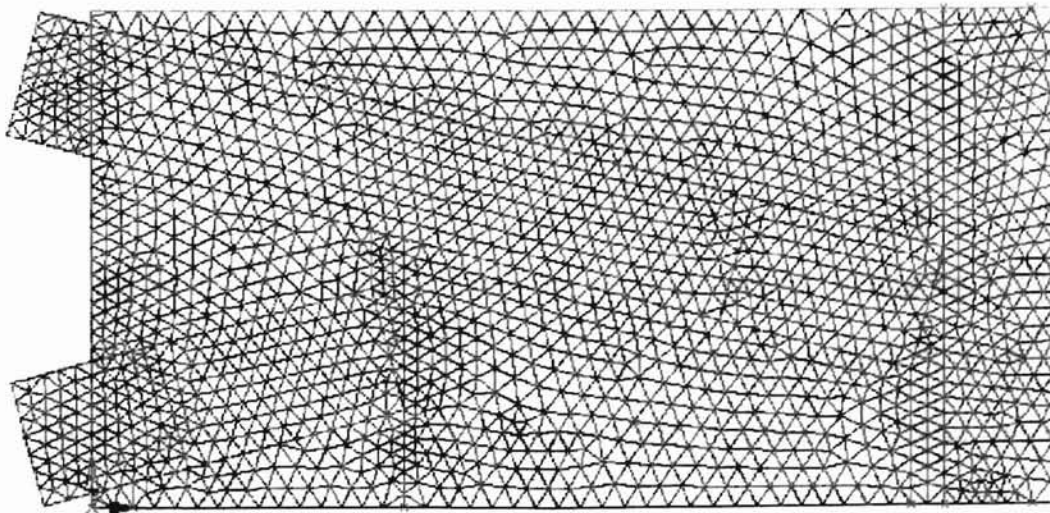


Figure E-11. P-Cube Generated Mesh for Front of Reactor

After all steps were carried out successfully, a viable computational model was achieved. The model as interpreted by solver can be represented by that shown in Figure E-12.



Figure E-12. Final Domain Rendering as Indicated by FLUENT/UNS

E.3 Leo

As explained in Chapter IV, Leo has many tools which allows assessment of the grid quality and potential problems. This tool was of great benefit in the initial learning stages with the FLUENT/UNS package. In the later stages, after grid development skills had improved, this tool was no longer needed. Again, however, its importance in the beginning stages cannot be neglected in troubleshooting tasks.

E.4 FLUENT/UNS

This section documents in detail the steps applied for setting up and running a computational solution in FLUENT/UNS for the research contained in this thesis. The case was created and ran on Oklahoma State University's Tesla unix system (tesla.ceatlabs.okstate.edu). Since the settings applied in FLUENT/UNS can have significant impact on the process solution, it was deemed important to document all the

relevant information. For most of the case runs, default parameters for some of the settings were used. For these occurrences, details of their specific settings are not covered. If users follow the material explained in this section and attempt to apply it elsewhere, be informed that additional parameter adjustment will more than likely be required.

Graphical representations of actual input and information panels have been provided to aid in explanation. These are designated by a number found in brackets located to the left of each panel. Some actions are fairly simple and panels have not been provided for them. They are however still discussed. Additionally, text surrounded by a box indicates a main menu choice and all of the menu choices are shown in bold. Filenames and some button press actions are indicated in quotation marks.

- Load the property database into the solver

File → **Read** → **Scheme** → "probdb.scm"

At this point an error message similar to the following may be encountered:

"ERROR: eval:unbound variable" and "ERROR OBJECT: Mixture-Template"

This appears to be encountered every time and seems to be inconsequential. Click "OK."

- Load the mesh file into the solver

File → **Read** → **Case** → "filename.msh"

- Check the grid

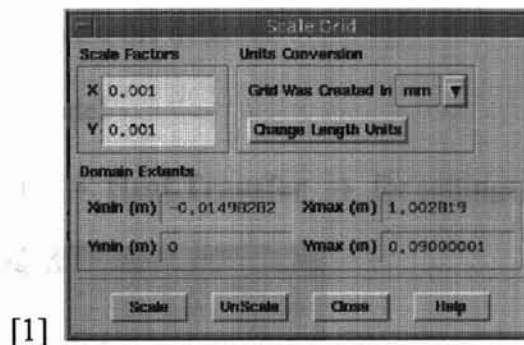
Grid → **Check**

Even if the user has confidence in the developed grid, it is a good idea to check it. Some potential problems that were not discovered earlier may be indicated at this point.

- Scale the grid

Grid → **Scale** → for settings see Panel 1 → “Scale” → “Close”

The scale button is pressed only once, as repeated pressing continues to scale the geometry even further.



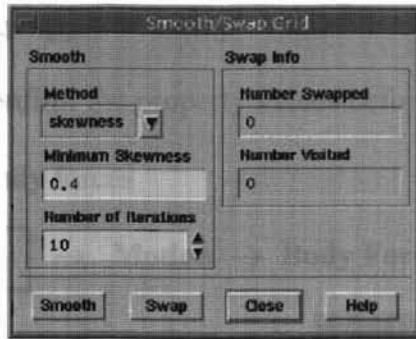
- Smooth the grid

Grid → **Smooth/Swap** → for typical settings see Panel 2 → Execute a few (approximately 2) alternating presses of “Smooth” and “Swap” → “Close”

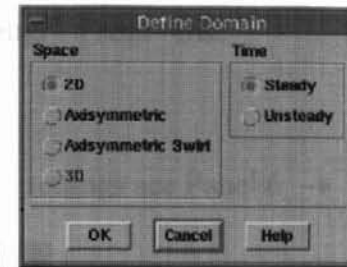
This effectively improves the grid an additional amount within the solver.

- Define the flow domain

Define → **Models** → **Domain** → for settings see Panel 3 → “OK”



[2]



[3]

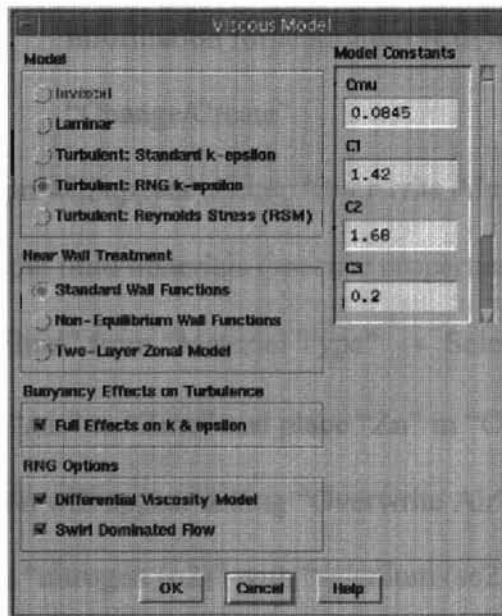
- Define the viscous flow model

Define → **Models** → **Viscous** → for settings see Panel 4 → “OK”

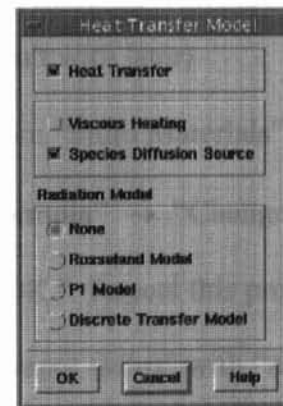
All model constants used were the defaults.

- Define the heat transfer model

Define → **Models** → **Heat Transfer** → for settings see Panel 5 → “OK”



[4]



[5]

- Enable the chemical reaction model

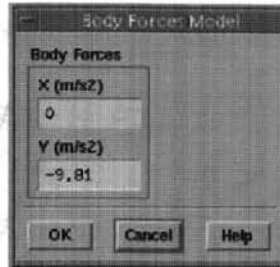
Define → **Models** → **Species Transport** → Select “Finite Rate Reactions”

→ “OK”

A message appears stating “Available material properties or methods have changed. Please confirm the property values before continuing.” Press “OK.”

- Define body forces

Define → **Models** → **Body Forces** → for settings see Panel 6 → “OK”



[6]

- Define quartz solid material

Define → **Materials** → Select “Solid” from “Material Type” → Replace all information for aluminum with that shown in Panel 7 → “Change/Create”

A question will appear asking “Overwrite Aluminum?” Press “OK.”

- Rename the fluid materials (specific properties will be dealt with later)

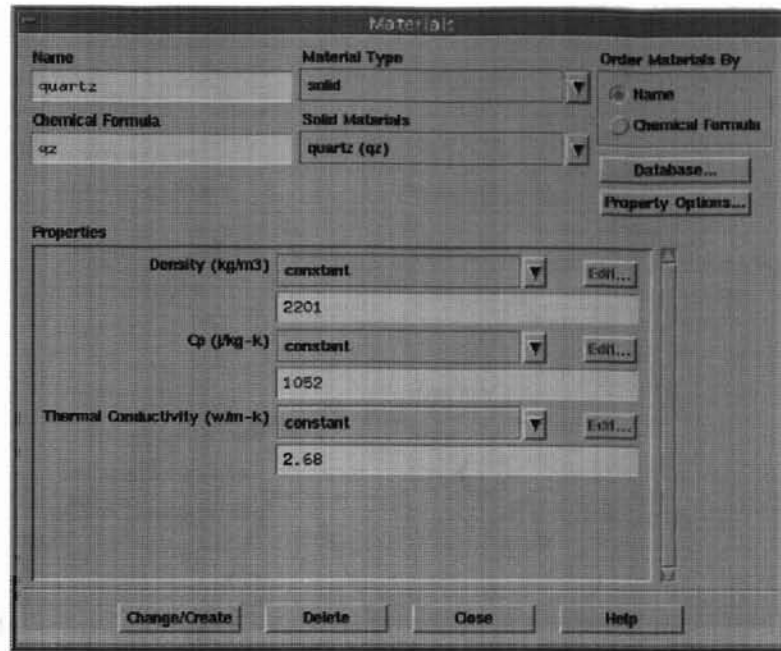
Select “Fluid” from “Material Type” → Select “Air” from “Fluid Materials” →

Rename “Air” to “Zinc” and place “Zn” in “Chemical Formula” → “Change/Create”

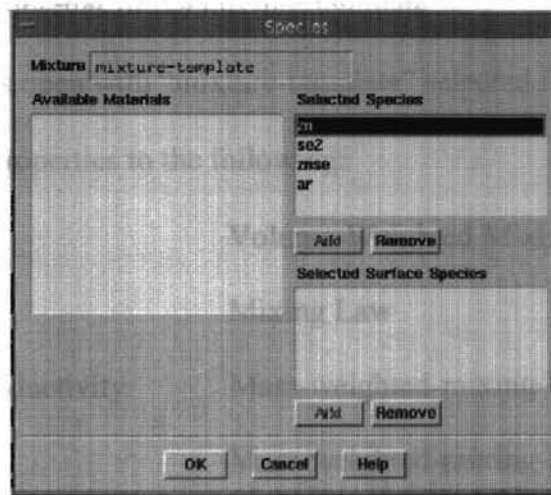
A question will appear asking “Overwrite Air?” Press “OK.” Repeat this procedure replacing “nitrogen (n2)” with “selenium (se2)”, “water-vapor (h2o)” with “zinc-selenide (znse)”, and “oxygen (o2)” with “argon (ar).”

- Select species to participate in simulation

Select “Mixture” from “Material Type” → Select “Edit” to the right of “Mixture Species” → Press “Add” and “Remove” while selecting species until the result shown in Panel 8 is obtained. → “OK”



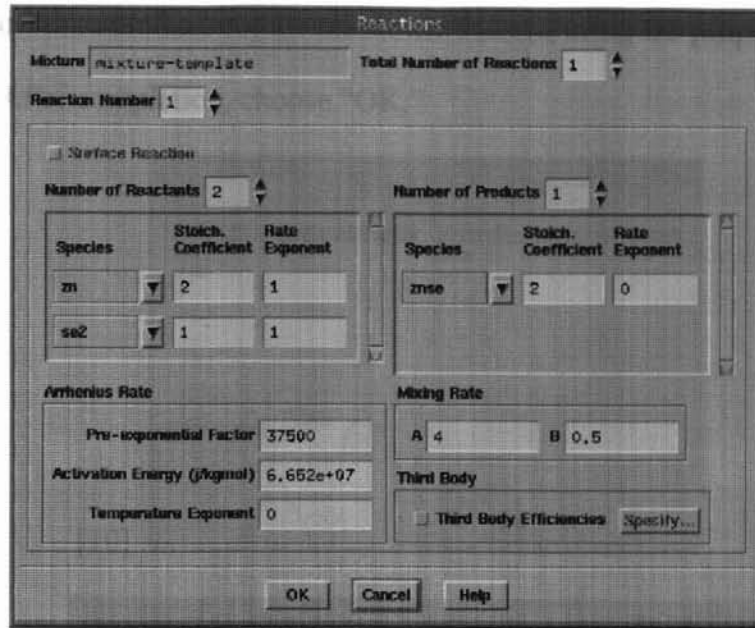
[7]



[8]

- Define the chemical reaction parameters

Select "Edit" to the right of "Reaction Model" → for settings see Panel 9 → "OK"



[9]

- Specify the collective properties of the mixture-template

Verify Materials panel is open with “mixture-template” selected from “Mixture Materials” → Set the properties to the following:

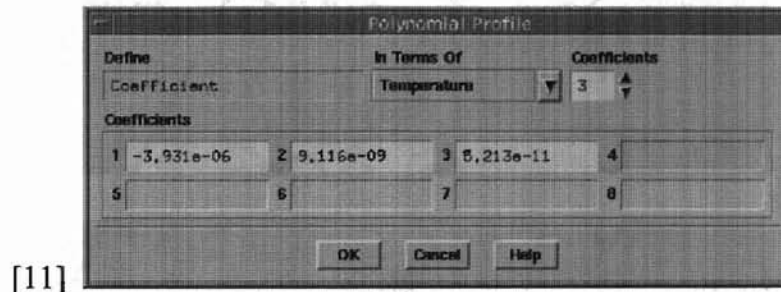
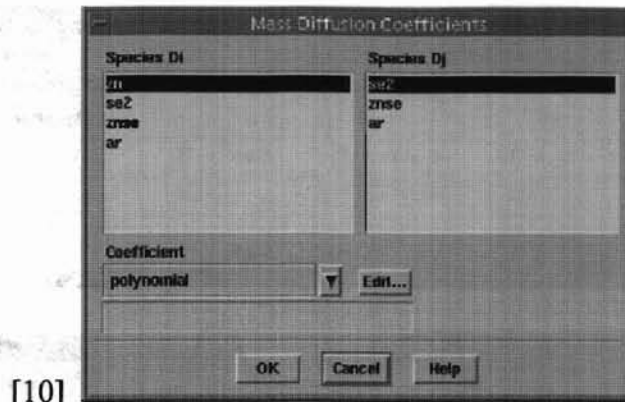
Density:	Volume-Weighted Mixing Law
Cp:	Mixing Law
Thermal Conductivity:	Mass-weighted-mixing-law
Viscosity:	Mass-weighted-mixing-law
Mass Diffusivity:	Multicomponent

After multicomponent mass diffusivities are chosen, the Mass Diffusion Coefficients Panel usually comes open automatically as shown in Panel 10.

- Specify multicomponent mass diffusivities

With species “zn” and “se2” highlighted, select “Polynomial” under “Coefficient” → select “Edit” → Input parameters until the result shown in Panel 11 is achieved. → “OK”

Repeat the procedure until all combinations are defined using the properties found in Section E.5. After completion, choose “OK.”



- Specify individual material properties

Select “Fluid” from “Material Type” → Select “Argon” from “Fluid Materials” →

Set properties to the following using the specified steps:

Density: Polynomial → Edit → Panel 12 → “OK”

Cp: Constant → 520.67

Thermal Conductivity: Polynomial → Edit → Panel 13 → “OK”

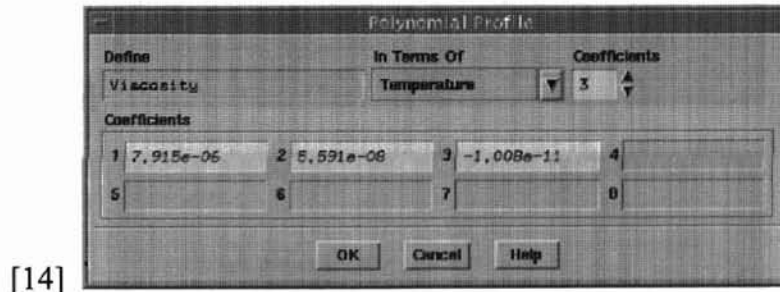
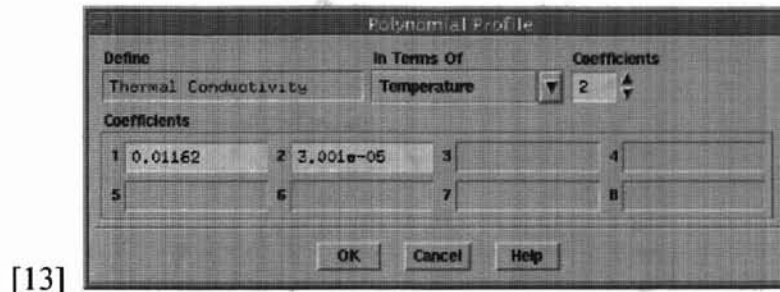
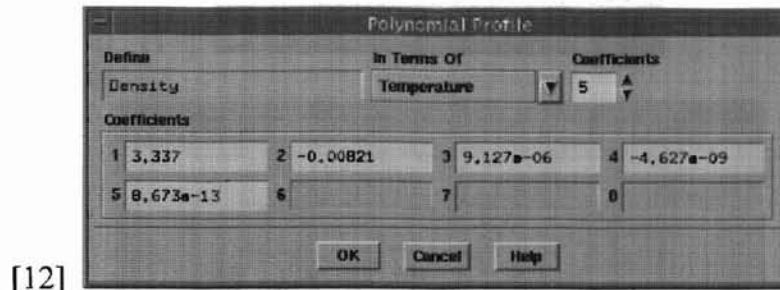
Viscosity: Polynomial → Edit → Panel 14 → “OK”

Molecular Weight: Constant → 39.948

Heat of Formation: Constant → 0

Reference Temperature: Constant → 298.15

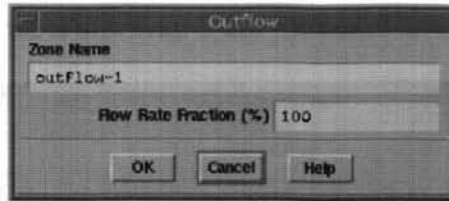
Press “Change/Create.” Repeat procedure until all properties as defined in Section E.5 are specified for all fluid materials. Press “Close” when complete.



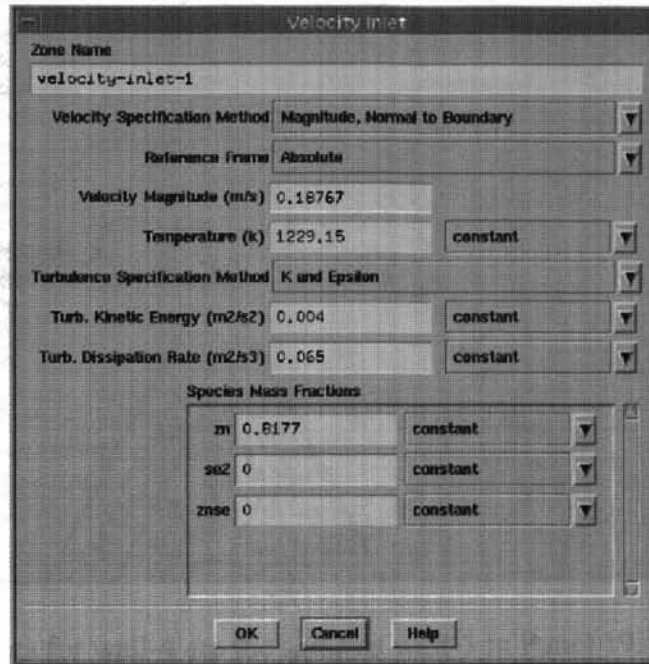
- Specify the boundary conditions

Define → **Boundary Conditions** → Select “Outflow-1” from “Zone” →
 Press “Set...” → See Panel 15 for settings. → “OK”

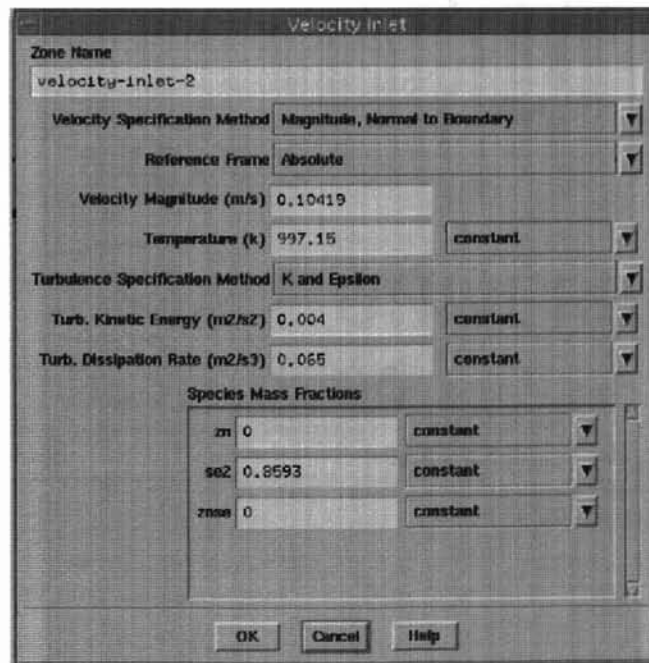
Continue setting boundary conditions (Panels 16 through 22) based on the remaining data. When all is complete, press “Close.”



[15]

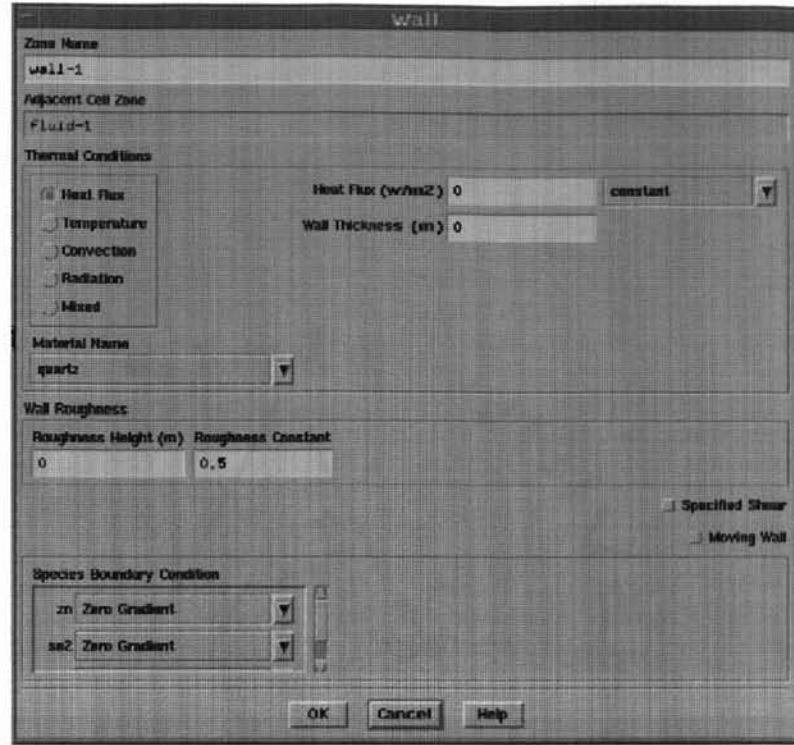


[16]



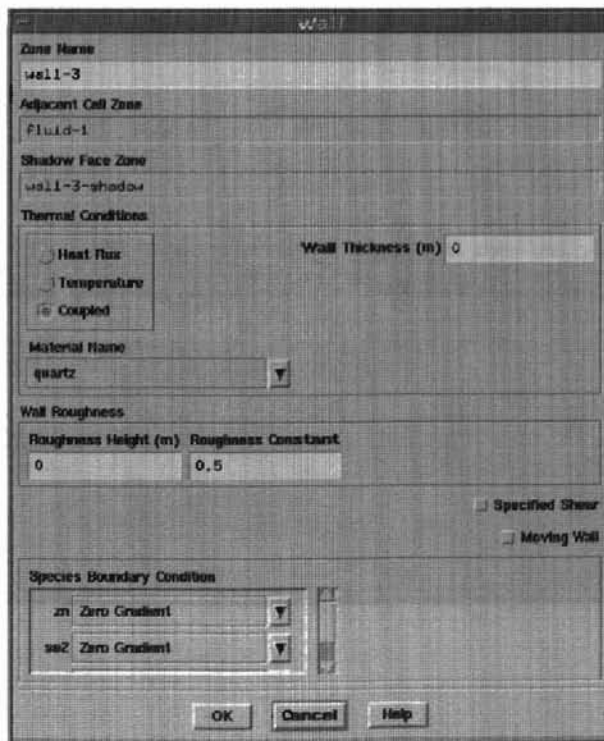
[17]

Note that the settings for wall-2 and wall-5 are the same as wall-1 in Panel 18.



[18]

Note that the settings for wall-4 are the same as wall-3 in Panel 19.



[19]

Zone Name
wall-6

Adjacent Cell Zone
fluid-3

Thermal Conditions

Heat Flux
 Temperature
 Convection
 Radiation
 Mixed

Temperature (K) 1273.15 constant

Wall Thickness (m) 0

Material Name
quartz

Wall Roughness

Roughness Height (m) Roughness Constant

0 0.5

Specified Shear
 Moving Wall

Species Boundary Condition

zn Zero Gradient

so2 Zero Gradient

OK Cancel Help

[20]

Zone Name
wall-7

Adjacent Cell Zone
fluid-3

Thermal Conditions

Heat Flux
 Temperature
 Convection
 Radiation
 Mixed

Temperature (K) 1263.15 constant

Wall Thickness (m) 0

Material Name
quartz

Wall Roughness

Roughness Height (m) Roughness Constant

0 0.5

Specified Shear
 Moving Wall

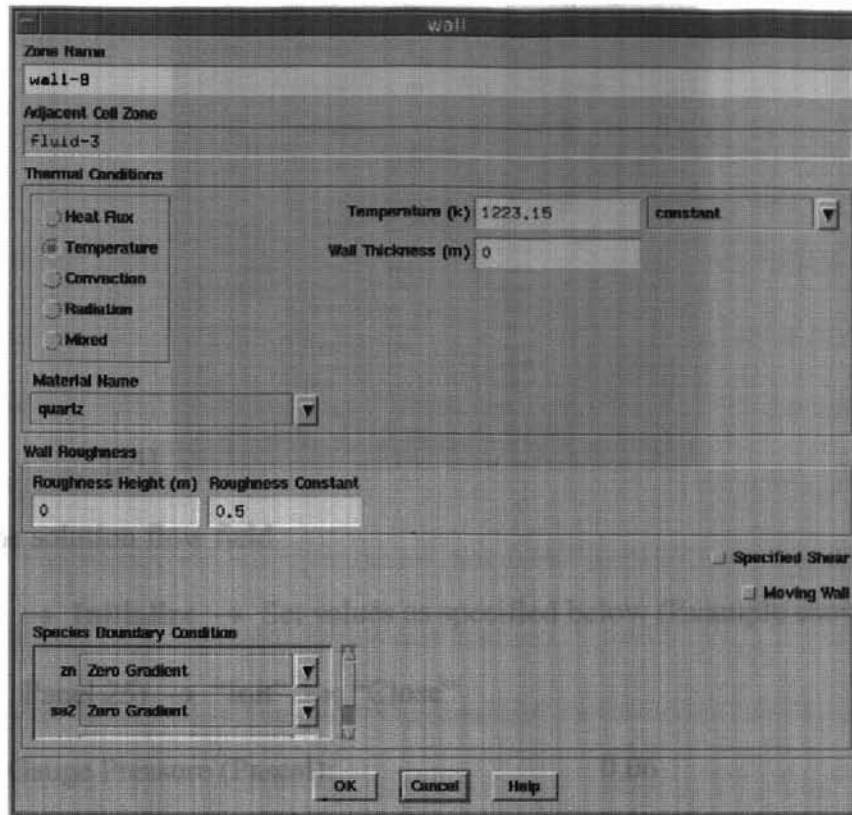
Species Boundary Condition

n Zero Gradient

so2 Zero Gradient

OK Cancel Help

[21]

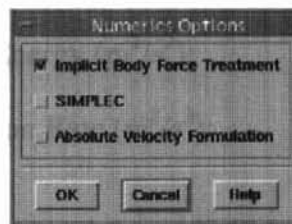


[22]

- Turn on implicit body force treatment since buoyant forces are important

Solve

→ **Controls** → **Numerics** → See Panel 23 for settings. → “OK”



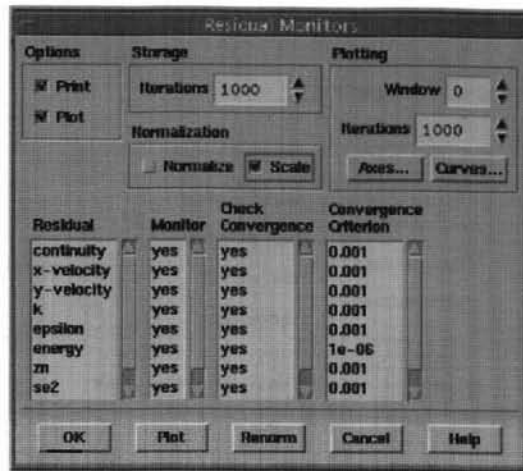
[23]

- Set residual monitoring and convergence properties

Solve

→ **Monitors** → **Residual** → see Panel 24 for settings. → “OK”

For the typical case the default convergence criterion were kept.



[24]

- Initialize the solution flow field

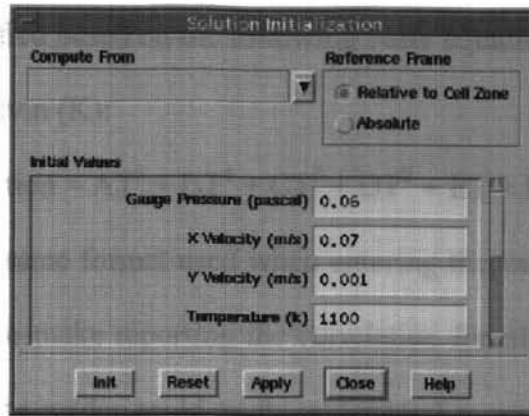
Solve

→ **Initialize** → Set values as specified below (Example shown in

Panel 25) → “Init” → “Close”

Gauge Pressure (Pascal):	0.06
X-velocity (m/s):	0.07
Y-velocity(m/s):	0.002
Temperature (K):	1100
Turbulence Kinetic Energy (m^2/s^2):	0.004
Turbulence Dissipation Rate (m^2/s^3):	0.065
Zn mass fraction:	0.3
Se2 mass fraction:	0.3
ZnSe mass fraction:	0.2

It must be noted the initial starting guesses can be extremely important. Values that deviate largely from those expected in the solution can cause the calculations to diverge or significantly lengthen the solution time.



[25]

- Iterate the solution

Solve → **Iterate** → Set “Number of iterations” to “150” → “Iterate”

- Save solution after desired convergence was attained

File → **Write** → **Case** → “filename.cas”

The procedures described above were used to obtain solutions for the case runs considered in this research. Due to the nature of computational work, the case runs were saved before and after iterating to avoid loss of input data settings and to keep a documented record of the results for further viewing and analysis.

E.5 Thermophysical Properties

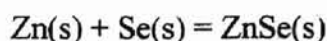
A compilation of thermophysical properties was needed to help complete the computational model. These values were either gathered from various indicated sources or estimated primarily by the use of kinetic theory formulations. Empirical polynomial formulations, when applicable, were created based on the data. The polynomial

coefficients are later specified based on the following basic equation and are a function of temperature in degrees Kelvin (K):

$$\text{Function} = AT^5 + BT^4 + CT^3 + DT^2 + ET + F \quad (\text{E-1})$$

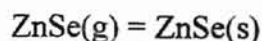
Please note this is not the same format used when entering the values in FLUENT/UNS. The method was adopted to make reporting the correlation function values easier and to provide them in a way so the reader could easily understand as well. Supplied along with the polynomial formulations are statistical correlation factors (indicated as R^2) obtained from Microsoft Excel. These values provide a way of evaluating how well the equations fit the supplied data with a value of 1 indicating an excellent fit. While the list of properties contained in this section is complete for the system under study, a substantial compilation of the available data in the literature can be found in the work by Morrison (1998).

Some of the first values determined for the model inputs were the heats of formation. These are shown in Table E-2 along with the molecular weight of each species. The heat of formation of ZnSe(g) was calculated based on outputs supplied from Outokumpu Research Oy (1997). Interpolating in Table C-3 in Appendix C at 298.15 K (25 °C) for the reaction:



resulted in a ΔH value of -1.591×10^8 J/kmol (corresponding to -38.01 kcal per mole of ZnSe(s) in the table). It is worth noting that Zn(s) and Se(s) are the stable forms of the elements (Kaldis, 1982) and form the basis for determination of the heat of formation. Interpolation was then performed in Table C-2 at 298.15 K (25 °C) to obtain a ΔH value

of -3.965×10^8 J/kmol (corresponding to the value of -94.700 kcal per mole of ZnSe(s) in the table) for the reaction:



Subtracting the second obtained value from the first provided a very reasonable estimate of 2.374×10^8 J/kmol for the heat of formation of ZnSe(g). Nearly identical values were obtained using the available data found in Barin et al. (1977). The related specific heats (c_p) can be found in the remaining portions of this section. The specific heat values were nearly constant across the temperature range considered for Zn(g) and Ar(g). These values were determined to be 317.9 J/kg-K for Zn(g) (Chase et al., 1985) and 520.7 J/kg-K for Ar(g) (Touloukian and Makita, 1970b).

Table E-2. Various Species Properties

Species	MW	Heat of Formation (J/kmol)	Temperature (K)	Source for Heat of Formation
Zn(g)	65.39	1.306×10^8	298.15	Kaldis (1982)
Se ₂ (g)	157.92	1.388×10^8	298.15	Kaldis (1982)
ZnSe(g)	144.35	2.374×10^8	298.15	See appendix text
Ar(g)	39.948	0	298.15	Perry et al. (1997)

Densities for all species involved were calculated based on the ideal gas formulation at standard pressure. Due to the mentioned scarcity of available literature on the subject, little relevant information was found.

Discussion of the viscosities marks the beginning for the utilization of kinetic theory methods for property evaluation. For viscosities, the Chapman-Enskog

formulation for pure monatomic gases at low density was employed (Bird et al., 1960) and is given as:

$$\mu = 2.6693(10^{-6}) \frac{\sqrt{MT}}{\sigma^2 \Omega_\mu} \quad (\text{E-2})$$

where μ is the dynamic viscosity, M is the molecular weight, T is the temperature, σ is known as a characteristic diameter, and Ω_μ is a function of the dimensionless temperature, $\kappa T/\epsilon$. For the dimensionless temperature, κ is the Boltzmann constant and ϵ is considered the maximum attractive energy between two molecules. This formulation has been known to produce favorable results when applied to polyatomic gases as well. Values of σ and ϵ/κ (known as Lennard-Jones parameters) can often be found in the literature for many materials. However, for this research, when the values were not available, Bird et al. (1960) provided techniques for estimation of these parameters. The following were used to calculate the Lennard-Jones parameters for the Zn(g) species (Bird et al., 1960):

$$\epsilon/\kappa = 1.92T_m \quad (\text{E-3})$$

$$\sigma = 1.222\tilde{V}_{m,sol.}^{1/3} \quad (\text{E-4})$$

where T_m is the melting point temperature and $\tilde{V}_{m,sol.}$ is the molar volume of the solid at the melting point. Values of 692.7 K and 9.5739 cm³/mol were arrived at for the melting point temperature and the molar volume of the solid at the melting point, respectively, based on information provided by Mathewson (1959). Calculations then produced values of 1329.89 for ϵ/κ and 2.595 for σ . Further, since adequate information could not be found on which to base an estimate, the Lennard-Jones parameters for Se₂ (g) were assumed for the ZnSe(g) species. All of the Lennard-Jones parameters can be found in

Table E-3 with the final results for the predicted viscosities found in the remaining portions of this appendix.

Table E-3. Lennard-Jones Parameters for Species

Species	σ (Angstroms)	ϵ/k (K)	Source
Zn(g)	2.595	1329.9	See appendix text
Se ₂ (g)	3.576	1130	Sha et al. (1995)
ZnSe(g)	Same as Se ₂ (g)	Same as Se ₂ (g)	
Ar(g)	3.418	124	Bird et al. (1960)

Kinetic theory estimation methods were also utilized to obtain the material thermal conductivities when needed. For monatomic gases at low density, such as Zn(g), a formulation based on Chapman-Enskog theory was once again applied and is given as (Bird et al., 1960):

$$k = 8.3280(10^{-2}) \frac{\sqrt{T/M}}{\sigma^2 \Omega_k} \quad (\text{E-5})$$

where k is the thermal conductivity and Ω_k is a function identical to Ω_μ found in the previous formulation for viscosity. With respect to the polyatomic Se₂(g) species in this research, the Eucken method was applied and is given as (Bird et al., 1960):

$$k = \left(c_p + \frac{5}{4} \frac{R}{M} \right) \mu \quad (\text{E-6})$$

where k is the thermal conductivity, c_p is the specific heat, R is the gas constant, M is the molecular weight, and μ is the dynamic viscosity. Using the values for the viscosities and specific heats, the thermal conductivities were calculated and are presented in the remaining portions of this appendix.

The last remaining parameters to be calculated using the kinetic theory estimation methods were the binary diffusivities. Assuming calculation at standard pressure, all binary diffusivities for all combinations were estimated based on the following formulation presented by Bird et al. (1960):

$$D_{AB} = 1.8583(10^{-7}) \frac{\sqrt{T^3 \left(\frac{1}{M_A} + \frac{1}{M_B} \right)}}{\sigma_{AB} \Omega_{D,AB}} \quad (\text{E-7})$$

where D_{AB} is the binary diffusion coefficient, M_A and M_B stand for the molecular weights of each species A and B, and $\Omega_{D,AB}$ is a molecular property characteristic of the detailed theory. Values for the molecular parameter, $\Omega_{D,AB}$, as a function of the dimensionless temperature ($\kappa T/\epsilon$) are located in sources such as Bird et al. (1960) and Cussler (1997). The needed parameters σ_{AB} and ϵ_{AB} were found based on the following formulations from Bird et al. (1960) for each pair of species:

$$\sigma_{AB} = \frac{1}{2}(\sigma_A + \sigma_B) \quad (\text{E-8})$$

$$\epsilon_{AB} = \sqrt{\epsilon_A \epsilon_B} \quad (\text{E-9})$$

Bird et al. (1960) state that deviation is typically within about 10 percent when this method is used.

FLUENT/UNS provided the means within the program to calculate all the needed values based on kinetic theory. The only needed inputs were the Lennard-Jones parameters. However, the program only provided an “all or nothing” approach and did not allow additional experimentation for some of the values. Therefore, based on the

desired experimentation at the beginning of this research, the empirical polynomial formulations were calculated and manually entered into the computer program.

Quartz

Table E-4. Thermophysical Properties for Quartz (Heraeus Amersil, 1986)

Property	Value	Indicated Evaluation Range
Density (kg/m^3)	2201	None
Specific Heat (J/kg-K)	1052	0... 1173.15 K
Thermal Conductivity (W/m-K)	2.68	1223.15 K

Zinc

Table E-5. Zn(g) Species Ideal Gas Density

Temperature (K)	Density (kg/m^3)	Temperature (K)	Density (kg/m^3)
298	2.674	1150	0.693
300	2.656	1200	0.664
350	2.277	1250	0.638
400	1.992	1300	0.613
450	1.771	1350	0.590
500	1.594	1400	0.569
550	1.449	1450	0.550
600	1.328	1500	0.531
650	1.226	1550	0.514
700	1.138	1600	0.498
750	1.063	1650	0.483
800	0.996	1700	0.469
850	0.938	1750	0.455
900	0.885	1800	0.443
950	0.839	1850	0.431
1000	0.797	1900	0.419
1050	0.759	1950	0.409
1100	0.724	2000	0.398

Table E-6. Zn(g) Species Dynamic Viscosity Based on Chapman-Enskog Theory (Bird et al., 1960)

Temperature (K)	Absolute Viscosity (Pa-s)	Temperature (K)	Absolute Viscosity (Pa-s)
298	1.821E-05	1150	6.335E-05
300	1.831E-05	1200	6.616E-05
350	2.072E-05	1250	6.896E-05
400	2.316E-05	1300	7.176E-05
450	2.564E-05	1350	7.455E-05
500	2.814E-05	1400	7.733E-05
550	3.069E-05	1450	8.009E-05
600	3.326E-05	1500	8.285E-05
650	3.588E-05	1550	8.558E-05
700	3.853E-05	1600	8.830E-05
750	4.121E-05	1650	9.100E-05
800	4.391E-05	1700	9.369E-05
850	4.665E-05	1750	9.635E-05
900	4.940E-05	1800	9.898E-05
950	5.217E-05	1850	1.016E-04
1000	5.495E-05	1900	1.042E-04
1050	5.775E-05	1950	1.068E-04
1100	6.055E-05	2000	1.093E-04

Table E-7. Zn(g) Species Thermal Conductivity Based on Monatomic Theory (Bird et al., 1960)

Temperature (K)	Thermal Conductivity (W/m-K)	Temperature (K)	Thermal Conductivity (W/m-K)
298	8.690E-03	1150	3.023E-02
300	8.736E-03	1200	3.156E-02
350	9.888E-03	1250	3.290E-02
400	1.105E-02	1300	3.424E-02
450	1.223E-02	1350	3.557E-02
500	1.343E-02	1400	3.689E-02
550	1.464E-02	1450	3.821E-02
600	1.587E-02	1500	3.953E-02
650	1.712E-02	1550	4.083E-02
700	1.838E-02	1600	4.213E-02
750	1.966E-02	1650	4.342E-02
800	2.095E-02	1700	4.470E-02
850	2.226E-02	1750	4.597E-02
900	2.357E-02	1800	4.723E-02
950	2.489E-02	1850	4.848E-02
1000	2.622E-02	1900	4.971E-02
1050	2.755E-02	1950	5.094E-02
1100	2.889E-02	2000	5.215E-02

Table E-8. Final Polynomial Coefficients and Constant Values for Zn(g) Species

Property	Units	A	B	C	D	E	F	R ²
Specific Heat	J/kg-K						3.179E+02	None
Density	kg/m ³		1.228E-12	-6.771E-09	1.386E-05	-1.295E-02	5.413E+00	0.998
Viscosity	Pa-s					5.431E-08	1.049E-06	1.000
Thermal Conductivity	W/m-K					2.591E-05	5.003E-04	1.000

Selenium

Table E-9. Se₂(g) Species Specific Heat (Barin, 1977)

Temperature (K)	Specific Heat (J/kg-K)
298	2.598E+02
300	2.600E+02
400	2.660E+02
500	2.679E+02
600	2.681E+02
700	2.676E+02
800	2.667E+02
900	2.655E+02
1000	2.642E+02
1100	2.628E+02

Temperature (K)	Specific Heat (J/kg-K)
1200	2.613E+02
1300	2.598E+02
1400	2.583E+02
1500	2.567E+02
1600	2.551E+02
1700	2.535E+02
1800	2.518E+02
1900	2.502E+02
2000	2.486E+02

Table E-10. Se₂(g) Species Ideal Gas Density

Temperature (K)	Density (kg/m ³)	Temperature (K)	Density (kg/m ³)
298	6.458	1150	1.674
300	6.415	1200	1.604
350	5.499	1250	1.540
400	4.812	1300	1.480
450	4.277	1350	1.426
500	3.849	1400	1.375
550	3.499	1450	1.327
600	3.208	1500	1.283
650	2.961	1550	1.242
700	2.749	1600	1.203
750	2.566	1650	1.166
800	2.406	1700	1.132
850	2.264	1750	1.100
900	2.138	1800	1.069
950	2.026	1850	1.040
1000	1.925	1900	1.013
1050	1.833	1950	0.987
1100	1.750	2000	0.962

Table E-11. Se₂(g) Species Dynamic Viscosity Based on Chapman-Enskog Theory (Bird et al., 1960)

Temperature (K)	Absolute Viscosity (Pa-s)	Temperature (K)	Absolute Viscosity (Pa-s)
298	1.566E-05	1150	5.638E-05
300	1.575E-05	1200	5.885E-05
350	1.792E-05	1250	6.130E-05
400	2.012E-05	1300	6.373E-05
450	2.236E-05	1350	6.615E-05
500	2.464E-05	1400	6.855E-05
550	2.696E-05	1450	7.093E-05
600	2.931E-05	1500	7.329E-05
650	3.169E-05	1550	7.562E-05
700	3.411E-05	1600	7.794E-05
750	3.654E-05	1650	8.022E-05
800	3.900E-05	1700	8.248E-05
850	4.147E-05	1750	8.472E-05
900	4.395E-05	1800	8.694E-05
950	4.644E-05	1850	8.912E-05
1000	4.893E-05	1900	9.129E-05
1050	5.142E-05	1950	9.343E-05
1100	5.390E-05	2000	9.554E-05

Table E-12. $\text{Se}_2(\text{g})$ Species Thermal Conductivity Based on the Eucken Method (Bird et al., 1960)

Temperature (K)	Thermal Conductivity (W/m-K)
298	5.098E-03
300	5.129E-03
400	6.675E-03
500	8.222E-03
600	9.788E-03
700	1.137E-02
800	1.297E-02
900	1.456E-02
1000	1.615E-02
1100	1.771E-02

Temperature (K)	Thermal Conductivity (W/m-K)
1200	1.925E-02
1300	2.075E-02
1400	2.222E-02
1500	2.363E-02
1600	2.501E-02
1700	2.633E-02
1800	2.761E-02
1900	2.885E-02
2000	3.004E-02

Table E-13. Final Polynomial Coefficients and Constant Values for $\text{Se}_2(\text{g})$ Species

Property	Units	A	B	C	D	E	F	R ²
Specific Heat	J/kg-K	2.134E-14	-1.400E-10	3.562E-07	-4.406E-04	2.511E-01	2.159E+02	0.998
Density	kg/m ³		2.965E-12	-1.635E-08	3.347E-05	-3.126E-02	1.307E+01	0.998
Viscosity	Pa-s					4.778E-08	1.086E-06	1.000
Thermal Conductivity	W/m-K					1.492E-05	9.463E-04	0.998

Zinc Selenide

Table E-14. $\text{ZnSe}(\text{g})$ Species Specific Heat (Barin, 1977)

Temperature (K)	Specific Heat (J/kg-K)
298	2.508E+02
300	2.509E+02
400	2.545E+02
500	2.562E+02
600	2.571E+02
700	2.577E+02
800	2.581E+02
900	2.583E+02
1000	2.585E+02
1100	2.587E+02

Temperature (K)	Specific Heat (J/kg-K)
1200	2.588E+02
1300	2.589E+02
1400	2.589E+02
1500	2.590E+02
1600	2.590E+02
1700	2.591E+02
1800	2.591E+02
1900	2.591E+02
2000	2.592E+02

Table E-15. ZnSe(g) Species Ideal Gas Density

Temperature (K)	Density (kg/m ³)	Temperature (K)	Density (kg/m ³)
290	6.066	1150	1.530
300	5.864	1200	1.466
350	5.026	1250	1.407
400	4.398	1300	1.353
450	3.909	1350	1.303
500	3.518	1400	1.257
550	3.199	1450	1.213
600	2.932	1500	1.173
650	2.707	1550	1.135
700	2.513	1600	1.100
750	2.346	1650	1.066
800	2.199	1700	1.035
850	2.070	1750	1.005
900	1.955	1800	0.977
950	1.852	1850	0.951
1000	1.759	1900	0.926
1050	1.675	1950	0.902
1100	1.599	2000	0.880

Table E-16. Final Polynomial Coefficients and Constant Values for ZnSe(g) Species

Property	Units	A	B	C	D	E	F	R ²
Specific Heat	J/kg-K	1.018E-14	-6.661E-11	1.691E-07	-2.086E-04	1.267E-01	2.277E+02	0.998
Density	kg/m ³		2.778E-12	-1.528E-08	3.118E-05	-2.900E-02	1.205E+01	0.998
Viscosity	Pa-s	Same as Se ₂ (g)						
Thermal Conductivity	W/m-K	Same as Se ₂ (g)						

Argon

Table E-17. Ar(g) Species Ideal Gas Density

Temperature (K)	Density (kg/m ³)	Temperature (K)	Density (kg/m ³)
290	1.679	750	0.649
300	1.623	760	0.641
310	1.571	770	0.632
320	1.521	780	0.624
330	1.475	790	0.616
340	1.432	800	0.609
350	1.391	810	0.601
360	1.352	820	0.594
370	1.316	830	0.587
380	1.281	840	0.580
390	1.248	850	0.573
400	1.217	860	0.566
410	1.187	870	0.560
420	1.159	880	0.553
430	1.132	890	0.547
440	1.106	900	0.541
450	1.082	910	0.535
460	1.058	920	0.529
470	1.036	930	0.524
480	1.014	940	0.518
490	0.994	950	0.512
500	0.974	960	0.507
510	0.955	970	0.502
520	0.936	980	0.497
530	0.919	990	0.492
540	0.902	1000	0.487
550	0.885	1050	0.464
560	0.869	1100	0.443
570	0.854	1150	0.423
580	0.839	1200	0.406
590	0.825	1250	0.389
600	0.811	1300	0.375
610	0.798	1350	0.361
620	0.785	1400	0.348
630	0.773	1450	0.336
640	0.761	1500	0.325
650	0.749	1550	0.314
660	0.738	1600	0.304
670	0.727	1650	0.295
680	0.716	1700	0.286
690	0.706	1750	0.278
700	0.696	1800	0.270
710	0.686	1850	0.263
720	0.676	1900	0.256
730	0.667	1950	0.250
740	0.658	2000	0.243

Table E-18. Ar(g) Species Dynamic Viscosity (Touloukian et al., 1970c)

Temperature (K)	Absolute Viscosity (Pa-s)
290	2.209E-05
300	2.272E-05
310	2.333E-05
320	2.394E-05
330	2.454E-05
340	2.513E-05
350	2.572E-05
360	2.629E-05
370	2.686E-05
380	2.742E-05
390	2.797E-05
400	2.852E-05
410	2.906E-05
420	2.959E-05
430	3.012E-05
440	3.064E-05
450	3.116E-05
460	3.167E-05
470	3.217E-05
480	3.267E-05
490	3.316E-05
500	3.365E-05
510	3.410E-05
520	3.460E-05
530	3.510E-05
540	3.560E-05
550	3.600E-05
560	3.650E-05
570	3.690E-05
580	3.740E-05
590	3.780E-05
600	3.830E-05
610	3.870E-05
620	3.910E-05
630	3.960E-05
640	4.000E-05
650	4.040E-05
660	4.090E-05
670	4.130E-05
680	4.170E-05
690	4.210E-05
700	4.250E-05
710	4.290E-05
720	4.330E-05
730	4.370E-05
740	4.410E-05

Temperature (K)	Absolute Viscosity (Pa-s)
750	4.450E-05
760	4.490E-05
770	4.530E-05
780	4.570E-05
790	4.600E-05
800	4.640E-05
810	4.680E-05
820	4.720E-05
830	4.750E-05
840	4.790E-05
850	4.830E-05
860	4.860E-05
870	4.900E-05
880	4.940E-05
890	4.970E-05
900	5.010E-05
910	5.040E-05
920	5.080E-05
930	5.110E-05
940	5.150E-05
950	5.180E-05
960	5.220E-05
970	5.250E-05
980	5.280E-05
990	5.320E-05
1000	5.350E-05
1050	5.520E-05
1100	5.680E-05
1150	5.830E-05
1200	5.990E-05
1250	6.130E-05
1300	6.280E-05
1350	6.420E-05
1400	6.560E-05
1450	6.700E-05
1500	6.840E-05
1550	6.970E-05
1600	7.100E-05
1650	7.230E-05
1700	7.350E-05
1750	7.480E-05
1800	7.600E-05
1850	7.720E-05
1900	7.840E-05
1950	7.950E-05
2000	8.070E-05

Table E-19. Ar(g) Species Thermal Conductivity (Touloukian et al., 1970a)

Temperature (K)	Thermal Conductivity (W/m-K)	Temperature (K)	Thermal Conductivity (W/m-K)
290	1.722E-02	750	3.530E-02
300	1.772E-02	760	3.560E-02
310	1.822E-02	770	3.590E-02
320	1.871E-02	780	3.620E-02
330	1.919E-02	790	3.660E-02
340	1.966E-02	800	3.690E-02
350	2.013E-02	810	3.720E-02
360	2.059E-02	820	3.750E-02
370	2.103E-02	830	3.780E-02
380	2.147E-02	840	3.810E-02
390	2.190E-02	850	3.840E-02
400	2.233E-02	860	3.870E-02
410	2.276E-02	870	3.900E-02
420	2.318E-02	880	3.930E-02
430	2.359E-02	890	3.960E-02
440	2.400E-02	900	3.980E-02
450	2.441E-02	910	4.010E-02
460	2.481E-02	920	4.040E-02
470	2.520E-02	930	4.070E-02
480	2.559E-02	940	4.100E-02
490	2.599E-02	950	4.130E-02
500	2.638E-02	960	4.160E-02
510	2.680E-02	970	4.180E-02
520	2.720E-02	980	4.210E-02
530	2.760E-02	990	4.240E-02
540	2.800E-02	1000	4.270E-02
550	2.830E-02	1050	4.410E-02
560	2.870E-02	1100	4.540E-02
570	2.900E-02	1150	4.680E-02
580	2.940E-02	1200	4.810E-02
590	2.970E-02	1250	4.950E-02
600	3.010E-02	1300	5.080E-02
610	3.050E-02	1350	5.210E-02
620	3.080E-02	1400	5.350E-02
630	3.110E-02	1450	5.480E-02
640	3.150E-02	1500	5.610E-02
650	3.190E-02	1550	5.750E-02
660	3.220E-02	1600	5.880E-02
670	3.260E-02	1650	6.020E-02
680	3.290E-02	1700	6.150E-02
690	3.330E-02	1750	6.280E-02
700	3.360E-02	1800	6.410E-02
710	3.390E-02	1850	6.540E-02
720	3.430E-02	1900	6.670E-02
730	3.460E-02	1950	6.800E-02
740	3.490E-02	2000	6.920E-02

Table E-20. Final Polynomial Coefficients and Constant Values for Ar(g) Species

Property	Units	A	B	C	D	E	F	R ²
Specific Heat	J/kg-K						5.207E+02	None
Density	kg/m ³		8.673E-13	-4.627E-09	9.127E-06	-8.210E-03	3.337E+00	0.998
Viscosity	Pa-s				-1.008E-11	5.591E-08	7.915E-06	0.999
Thermal Conductivity	W/m-K					3.001E-05	1.162E-02	0.991

Binary Diffusivities

Table E-21. Binary Diffusion Coefficients for Ar(g)-Se₂(g) Combination

Temperature (K)	D _{AB} (m ² /s)	Temperature (K)	D _{AB} (m ² /s)
250	6.005E-06	1150	1.114E-04
300	8.688E-06	1200	1.201E-04
350	1.185E-05	1250	1.290E-04
400	1.546E-05	1300	1.382E-04
450	1.949E-05	1350	1.476E-04
500	2.392E-05	1400	1.572E-04
550	2.874E-05	1450	1.671E-04
600	3.395E-05	1500	1.772E-04
650	3.947E-05	1550	1.875E-04
700	4.531E-05	1600	1.980E-04
750	5.151E-05	1650	2.087E-04
800	5.799E-05	1700	2.197E-04
850	6.481E-05	1750	2.309E-04
900	7.187E-05	1800	2.423E-04
950	7.926E-05	1850	2.539E-04
1000	8.691E-05	1900	2.656E-04
1050	9.481E-05	1950	2.775E-04
1100	1.030E-04	2000	2.896E-04

Table E-22. Binary Diffusion Coefficients for Ar(g)-Zn(g) Combination

Temperature (K)	D_{AB} (m^2/s)	Temperature (K)	D_{AB} (m^2/s)
250	8.820E-06	1150	1.671E-04
300	1.277E-05	1200	1.803E-04
350	1.744E-05	1250	1.938E-04
400	2.280E-05	1300	2.077E-04
450	2.879E-05	1350	2.218E-04
500	3.540E-05	1400	2.365E-04
550	4.261E-05	1450	2.514E-04
600	5.040E-05	1500	2.667E-04
650	5.868E-05	1550	2.823E-04
700	6.749E-05	1600	2.983E-04
750	7.674E-05	1650	3.145E-04
800	8.657E-05	1700	3.311E-04
850	9.676E-05	1750	3.481E-04
900	1.074E-04	1800	3.653E-04
950	1.185E-04	1850	3.830E-04
1000	1.302E-04	1900	4.008E-04
1050	1.421E-04	1950	4.191E-04
1100	1.544E-04	2000	4.375E-04

Table E-23. Binary Diffusion Coefficients for ZnSe(g)-Se₂(g) Combination
(Calculated as Se₂(g)-Se₂(g))

Temperature (K)	D_{AB} (m^2/s)	Temperature (K)	D_{AB} (m^2/s)
350	4.083E-06	1200	4.865E-05
400	5.316E-06	1250	5.274E-05
450	6.723E-06	1300	5.700E-05
500	8.298E-06	1350	6.139E-05
550	1.007E-05	1400	6.589E-05
600	1.200E-05	1450	7.056E-05
650	1.412E-05	1500	7.534E-05
700	1.641E-05	1550	8.028E-05
750	1.890E-05	1600	8.536E-05
800	2.155E-05	1650	9.055E-05
850	2.437E-05	1700	9.587E-05
900	2.734E-05	1750	1.014E-04
950	3.051E-05	1800	1.069E-04
1000	3.382E-05	1850	1.126E-04
1050	3.730E-05	1900	1.184E-04
1100	4.093E-05	1950	1.243E-04
1150	4.473E-05	2000	1.303E-04

Table E-24. Binary Diffusion Coefficients for Zn(g)-Se₂(g) Combination

Temperature (K)	D _{AB} (m ² /s)	Temperature (K)	D _{AB} (m ² /s)
400	8.961E-06	1250	8.904E-05
450	1.132E-05	1300	9.619E-05
500	1.398E-05	1350	1.037E-04
550	1.694E-05	1400	1.114E-04
600	2.018E-05	1450	1.194E-04
650	2.373E-05	1500	1.276E-04
700	2.758E-05	1550	1.359E-04
750	3.176E-05	1600	1.447E-04
800	3.624E-05	1650	1.534E-04
850	4.094E-05	1700	1.627E-04
900	4.598E-05	1750	1.720E-04
950	5.130E-05	1800	1.815E-04
1000	5.693E-05	1850	1.913E-04
1050	6.282E-05	1900	2.013E-04
1100	6.896E-05	1950	2.115E-04
1150	7.540E-05	2000	2.219E-04
1200	8.208E-05		

Table E-25. Final Polynomial Coefficients for Binary Diffusivity Combinations

Species	Units	A	B	C	D	E	F	R ²
Ar(g)-Se ₂ (g)	m ² /s				5.284E-11	4.576E-08	-1.138E-05	1.000
Ar(g)-Zn(g)	m ² /s				8.111E-11	6.631E-08	-1.682E-05	1.000
Ar(g)-ZnSe(g)	m ² /s	Same as Ar(g)-Se ₂ (g)						
Zn(g)-Se ₂ (g)	m ² /s				5.213E-11	9.116E-09	-3.931E-06	1.000
Zn(g)-ZnSe(g)	m ² /s	Same as Zn(g)-Se ₂ (g)						
Se ₂ (g)-ZnSe(g)	m ² /s				3.022E-11	6.335E-09	-2.489E-06	1.000

APPENDIX F

COMPUTATIONAL STUDY DATA

This appendix contains all of the boundary condition data entered into the FLUENT/UNS model and the results obtained.

Table F-1a. Computational Study Data

Case Number	Case Descriptor	Explanation	Number of Nodes	Number of Iterations	Front Zone Temperature	Middle Zone Temperature	Rear Zone Temperature
					K	K	K
1	k1-1	Pre-exponential factor = $2 \times 10^4 \text{ m}^3/\text{kmol-s}$	5009	150	1273.15	1263.15	1223.15
2	k1-2	Pre-exponential factor = $4 \times 10^4 \text{ m}^3/\text{kmol-s}$	5009	150	1273.15	1263.15	1223.15
3	k1-3	Pre-exponential factor = $5 \times 10^4 \text{ m}^3/\text{kmol-s}$	5009	150	1273.15	1263.15	1223.15
4	k2-1	Pre-exponential factor = $5 \times 10^4 \text{ m}^3/\text{kmol-s}$	5009	150	1373.15	1368.15	1293.15
5	k2-2	Pre-exponential factor = $2.5 \times 10^4 \text{ m}^3/\text{kmol-s}$	5009	150	1373.15	1368.15	1293.15
6	corr1-1	Pre-exponential factor = $3.75 \times 10^4 \text{ m}^3/\text{kmol-s}$	5009	150	1273.15	1263.15	1223.15
7	corr2-1	Pre-exponential factor = $3.75 \times 10^4 \text{ m}^3/\text{kmol-s}$	5009	150	1373.15	1368.15	1293.15
8	nograv	Gravity Effects Turned Off	5009	130	1273.15	1263.15	1223.15
9	temp1-1	Front Zone Temperature Variation	5009	150	1400	1263.15	1223.15
10	temp1-2	Front Zone Temperature Variation	5009	150	1350	1263.15	1223.15
11	temp1-3	Front Zone Temperature Variation	5009	150	1300	1263.15	1223.15
12	temp1-4	Front Zone Temperature Variation	5009	150	1250	1263.15	1223.15
13	temp1-5	Front Zone Temperature Variation	5009	150	1200	1263.15	1223.15
14	temp2-1	Middle Zone Temperature Variation	5009	150	1273.15	1400	1223.15
15	temp2-2	Middle Zone Temperature Variation	5009	150	1273.15	1350	1223.15
16	temp2-3	Middle Zone Temperature Variation	5009	150	1273.15	1300	1223.15
17	temp2-4	Middle Zone Temperature Variation	5009	150	1273.15	1250	1223.15
18	temp2-5	Middle Zone Temperature Variation	5009	150	1273.15	1200	1223.15
19	temp3-1	Rear Zone Temperature Variation	5009	150	1273.15	1263.15	1400
20	temp3-2	Rear Zone Temperature Variation	5009	150	1273.15	1263.15	1350
21	temp3-3	Rear Zone Temperature Variation	5009	150	1273.15	1263.15	1300
22	temp3-4	Rear Zone Temperature Variation	5009	150	1273.15	1263.15	1250
23	temp3-5	Rear Zone Temperature Variation	5009	150	1273.15	1263.15	1200

Table F-1b. Computational Study Data (Continued)

Case Number	Zn Inlet Temperature	Zn Mass Flow Rate	Ar (Zn) Mass Flow Rate	Zn Mass Fraction	Ar (Zn) Mass Fraction	Zn Inlet Velocity	Se ₂ Inlet Temperature	Se ₂ Mass Flow Rate	Ar (Se ₂) Mass Flow Rate	Se ₂ Mass Fraction	Ar (Se ₂) Mass Fraction	Se ₂ Inlet Velocity
	K	kg/s	kg/s			m/s	K	kg/s	kg/s			m/s
1	1229.15	3.7037E-05	8.2583E-06	0.8177	0.1823	1.8767E-01	997.15	5.0719E-05	8.3063E-06	0.8593	0.1407	1.0419E-01
2	1229.15	3.7037E-05	8.2583E-06	0.8177	0.1823	1.8767E-01	997.15	5.0719E-05	8.3063E-06	0.8593	0.1407	1.0419E-01
3	1229.15	3.7037E-05	8.2583E-06	0.8177	0.1823	1.8767E-01	997.15	5.0719E-05	8.3063E-06	0.8593	0.1407	1.0419E-01
4	1223.15	4.6361E-05	5.9514E-06	0.8862	0.1138	2.0725E-01	991.15	6.3380E-05	6.1225E-06	0.9119	0.0881	1.0856E-01
5	1223.15	4.6361E-05	5.9514E-06	0.8862	0.1138	2.0725E-01	991.15	6.3380E-05	6.1225E-06	0.9119	0.0881	1.0856E-01
6	1229.15	3.7037E-05	8.2583E-06	0.8177	0.1823	1.8767E-01	997.15	5.0719E-05	8.3063E-06	0.8593	0.1407	1.0419E-01
7	1223.15	4.6361E-05	5.9514E-06	0.8862	0.1138	2.0725E-01	991.15	6.3380E-05	6.1225E-06	0.9119	0.0881	1.0856E-01
8	1229.15	3.7037E-05	8.2583E-06	0.8177	0.1823	1.8767E-01	997.15	5.0719E-05	8.3063E-06	0.8593	0.1407	1.0419E-01
9	1229.15	3.7037E-05	8.2583E-06	0.8177	0.1823	1.8767E-01	997.15	5.0719E-05	8.3063E-06	0.8593	0.1407	1.0419E-01
10	1229.15	3.7037E-05	8.2583E-06	0.8177	0.1823	1.8767E-01	997.15	5.0719E-05	8.3063E-06	0.8593	0.1407	1.0419E-01
11	1229.15	3.7037E-05	8.2583E-06	0.8177	0.1823	1.8767E-01	997.15	5.0719E-05	8.3063E-06	0.8593	0.1407	1.0419E-01
12	1229.15	3.7037E-05	8.2583E-06	0.8177	0.1823	1.8767E-01	997.15	5.0719E-05	8.3063E-06	0.8593	0.1407	1.0419E-01
13	1229.15	3.7037E-05	8.2583E-06	0.8177	0.1823	1.8767E-01	997.15	5.0719E-05	8.3063E-06	0.8593	0.1407	1.0419E-01
14	1229.15	3.7037E-05	8.2583E-06	0.8177	0.1823	1.8767E-01	997.15	5.0719E-05	8.3063E-06	0.8593	0.1407	1.0419E-01
15	1229.15	3.7037E-05	8.2583E-06	0.8177	0.1823	1.8767E-01	997.15	5.0719E-05	8.3063E-06	0.8593	0.1407	1.0419E-01
16	1229.15	3.7037E-05	8.2583E-06	0.8177	0.1823	1.8767E-01	997.15	5.0719E-05	8.3063E-06	0.8593	0.1407	1.0419E-01
17	1229.15	3.7037E-05	8.2583E-06	0.8177	0.1823	1.8767E-01	997.15	5.0719E-05	8.3063E-06	0.8593	0.1407	1.0419E-01
18	1229.15	3.7037E-05	8.2583E-06	0.8177	0.1823	1.8767E-01	997.15	5.0719E-05	8.3063E-06	0.8593	0.1407	1.0419E-01
19	1229.15	3.7037E-05	8.2583E-06	0.8177	0.1823	1.8767E-01	997.15	5.0719E-05	8.3063E-06	0.8593	0.1407	1.0419E-01
20	1229.15	3.7037E-05	8.2583E-06	0.8177	0.1823	1.8767E-01	997.15	5.0719E-05	8.3063E-06	0.8593	0.1407	1.0419E-01
21	1229.15	3.7037E-05	8.2583E-06	0.8177	0.1823	1.8767E-01	997.15	5.0719E-05	8.3063E-06	0.8593	0.1407	1.0419E-01
22	1229.15	3.7037E-05	8.2583E-06	0.8177	0.1823	1.8767E-01	997.15	5.0719E-05	8.3063E-06	0.8593	0.1407	1.0419E-01
23	1229.15	3.7037E-05	8.2583E-06	0.8177	0.1823	1.8767E-01	997.15	5.0719E-05	8.3063E-06	0.8593	0.1407	1.0419E-01

Table F-1c. Computational Study Data (Continued)

Case Number	FLUENT/UNS 2-D Zn Exit Mass Flow Rate kg/s	FLUENT/UNS 2-D Se ₂ Exit Mass Flow Rate kg/s	FLUENT/UNS 2-D ZnSe Exit Mass Flow Rate kg/s	Yield %
1	1.096E-03	1.597E-03	2.306E-03	46.1
2	8.002E-04	1.259E-03	3.031E-03	59.6
3	7.044E-04	1.091E-03	3.216E-03	64.2
4	8.126E-04	1.127E-03	4.151E-03	68.1
5	1.124E-03	1.646E-03	3.465E-03	55.6
6	8.5900E-04	1.2410E-03	2.9369E-03	58.3
7	9.8443E-04	1.4464E-03	3.9067E-03	61.6
8	8.2670E-04	1.2172E-03	2.9050E-03	58.7
9	8.531E-04	1.134E-03	3.068E-03	60.7
10	8.460E-04	1.204E-03	3.012E-03	59.5
11	8.534E-04	1.193E-03	2.977E-03	59.3
12	8.334E-04	1.267E-03	2.917E-03	58.1
13	8.292E-04	1.268E-03	2.881E-03	57.9
14	6.886E-04	1.080E-03	3.235E-03	64.7
15	7.534E-04	1.122E-03	3.105E-03	62.3
16	8.188E-04	1.174E-03	2.994E-03	60.0
17	8.404E-04	1.232E-03	2.907E-03	58.4
18	9.138E-04	1.357E-03	2.788E-03	55.1
19	7.719E-04	1.203E-03	3.064E-03	60.8
20	7.696E-04	1.214E-03	2.968E-03	59.9
21	7.897E-04	1.249E-03	2.970E-03	59.3
22	8.154E-04	1.244E-03	2.946E-03	58.9
23	8.601E-04	1.218E-03	2.899E-03	58.2

Table F-1d. Computational Study Data (Continued)

Case Number	Case Descriptor	Explanation	Number of Nodes	Number of Iterations	Front Zone Temperature	Middle Zone Temperature	Rear Zone Temperature
					K	K	K
24	arzn1	Ar (Zn) Flow Rate -50%	6610	200	1273.15	1263.15	1223.15
25	arzn2	Ar (Zn) Flow Rate -25%	5009	150	1273.15	1263.15	1223.15
26	arzn3	Ar (Zn) Flow Rate +25%	5009	150	1273.15	1263.15	1223.15
27	arzn4	Ar (Zn) Flow Rate +50%	5009	150	1273.15	1263.15	1223.15
28	arse1	Ar (Se ₂) Flow Rate -50%	5009	150	1273.15	1263.15	1223.15
29	arse2	Ar (Se ₂) Flow Rate -25%	5009	150	1273.15	1263.15	1223.15
30	arse3	Ar (Se ₂) Flow Rate +25%	6610	200	1273.15	1263.15	1223.15
31	arse4	Ar (Se ₂) Flow Rate +50%	5009	150	1273.15	1263.15	1223.15
32	zn1	Zn Flow Rate -50%	5009	150	1273.15	1263.15	1223.15
33	zn2	Zn Flow Rate -25%	5009	150	1273.15	1263.15	1223.15
34	zn3	Zn Flow Rate +25%	5009	150	1273.15	1263.15	1223.15
35	zn4	Zn Flow Rate +50%	5009	150	1273.15	1263.15	1223.15
36	stoich1	Stoichiometric Flow -50%	5009	150	1273.15	1263.15	1223.15
37	stoich2	Stoichiometric Flow -25%	5009	150	1273.15	1263.15	1223.15
38	stoich3	Stoichiometric Flow	5009	150	1273.15	1263.15	1223.15
39	stoich4	Stoichiometric Flow +25%	5009	150	1273.15	1263.15	1223.15
40	stoich5	Stoichiometric Flow +50%	5009	200	1273.15	1263.15	1223.15
41	opt1	Optimum Conditions	6610	200	1350	1350	1300
42	opt1mod	Optimum Conditions -Mod Underrelax Factors	6610	198	1350	1350	1300
43	opt1ng	Optimum Conditions - No Gravity	6610	141	1350	1350	1300

Table F-1e. Computational Study Data (Continued)

Case Number	Zn Inlet Temperature	Zn Mass Flow Rate	Ar (Zn) Mass Flow Rate	Zn Mass Fraction	Ar (Zn) Mass Fraction	Zn Inlet Velocity	Se ₂ Inlet Temperature	Se ₂ Mass Flow Rate	Ar (Se ₂) Mass Flow Rate	Se ₂ Mass Fraction	Ar (Se ₂) Mass Fraction	Se ₂ Inlet Velocity
	K	kg/s	kg/s			m/s	K	kg/s	kg/s			m/s
24	1229.15	3.7037E-05	4.1292E-06	0.8997	0.1003	1.6258E-01	997.15	5.0719E-05	8.3063E-06	0.8593	0.1407	1.0419E-01
25	1229.15	3.7037E-05	6.1937E-06	0.8567	0.1433	1.7513E-01	997.15	5.0719E-05	8.3063E-06	0.8593	0.1407	1.0419E-01
26	1229.15	3.7037E-05	1.0323E-05	0.7820	0.2180	2.0022E-01	997.15	5.0719E-05	8.3063E-06	0.8593	0.1407	1.0419E-01
27	1229.15	3.7037E-05	1.2387E-05	0.7494	0.2506	2.1276E-01	997.15	5.0719E-05	8.3063E-06	0.8593	0.1407	1.0419E-01
28	1229.15	3.7037E-05	8.2583E-06	0.8177	0.1823	1.8767E-01	997.15	5.0719E-05	4.1532E-06	0.9243	0.0757	8.3719E-02
29	1229.15	3.7037E-05	8.2583E-06	0.8177	0.1823	1.8767E-01	997.15	5.0719E-05	6.2297E-06	0.8906	0.1094	9.3956E-02
30	1229.15	3.7037E-05	8.2583E-06	0.8177	0.1823	1.8767E-01	997.15	5.0719E-05	1.0383E-05	0.8301	0.1699	1.1443E-01
31	1229.15	3.7037E-05	8.2583E-06	0.8177	0.1823	1.8767E-01	997.15	5.0719E-05	1.2459E-05	0.8028	0.1972	1.2467E-01
32	1159	1.8560E-05	8.2583E-06	0.6921	0.3079	1.1229E-01	997.15	5.0719E-05	8.3063E-06	0.8593	0.1407	1.0419E-01
33	1199	2.7810E-05	8.2583E-06	0.7710	0.2290	1.4966E-01	997.15	5.0719E-05	8.3063E-06	0.8593	0.1407	1.0419E-01
34	1254	4.6393E-05	8.2583E-06	0.8489	0.1511	2.2690E-01	997.15	5.0719E-05	8.3063E-06	0.8593	0.1407	1.0419E-01
35	1275	5.5715E-05	8.2583E-06	0.8709	0.1291	2.6660E-01	997.15	5.0719E-05	8.3063E-06	0.8593	0.1407	1.0419E-01
36	1171	2.1018E-05	8.3063E-06	0.7167	0.2833	1.2242E-01	935.5	2.5348E-05	8.3063E-06	0.7532	0.2468	6.8070E-02
37	1212	3.1525E-05	8.3063E-06	0.7915	0.2085	1.6517E-01	969	3.8013E-05	8.3063E-06	0.8207	0.1793	8.5856E-02
38	1243	4.2040E-05	8.3063E-06	0.8350	0.1650	2.0887E-01	997.15	5.0718E-05	8.3063E-06	0.8593	0.1407	1.0419E-01
39	1268	5.2453E-05	8.3063E-06	0.8633	0.1367	2.5295E-01	1023	6.3204E-05	8.3063E-06	0.8838	0.1162	1.2287E-01
40	1290	6.3254E-05	8.3063E-06	0.8839	0.1161	2.9941E-01	1051	7.6213E-05	8.3063E-06	0.9017	0.0983	1.4333E-01
41	1231	3.7676E-05	7.8910E-06	0.8268	0.1732	1.8810E-01	986	4.5512E-05	7.8910E-06	0.8522	0.1478	9.4585E-02
42	1231	3.7676E-05	7.8910E-06	0.8268	0.1732	1.8810E-01	986	4.5512E-05	7.8910E-06	0.8522	0.1478	9.4585E-02
43	1231	3.7676E-05	7.8910E-06	0.8268	0.1732	1.8810E-01	986	4.5512E-05	7.8910E-06	0.8522	0.1478	9.4585E-02

Table F-1f. Computational Study Data (Continued)

Case Number	FLUENT/UNS 2-D Zn Exit Mass Flow Rate kg/s	FLUENT/UNS 2-D Se ₂ Exit Mass Flow Rate kg/s	FLUENT/UNS 2-D ZnSe Exit Mass Flow Rate kg/s	Yield %
24	6.841E-04	1.102E-03	3.176E-03	64.0
25	8.362E-04	1.209E-03	3.026E-03	59.7
26	8.630E-04	1.332E-03	2.856E-03	56.5
27	9.253E-04	1.326E-03	2.768E-03	55.1
28	7.796E-04	1.131E-03	3.034E-03	61.4
29	8.315E-04	1.189E-03	2.942E-03	59.3
30	8.892E-04	1.284E-03	2.836E-03	56.6
31	9.175E-04	1.325E-03	2.756E-03	55.1
32	1.836E-04	1.745E-03	1.965E-03	50.5
33	4.876E-04	1.446E-03	2.528E-03	56.7
34	1.212E-03	1.153E-03	3.195E-03	57.5
35	1.642E-03	1.039E-03	3.368E-03	55.7
36	4.322E-04	3.674E-04	1.830E-03	69.6
37	6.766E-04	7.701E-04	2.470E-03	63.1
38	1.105E-03	1.166E-03	3.064E-03	57.4
39	1.436E-03	1.587E-03	3.552E-03	54.0
40	1.910E-03	2.035E-03	4.045E-03	50.6
41	7.818E-04	8.090E-04	3.118E-03	66.2
42	8.114E-04	8.574E-04	3.042E-03	64.6
43	7.845E-04	8.291E-04	3.060E-03	65.5

VITA

Brent L. Foster

Candidate for the Degree of

Master of Science

Thesis: 2-D RENDERING AND ANALYSIS OF A HORIZONTAL ZINC SELENIDE
AEROSOL REACTOR VIA COMPUTATIONAL FLUID DYNAMICS

Major Field: Mechanical Engineering

Biographical:

Personal Data: Born in McAlester, Oklahoma, on July 7, 1973, the second son of Curley L. and Patsy J. Foster.

Education: Graduated from Union High School, Tulsa, Oklahoma, in May 1991; received Bachelor of Science degree in Mechanical Engineering from Oklahoma State University, Stillwater, Oklahoma, in May 1997; completed requirements for Master of Science degree in Mechanical Engineering at Oklahoma State University, Stillwater, Oklahoma, in July 1999.

Professional Experience: Employed as research and teaching assistant at Oklahoma State University, School of Mechanical and Aerospace Engineering, 1997-1999; employed as engineering intern, Phillips Petroleum – Woods Cross Refinery, Woods Cross, Utah, summers of 1996 and 1997.

Professional Memberships: American Society of Mechanical Engineers, Tau Beta Pi Engineering Honor Society, Pi Tau Sigma Mechanical Engineering Honor Society.